CONTINUOUS MICRODIALYSIS OF BLOOD PROTEINS DURING CARDIOPULMONARY BYPASS

by

ALEXANDER FOK

A Thesis submitted to the
Graduate School – New Brunswick
Rutgers, The State University of New Jersey
And
The Graduate School of Biomedical Sciences
University of Medicine and Dentistry of New Jersey
in partial fulfillment of the requirements
for the degree of
Master of Science
Graduate Program in Biomedical Engineering
written under the direction of
Professor Jeffrey D. Zahn
and approved by

_____

_____

_____

_____

New Brunswick, New Jersey

October 2009

ABSTRACT OF THE THESIS

Continuous Microdialysis of Blood Proteins During Cardiopulmonary Bypass

By Alexander Fok

Thesis Director: Jeffrey Zahn, PhD

Cardiopulmonary bypass is a procedure that temporarily substitutes a patients' heart and lung functions with an extracorporeal heart-lung machine. This allows surgeons to operate on motionless heart and lungs, while still providing the body with proper blood circulation. However, the heart-lung machine has been shown to activate the body's systemic inflammatory response, resulting in short- and long- term organ dysfunction, and even death. The severity of this inflammatory response is strongly correlated to the production levels of specific cytokines and complements found in the bloodstream. Current detection methods require taking discrete blood samples during surgery and waiting at least several hours, but typically one to two weeks when including laboratory queue times in hospitals, for results. I propose a microdialysis device that continuously samples the patient's blood for biomarkers during surgery. The primary function of this device is to prepare a purified solution, with complement concentrations that closely matches that of the patient's bloodstream, to be used in a continuous microimmunoassay device.

The microdialysis device was fabricated using photolithography and softlithography techniques to create microfluidic channels and bonded to commercially available semi-permeable membranes with biocompatible epoxy. The device was designed based on computational simulations and fabrication constraints for optimal

performance. It was tested for its analyte-recovery capabilities for complements C3a, C4a, and C5a, in human blood continually circulating through a mock heart-lung machine.

Two slightly different designs were tested, one using a membrane pore-diameter of 0.1 μm and the other using 0.4 μm. Both devices operated at a perfusion flowrate of 4.1 μL/min, which is considered to be relatively fast for microdialysis probes. For the 0.1 μm pore membrane device, the relative recoveries were 79%, 75%, and 70% for C3a, C4a, and C5a, respectively. For the 0.4 μm pore membrane device, the relative recoveries were 112%, 135%, and 101% for C3a, C4a, and C5a, respectively. These findings show promising results for the proposed microdialysis device, but further investigation is needed to improve statistical significance.

ACKNOWLEDGEMENTS

This work would not have been possible without the guidance of my advisor, Dr. Jeffrey Zahn. His combination of technical expertise and creative ideas has shown me what it takes to approach new problems and how to solve them. I will continue to use these lessons in whatever career comes my way and in my own life.

I would also like to thank our collaborator, Dr. Akif Undar, who has supported this project in many ways. His generosity and willingness to share his laboratory space and resources at Hershey Medical Center was vital for conducting experiments.

I thank my committee members, Dr. David Schreiber and Dr. Li Cai, who were also my instructors at Rutgers University, for broadening my knowledge in the biomedical engineering field. Their dedication to helping students learn has been influential to me.

To my friends and colleagues at Rutgers University, I thank them for creating a supportive and positive learning environment. Special acknowledgements go to the members of my lab, whom I also consider as friends: Mercedes Morales, Kiana Aran, Larry Sasso, and Pantelis Athanasiou, who have provided immense support with my research and life in general.

To the faculty and administrative staff of Rutgers' Biomedical Engineering Department, I would like to express my appreciation for their help, advice, and friendly demeanor that made for a pleasant experience at Rutgers University.

Finally, to the most important people in my life, I would like to thank my parents and my brother for their seemingly infinite love and support.

DEDICATION

To my family and friends for their love and support.

TABLE OF CONTENTS

LIST OF TABLES

LIST OF ILLUSTRATIONS

Chapter 1 - Introduction

1.1 The Need for Microdialysis during CPB

Cardiopulmonary bypass (CPB) is a procedure where a patients' heart and lung functions are temporarily taken over by, what is commonly referred to as, an extracorporeal "heart-lung machine" (Fig. 1.1) to maintain the circulation and oxygenation of blood in the body. This procedure is usually necessary when a surgeon needs to operate on a motionless heart or lung, such as when repairing internal heart defects or heart valves [1], but can also be done on a beating heart, such as for minimally invasive off-pump coronary artery bypass surgery [2]. The CPB circuit consists of: pumps to circulate blood through the machine, an oxygenator to exchange carbon dioxide with oxygen in the blood, filters to remove emboli and gas bubbles, ports to introduce drugs such as the anticoagulant heparin and anesthesia agents, tubing to transport blood from one part of the circuit to another, and cannulas to remove and deliver blood, to and from, a patient's circulatory system [1].

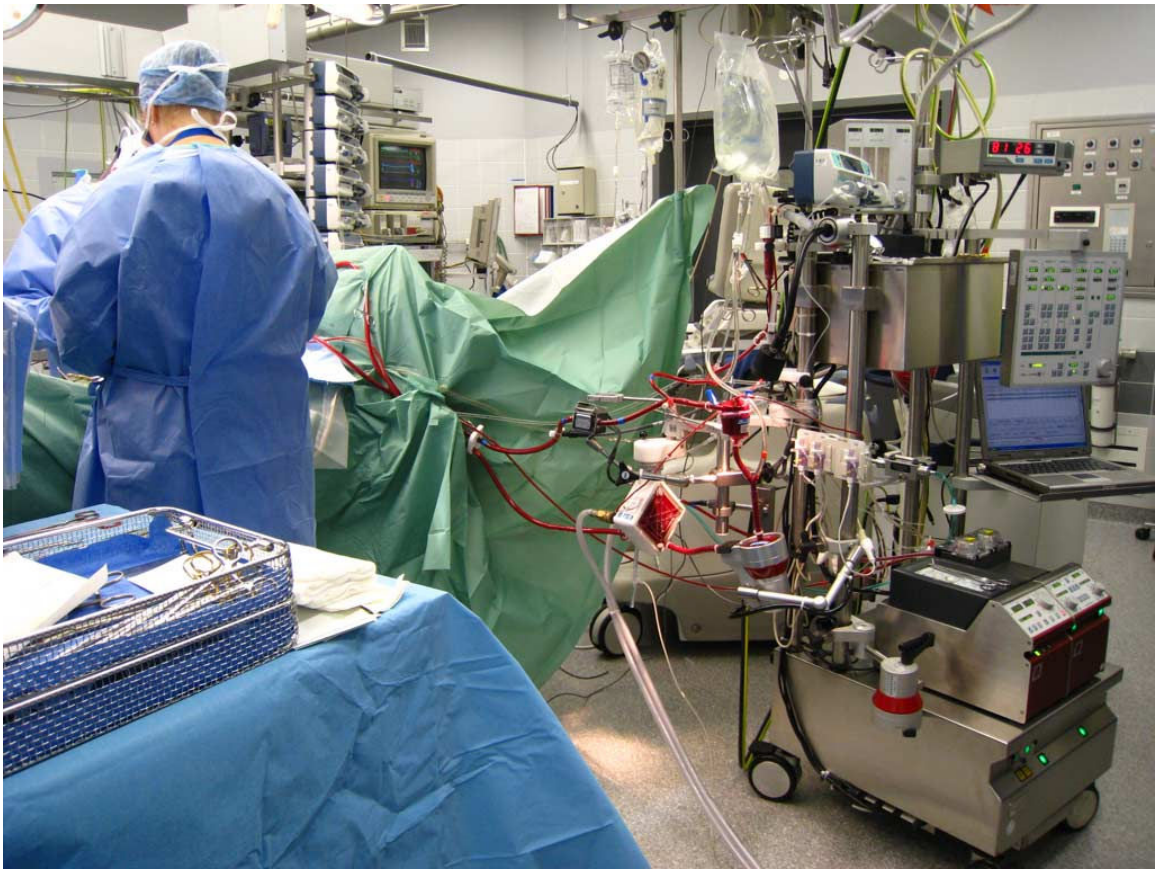

Figure 1.1: A cardiopulmonary bypass machine being used during surgery [3]

Although cardiac surgeries are usually life-saving procedures and the patient is typically only on the CPB pump for several hours, a major disadvantage of using a heart-lung machine is the damage it imposes on the circulating blood due to hemolysis [4, 5] and a systemic inflammatory response [6, 7]. As blood circulates through various components in the circuit, it can experience high shear stresses, and be exposed to immunological-activating surfaces and endotoxins, all of which may induce a systemic inflammatory response. As a result, short- or long-term multiple organ dysfunction, or even death can occur [8-12].

Researchers are currently working on correlating the expected degree of organ dysfunction with the degree of a patient's inflammatory response, which is done by measuring blood for levels of specific biomarkers such as complements. Since complement levels may fluctuate during and even after surgery, multiple discrete blood samples are taken between pre- and post-surgery and sent to a lab for analysis, which can typically take several hours to perform (though results may not be available for days or weeks, depending on laboratory queue time). Given the ability to monitor complement levels continuously and in near real-time, surgeons may be able to prevent or limit organ dysfunction by administering therapeutic drugs at times and doses tailored to individual patients.

This thesis is based on previous work and advances made by Zahn's group in the field of microfluidics and microfabrication. Hsieh et al. developed an on-chip, continuous microdialysis and glucose sensing device for the treatment of diabetic patients [13, 14]. This device incorporated a microdialysis device with in-line sensing electrodes to continuously track concentration changes with impressive glucose recovery and sensing capabilities. Yang et al. developed a microfluidic device that continuously separate splasma from whole blood [15] and another device that continuously monitors blood plasma proteins via fluorescence intensity detection using biotinylated FITC solution and streptavidin-coated microbeads [16], both devices utilizing the Zweifach-Fung effect [17, 18].

In this work, a microdialysis chip capable of continuously dialyzing blood proteins, while excluding cells, is presented. The device uses photolithography and softlithography techniques to fabricate microfluidic channels on a biocompatible

polymer, and an epoxy stamping technique to directly bond two layers of microchannels on opposite sides of a porous membrane. The porous membrane allows for small analytes in blood, such as proteins, to cross the membrane into an analyte-free, isotonic solution while preventing cells and large cellular fragments from crossing and contaminating the aforementioned isotonic solution.

In Chapter 2, some background information about the invention, design, and detrimental effects of the heart-lung machine (CPB pump) are discussed. The design of these components, such as the oxygenator and blood pumps, has a significant impact on the degree of a patient's inflammatory response. Current microdialysis techniques are also introduced here.

In Chapter 3, the methodology for designing the proposed microdialysis chip is explained as well as the fabrication techniques used. Initial bench-top experiments were performed using a saline solution doped with glucose, using the sugar molecule as the analyte of interest, and an analyte-free saline solution as the perfusate. Glucose recovery ranged from 91% to 95%, over a broad range of flowrates, despite large pressure gradient changes across the membrane. Further experimentation was performed on a mock CPB circuit using a full heart-lung machine setup but with several units of human blood in a blood bag instead of using an actual patient. The concentration levels for complements C3a, C4a, and C5a were measured at constant flowrate settings, over a period of 90 minutes, for a device using 0.1 μm pore diameter membrane and another using 0.4 μm pore diameter membrane. Analyte recovery performance varied depending on the pore size of the membrane as well as the specific complement being measured.

Finally, conclusions and future works are discussed in Chapter 4. Though inconsistencies were observed, the overall results show a promising path for designing an improved microdialysis system. Based on the evidence from the experiments, further investigation is necessary to explain several inconsistent observations such as why complement levels in blood samples from the CPB circuit were sometimes lower than that of the recovered dialysate; and why the complement levels in the solution recovered from the reservoir channel's outlet were significantly lower than that of the blood flowing in the CPB circuit. The system should then be incorporated into a microimmunoassay chip, which would continuously measure analyte concentration directly on the chip itself.

Chapter 2 - Background

In this chapter, CPB, its development, usage, and physiological complications are introduced. Studies have shown that the body induces systemic inflammatory responses during cardiac surgery, especially when cardiopulmonary bypass is used [11, 19-32]. Although much time and effort have gone into developing each component of the CPB machine, almost every component is still responsible for cell damage and immune activation to some degree. Clinical evidence has shown a strong correlation between specific inflammatory response levels with postoperative complications, such as organ dysfunction, which can potentially lead to death. At present, studies are done by taking blood samples from the patient pre-, during, and post-operation. Typically, concentration levels are then analyzed via enzyme-linked immunosorbent assay (ELISA) or immuno-fluorocytometry. By being able to monitor a patient's inflammatory response in near-real-time and continuously during CPB, doctors may one day be able to offer effective treatments during surgery, or at least understand the syndrome and its causes better.

2.1 Cardiopulmonary Bypass Procedure

Today, over 400,000 open-heart operations are performed each year in the United States [1]. Cardiopulmonary bypass is a procedure that replaces the function of the heart and lungs during operations that require the patients' own heart and lungs to be stopped. A cardiopulmonary bypass pump (often referred to as heart-lung machine or mechanical pump-oxygenator) is used to maintain the patient's blood circulation, which keeps tissues alive by providing nutrients and supplying oxygen to the blood while removing carbon dioxide. This procedure is used on patients ranging from neonates to seniors and for reasons ranging from heart-lung transplants to cardiac valve repair and/or replacement.

2.1.1 History of Development

During the 1930's and 1940's, prior to the invention of the heart-lung machine, only simple extracardiac (outside of the heart) surgeries were possible. As doctors gained experience and confidence from this, they began to expand into intracardiac surgeries, where repairs are made inside the heart [1]. In order to support a patient's life during this more complex type of cardiac repair, surgeons had to somehow support the patient's blood circulation and blood-gas transfer. While several worldwide teams began to work on mechanical pump-oxygenators, C. Walton Lillehei, at the University of Minnesota, developed a controlled cross circulation procedure where another person's oxygenated blood (typically the patient's parent) was cannulated from their femoral vessel and pumped into the patient requiring cardiac repair [26]. Lillehei began clinical cases in 1954 and observed a 40% mortality rate (18 deaths out of 45 total cases) [33]. This procedure also introduced potential risk to the donor. Nevertheless, the procedure was

seen as a success and many recommended abandoning further research into mechanical CPB pumps.

John H. Gibbon, Jr. developed his CPB machine while working at Jefferson Medical College in Philadelphia, PA, with partial financial support from Thomas J. Watson, chairman of IBM. In 1952, Gibbon's first attempt at using his mechanical pump with a screen oxygenator was unsuccessful due to a fatal misdiagnosis of the one year old patient's condition [1]. Gibbon's only success with his machine came in May 1953 for an 18 year old woman suffering from atrial septal defect (ASD). Gibbons made several more unsuccessful cardiac surgical attempts, but the patients died and no further attempts were made [1].

In 1952, John W. Kirklin gathered a team of experts in pathology, physiology, cardiology, anesthesiology, and mechanical engineering at the Mayo Clinic to develop a mechanical pump-oxygenator. Using the Gibbon-IBM machine's blueprint as a starting point, Kirklin modified and refined the design for 2½ years before its first use in 1955 (Fig. 2.1). In that year, a clinical series of open heart surgeries where Gibbon's CPB pump was used on 8 patients (aged between 4 months to 11 years old), where 4 died postoperatively. Patients were under cardiopulmonary bypass for 20 to 73 minutes, with blood flowrates of 100 ml/kg [34]. This pioneering effort led by the Mayo Clinic team, brought forth a new era in intracardiac surgery.

Figure 2. 1: The Gibbon type cardiopulmonary bypass machine first used in March 1955 by Kirklin's team at the Mayo Clinic [1]

2.1.2 Main CPB Components

A modern-day CPB machine consists of two main components: the pump and the oxygenator. Secondary components are tubing, which connects components from one part of the circuit to another, and cannulae, which are tubes that connect to the patients' veins and arteries. Each component has continually gone through design changes, with the motive of minimizing physiological effects such as systemic inflammatory response, hemolysis, and microembolisms.

2.1.2.1 Pumps

Performance characteristics that an ideal CPB pump should have are: 1) the ability to pump blood at 7 l/min against a pressure of 500 mm Hg for an adult, 2) should not cause damage to cellular or acellular blood components, 3) should not have dead

spaces where blood can stagnate or experience turbulent flow, 4) reproducible pump flowrates, and 5) ability to be operated manually in case of power failure [26]. Roller pumps and centrifugal pumps, as seen in Fig. 2.2, are the two most common types of extracorporeal pumps currently used for blood perfusion.

For the last five decades, the roller pump has been the most commonly used type for CPB, though recent improvements in centrifugal pumps have helped them gain popularity. In a roller pump, a length of tubing is located alongside a curved raceway, which is placed at the travel perimeter of rollers mounted on the ends of rotating arms. The arms are oriented such that at least one roller pinches the tubing at all times. As the roller begins to pinch the tubing at the beginning of the raceway, the volume of blood in the tubing ahead of the pinched section is pushed forward. This action allows for continuous blood flow, where flowrate is determined by the inside diameter of the tubing and the speed of the rollers moving along the raceway. Although pumps with varying amounts of rollers exist, a two-roller pump provides a relatively nonpulsatile flow compared to a single-roller pump and causes less hemolysis than a multiple-roller pump.

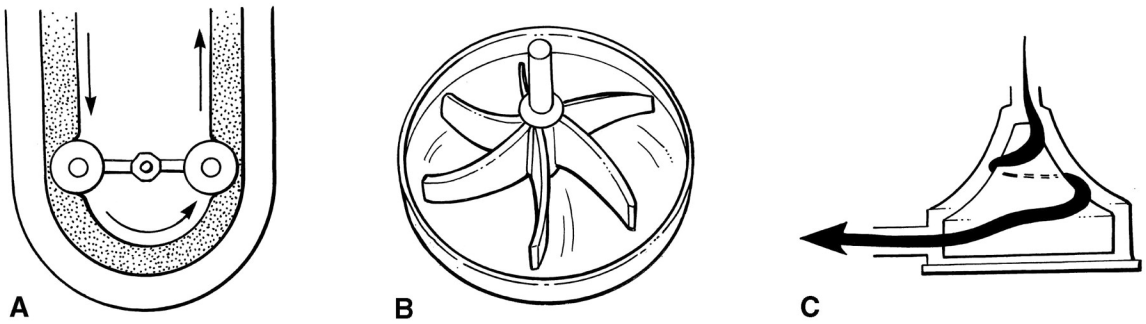

Figure 2.2: Blood pump designs. (A) Two-roller, roller pump. The tubing sits on the inner surface of the raceway. (B) Impeller pump with vanes connected to a rotating shaft. (C) Centrifugal pump. The inner concentric cone rotates rapidly, propelling blood radially outwards. [22]

When using roller pumps, several complications can arise during an operation. If a blockage occurs somewhere in the outflow end, pressure in the line can increase progressively until a tubing or connector fails. If a blockage occurs somewhere in the inflow end, a high negative pressure in the line can induce blood cavitation (the production of microscopic air bubbles) or suction of room air through loose valves or connections. Normal wear in the tubing, caused by the rollers, can create pinhole leaks, where microscopic air bubbles can enter the line and head towards the patient [35]. In a study by Stoney et al., line embolism from roller pumps were responsible for 92 deaths and 61 permanent injuries between 1972 and 1977 [36].

Centrifugal pumps have already replaced roller pumps at many institutions. Its basic design components consist of an impeller with a series of vanes or a stack of smooth plastic cones inside a plastic housing. The impeller is either driven directly by a shaft or indirectly by a magnetic coupling. Typically, fluid enters at the center of rotation. Then, as the impeller rotates, the fluid is propelled radially outwards due to centrifugal force, where it exits the pump. Unlike roller pumps, which rely on some amount of occlusion (closure via pinching) in the tubing, centrifugal pumps are nonocclusive. Because of this, the degree to which centrifugal pumps can experience extreme positive or negative pressures are low, when compared to roller pumps. Therefore, the chances of cavitation and microembolism issues are reduced [35]. Another major advantage is the reduced risk of introducing macroscopic and microscopic air bubbles, possibly due to a combination of shear force and positive pressure generation within the pump head [26].

Centrifugal pumps also suffer from several disadvantages. Due to the centrifugal pump's nonocclusive design, retrograde flow is possible when the pump stops or slows.

Also inherent to this design, even when the rotational speed is fixed, the flowrate can change automatically when the systemic vascular resistance changes; therefore the arterial outflow must be monitored with a flow probe.

Although both types of pumps mentioned have advantages and disadvantages, the medical community has not been able to reach a unanimous opinion on which is ultimately safer for patients. Some studies have shown less hemolysis with centrifugal pumps versus roller pumps [37, 38], while others have shown contradictory results [39, 40] or no difference at all [41, 42].

2.1.2.2 Oxygenators

Oxygenators serve several purposes during CPB, besides oxygenating blood. It acts as an entry point for anesthesia, and as a gas exchanger for oxygen, carbon dioxide, and other gases. They also serve as a heat exchanger and blood filter. Because of the natural lung's complex and highly efficient structures of pulmonary alveoli and capillaries, the artificial lung was one of the primary challenges for CPB designers.

Although several types of membrane oxygenators exist, the cross-current hollow fiber membrane (Fig. 2.3) is most commonly used. The hollow polypropylene fibers have pores of 1 μm in diameter that prevents both gas and blood from crossing the membrane. Fresh air flows through the inside of bundles of hollow membrane fibers, while blood flows perpendicularly outside of the fiber. The cross-flow design takes advantage of secondary-flow that is induced by the fibers "tripping" fluid flowing past it, which reduces the diffusion boundary layer and improves gas exchange.

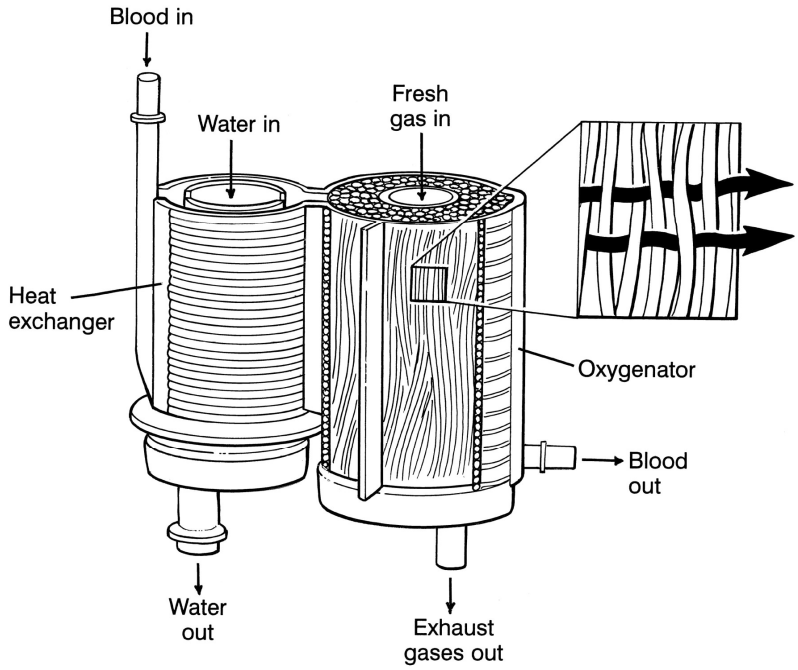

Figure 2.A: Diagram of a hollow fiber membrane oxygenator and heat exchanger unit. Blood flows through the heat exchanger, over temperature-controlled coils and then enters the oxygenator, which is made up of woven strands of hollow fibers. Oxygen flows from one end of the fiber to the other, supplying oxygen and exchanging carbon dioxide with blood. [22]

2.1.2.3 Heat Exchangers

Heat exchangers are coupled with the oxygenator and can either cool down or warm up blood circulating through it. Typically, blood flows through spiraling coils made of stainless steel or aluminum, which are submerged into circulating non-sterile water. The inner walls of the coils are coated with polymers to limit blood-surface interactions. The circulating water is chilled to nearly 0^{o}C in an ice bath and heated by an electric resistance coil to an absolute maximum of 42^{o}C, at which point blood proteins begin to denature [26]. Blood temperature plays a crucial role during CPB, as it can lead to serious short- and long-term health issues for the patient.

Inducing hypothermia at the onset of CPB reduces the patient's metabolism, blood oxygen requirements, complement activation, and overall systemic inflammation [1, 10, 43]. The blood is cooled as quickly as possible and is only limited by thermal and fluid dynamics. Conversely, re-warming of the blood is performed at the end of the procedure and its heating rate is carefully controlled to prevent blood damage, which can ultimately lead to cerebral injury. Furthermore, overheating blood too quickly can produce bubble formation due to the decrease in gas solubility, producing gaseous microemboli.

2.1.3 Systemic Inflammatory Response

SIRS, an acronym for "systemic inflammatory response syndrome," is a term used to associate cardiopulmonary bypass with a wide range of ailments due to a "whole body" inflammatory response such as pulmonary, renal, gut, central nervous system, and myocardial dysfunctions; vasoconstriction; vasodilatation; hemolysis; leukocytosis; and an increased risk to infections [11, 27, 28, 32, 35, 44]. Neither the severity of the response nor the specific ailment(s) to occur, are predictable. However, the duration of CPB, age, and complexity of the procedure are commonly regarded as risk factors [23, 27, 45, 46].

The origin of SIRS response can be attributed to the damage of cellular and noncellular (humoral) components of blood, primarily caused by altered arterial blood flow patterns and blood-surface contact within CPB components [26]. This can then result in microemboli formation, hemostasis disruption, and most importantly, a chain-reaction of cytokine-mediated and neutrophil-mediated inflammatory injury.

2.1.3.1 Inflammatory Cascade

The inflammatory cascade is primarily caused by the activation of factor XII, a plasma protein, to factor XIIa, which triggers several inflammatory systems (Fig. 2.4). To start, surface contact causes factor XII to undergo a conformational change and become attached to high-molecular-weight kininogen [26]. This complex then adheres to the foreign surface, undergoes limited proteolysis, then releases kallikrein, bradykinin, and factor XIIa. A positive feedback system involving factor XIIa and kallikrein, which activates neutrophils, can further activate the inflammatory cascade via production of oxygen free radicals and proteolytic enzymes [26].

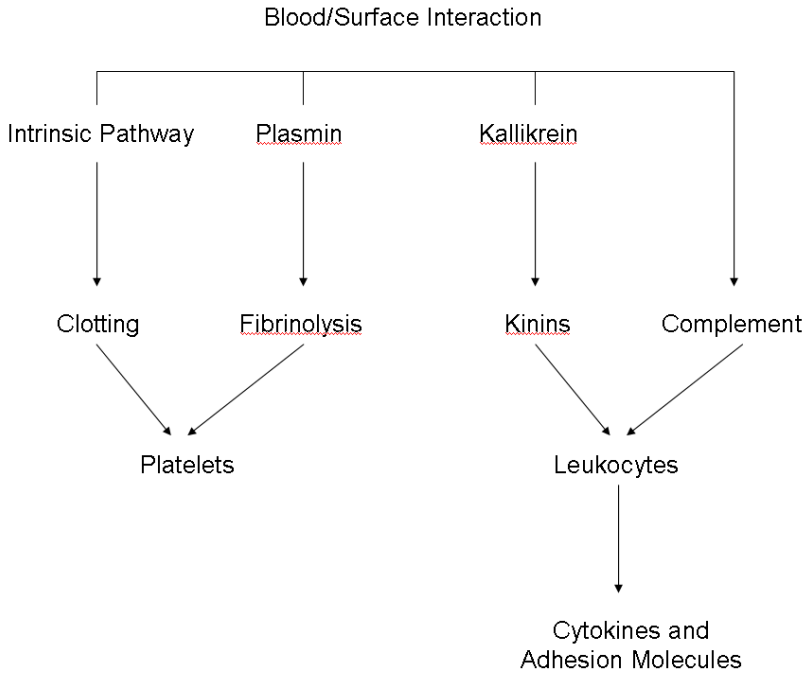

Figure 2.B: Contact activation cascade systems that cause SIRS [26]

2.1.3.2 Complement System

The complement system plays several key roles in the inflammatory process, such as mediating inflammation, opsonization of antigenic particles, and damaging pathogen membranes [26]. The product from a complement component interaction becomes the enzyme for the next step, as shown in Fig. 2.5. The complement system cascade can be triggered by just a small initial stimulus and result in massive amplification of the initial activating event. Fortunately, this system is tightly controlled by regulatory molecules, which makes up half the proteins in the complement system.

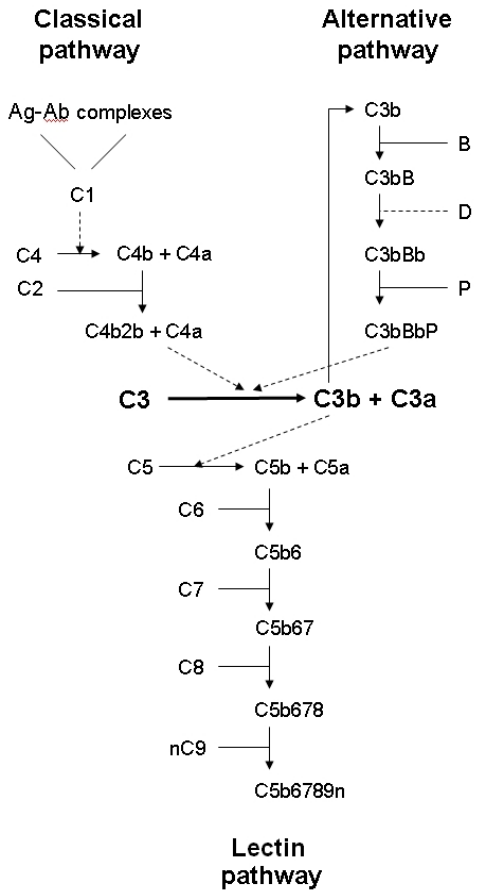

Figure 2.C: The three pathways of the complement system: Classical pathway, Alternative pathway, and Lectin pathway [26]

There are two activation pathways in the complement system: the classical pathway and alternative pathway. The classic pathway, which is the least important in this discussion, is initiated when antibodies bind to target antigens on a surface. Its cascade leads to the production of the classical pathway C3 convertase, C4b2b. This convertase then cleaves C3, the central component of the system, into C3a and C3b fragments. The alternative pathway has a feedback loop that begins at the C3b component and leads to the generation of the alternative pathway C3 convertase, C3bBbP. This convertase also cleaves C3 into its C3a and C3b fragments, where the C3b product can then be re-initiated to the beginning of the alternative pathway. Although the spontaneous activation of C3 occurs on a continuous basis, albeit at a low level, the triggering of the full cascade can be prevented by cellular expression of regulatory proteins that inactivates C3bBbP [26].

A third and final pathway in the complement system is the lectin pathway. This pathway uses C3b, from either the classical or alternative pathway, to activate C5 to produce C5a and C5b. C5a is a soluble molecule, while C5b binds to cell surfaces. As a result, C6, C7, and C8 binds to the cell surface and C9 polymerizes to form a pore through the cell membrane; thus resulting in a membrane attack complex (MAC) [26].

During CPB, activation of the complement system can be observed by monitoring the consumption of components [47] and the presence of C3a and C5a in the circulation [26]. Several factors have been shown to activate the cascade during CPB including: surface biocompatibility, release of endotoxin into the system, and the breakdown of C3 caused by blood interaction with oxygen bubbles.

2.1.3.3 Red Blood Cell Damage

Red blood cells (RBCs) primarily damaged by shear stress have reduced deformability due to mechanical damage [48]. Red blood cell deformability affects the rheological properties of blood and is particularly important to maintain tissue metabolism and oxygenation. Membrane damage also disrupts the normal function of ionic pumps and causes an abnormal accumulation of cations within the cell [49]. The membrane attack complex (MAC), generated during complement activation [11], attacks the plasma membrane by forming pores, which allow free diffusion of molecules to pass in and out of the cell. When enough pores are formed, hemolysis can occur. Death or even damage to RBCs may be one reason for post-operative anemia frequently observed in patients[50], as RBC damage shortens cell lifespan.

Besides anemia, RBC injury has a destructive effect at cellular, tissue, and organ levels. An increase in plasma hemoglobin levels increases the plasma oncotic pressure and viscosity, which is detrimental to tissue function. The auto-oxidation of hemoglobin releases cytotoxic oxygen free radicals. Potassium released from RBCs and into extracellular fluid may impair cardiac conduction and cause arrhythmias. Fragments of RBC lipid membranes can also block microcirculations (arterioles, capillaries, and venules) and cause organ dysfunction.

2.1.3.4 Neutrophil and Vascular Endothelium

Neutrophils make up most of the leukocytes in the body and are essential against fighting infections and foreign materials. On the other hand, activated vascular endothelium triggers neutrophil activation when the two come into contact, resulting in

much of the SIRS maladies. CPB circulation triggers a humoral cascade that leads to the activation of the vascular endothelium. Neutrophil activation occurs via IL-8, C5a, or platelet activation factor (PAF) to express adhesion molecules on its surface, causing the activated neutrophils to adhere to activated endothelium. At this stage, cytotoxic proteases and oxygen-derived free radicals are released by the neutrophils, causing some of the post-CPB end-organ damage [26].

Under normal physiological circumstances, the vascular endothelium is relatively inert and allows blood to circulate freely. Inflammatory signals (such as complement activation products, oxygen-derived free radicals, and cytokines) cause the endothelial cells to change their gene expression, prompting the release of cytokines and protein expressions, which leads to inflammatory reactions and thrombosis [19, 51]. Typically, endothelial activation occurs at a local site, where neutrophil recruitment and coagulation can occur to contain the local infection. However, cytokines released during CPB causes this reaction to occur on a systemic level. As a result, large areas of endothelium are activated, followed by large scale neutrophil activation, adhesion, and release of cytotoxic proteases and oxygen-derived free radicals. The body's feedback mechanism that is normally able to cope with attenuating the response at a local level is not able to cope proportionately at a systemic level. End-organ damage, microemboli, and clotting factor depletion are contributing factors to coagulopathy (clotting disorder) complications after open-heart surgery [24, 25, 52, 53]. Neutrophil-endothelium adhesion can cause capillaries to become blocked, causing local ischemia [20]. Finally, cytotoxic products released by activated neutrophils can damage cells directly.

2.1.3.5 Organ Dysfunction

Organs that are affected by CPB may include: the lung and pulmonary circulation, kidneys, brain, and gut. At the end of CPB, the entire cardiac output is sent to the pulmonary circulation, which will be exposed to a large number of activated cells passing through. Studies have shown that activated neutrophils are more likely to become lodged in the pulmonary circulation [54, 55] and release free radicals that cause lung injury. Studies have shown that intravenous injection of oxygen radical scavengers, such as superoxide dismutase or catalase, can attenuate pulmonary damage [56]. Renal function is reduced by the effects of (CPB-induced) hypothermia, which increases vascular resistance and vasoconstriction. To remedy this during CPB, hemodilution is used to improve plasma flow and help prevent renal injury [31]. Blood cell aggregates (microemboli) can cause brain swelling and lead to postoperative cerebral dysfunction [57].

2.1.3.6 Ischemia Reperfusion Injury

During an on-pump open heart surgery, where the heart is intentionally stopped and isolated from blood circulation via an aortic cross-clamp, the heart tissue is damaged due to the lack of oxygen and nutrients, and inability to remove metabolic waste [26]. However, further injury is incurred when blood flow is reintroduced, towards the end of surgery; this is known as ischemia reperfusion injury. Several mechanisms of reperfusion injury exist, including: oxidative stress, where the oxygen in the returned blood exposes cells to damaging oxygen free radicals; neutrophil activation, partially caused by blood contact with extracorporeal surfaces; and activation of the complement cascade, primarily

through the alternative pathway, which produces complement fragments (such as C3a and C5a) that further activates neutrophils [58]. Examples of reperfusion injury include myocardial necrosis, endothelial dysfunction, and apoptosis [26]. By monitoring the levels of specific biomarkers such as complement fragments in circulating blood, it would be possible to finely tuned doses of complement pathway inhibitors to counteract the inflammatory response in near-real-time.

2.2 Measuring Complement Components

Immunoassay techniques used in hospitals today (such as radioimmunoassay, enzyme-linked immunosorbent assay, or cytometric bead assay kit) involve machines that are typically cumbersome and expensive to operate. Multiple sample-preparation steps are required from the end-user, especially if the sample contains whole blood. Blood samples must be collected in tubes and kept on ice until it is ready to be centrifuged at 4^{o}C, at which point, the separated plasma is extracted and frozen at -70^{o}C [59, 60]. The centrifuging process removes red blood cells, leukocytes, platelets, and other debris from plasma since there is evidence that shows blood stored at 4^{o}C contributes to complement activation via the classical or alternate pathway [61]. Another contributing factor via the alternate pathway has been reported to be a result of blood contacting plastic surfaces during storage [62]. As one can see, careful steps must be taken to ensure validity of the samples such that there is no change in complement concentration from the time at which they were collected.

2.3 Microdialysis

Microdialysis sampling is a technique used to collect analytes from extracellular fluid (ECF) for analysis. The primary component of all microdialysis devices is its semi-porous membrane that is placed in between ECF and perfusion fluid. Substances travel from areas of higher concentration to lower concentration. Small analytes from the ECF (such as proteins, peptides, and other chemicals) diffuse through the membrane pores and into the perfusate while large particles (such as cells, platelets, large proteins, etc.) are excluded. In other words, the device provides "clean" samples to make chemical analysis easier or even possible.

2.3.1 Development of microdialysis

Microdialysis sampling began as a means to measure the chemical composition from rodent brain in real-time. By placing a microdialysis probe at specific target sites instead of using a needle to draw blood samples from the bloodstream, it provides both temporal and spatial references to the data. Today, it is used essentially on every organ for applications ranging from endocrinology, immunology, metabolism, and pharmacokinetics, though a vast majority of biomedical literature has focused in neuroscience [63]. However, more and more life scientists are realizing the potential uses for microdialysis sampling beyond neuroscience.

2.3.2 Basic Principles of Operation

Currently, microdialysis sampling devices most commonly exist in the form of a microdialysis probe located at the tip of two concentric cannulae (the “inner” cannula and “outer” cannula) (Fig. 2.6). Depending on the organ’s fragility, the cannulae can be made out of rigid or flexible materials. The perfusion fluid (“perfusate”) flows down the interior of the inner cannula, where it exits the tip of the inner cannula, and then flows upwards (away from the tip) in between the outer and inner cannulae. At the probe end, a section of the outer cannula is made of a semipermeable membrane and is the region that comes into direct contact with the tissue site or fluid-filled space. Analytes from the probe’s exterior diffuse across the membrane and into the perfusion fluid (referred to as the “dialysate”), where it then exits the microdialysis device to be collected or analyzed further downstream.

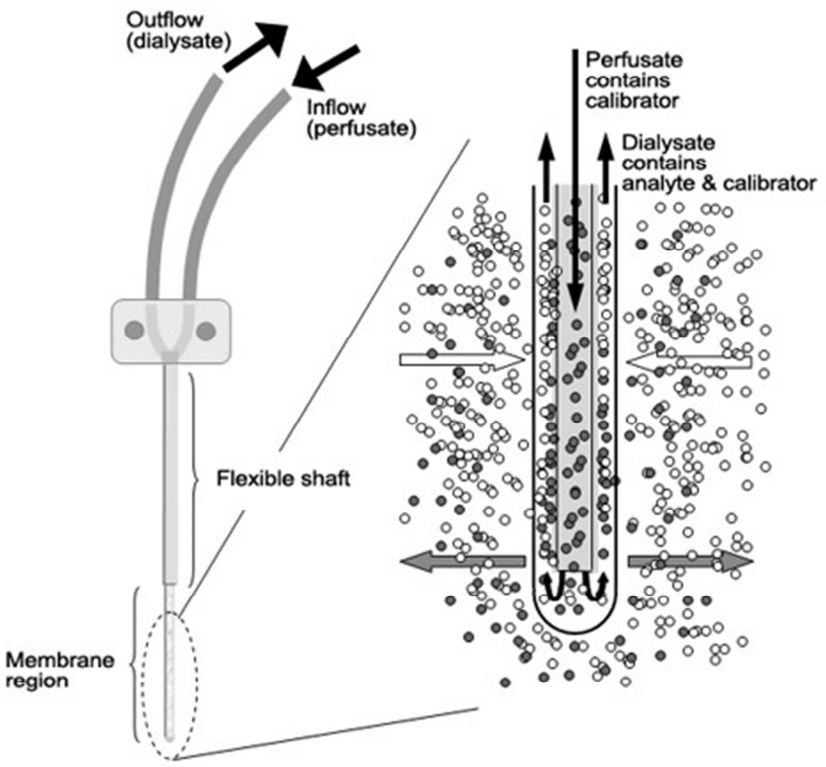

Figure 2.6: A cannula-based commercial microdialysis probe. The cannula tip is placed in extracellular fluid or on bare tissue, where analytes diffuse across the membrane and into the analyte-free perfusate solution. [64]

2.3.2.1 Perfusate

The particular perfusate solution is chosen carefully to match the ionic and osmotic strength of the ECF, which helps maintains fluid and ion balance across the membrane. An improperly balanced osmotic pressure across the membrane can cause perfusion fluid to be gained or lost, thereby affecting the analyte concentration to be measured as well as the normal physiological environment. An improperly balanced ionic gradient across the membrane can also damage sensitive organs such as the brain. For these reasons, a form of Ringer's solution is used as the perfusate and typically contains 150 mM NaCl, 4 mM KCl, and 2.4 mM $CaCl_2$. The solution can also be

supplemented with glucose and ionic salts [64]. If properly balanced, the primary mode of transport is diffusion, driven by the analytes' concentration gradients.

2.3.2.2 Membrane Material

The same semipermeable porous hollow fiber membranes used in kidney dialysis is also used in microdialysis probes (Fig. 2.7). Until recently, membranes were only able to recover low-molecular mass mediators, metabolites, and xenobiotics. With the current availability of high molecular weight cutoff (MWCO) membranes, larger molecules such as plasma proteins, complements, and growth factors can now be recovered as well [65]. Commonly used materials include polycarbonate/polyether blends (PC), polyethersulfone (PES), polyacrylonitrile (PAN), and cuprophan (CUP), and can have MWCO ranging from 5 kDa to 100 kDa. Due to its manufacturing process, porous hollow fiber membranes are made up of a range of pore sizes and its pore size distribution can be wide or narrow. The manufacturers typically define MWCO as the absolute maximum molecular weight by which anything greater is rejected but only a small fraction of molecules at or near that molecular weight will pass through (typically significantly less than 1%). As another example, a 10 kDa protein crossing a commercial 100 kDa MWCO membrane at a perfusion flowrate of 1 μl/min typically has a relative recovery below 5% [66], where relative recovery is simplified to be defined as the ratio of concentration "recovered" at the perfusion outlet to the concentration at the target site. A more in-depth explanation of this term is given in the next section.

A common problem associated with large MWCO membranes during microdialysis is ultrafiltration. Ultrafiltration occurs when the perfusate side of the

membrane is over-pressured, driving a convective flow of perfusion fluid through the pores and out of the probe. This is seen more commonly in large MWCO because of the inherently lower hydraulic resistance in the pores. If observed, the perfusion flow rate should be decreased since ultrafiltration dilutes analyte concentration in the tissue.

A membrane's MWCO cannot be relied upon as a good predictor for recovery performance during microdialysis [67]. The interaction between membrane material ("chemistry") and a particular analyte can also affect performance. For example, hydrophobic analytes are difficult to recover [68, 69], with little exception [65], and negatively charged analytes are typically rejected by negatively charged membrane materials such as polyacrylonitrile [70].

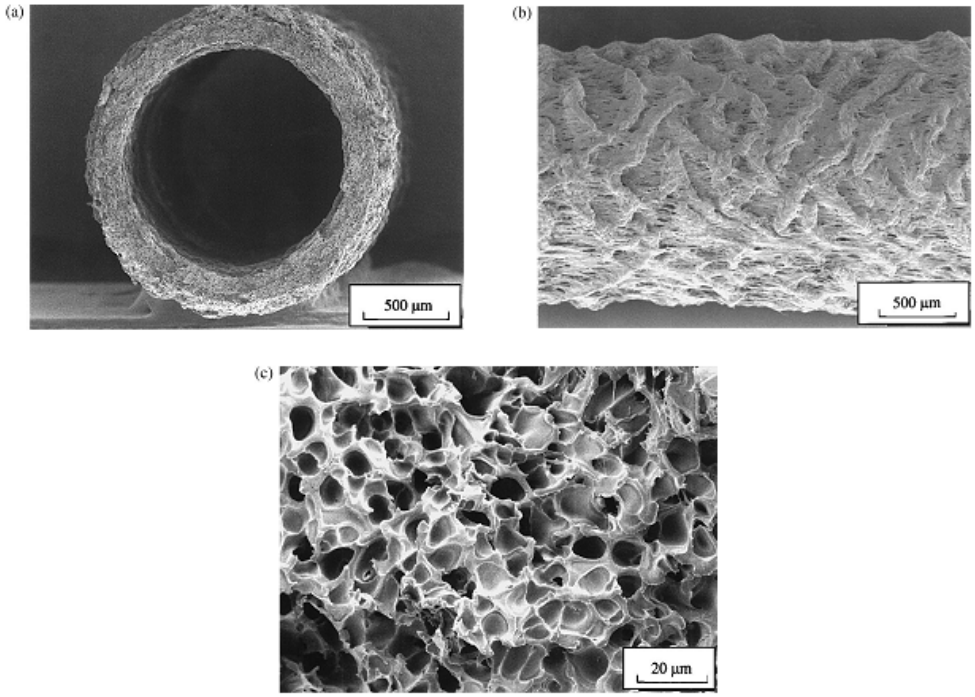

Figure 2.D: Scanning electron micrographs of a polycarbonate hollow fiber: (a) cross-sectional view; (b) outer surface; (c) cross-section under higher magnification. [71]

2.3.3 Quantitative Microdialysis Models

The microdialysis extraction fraction, E_d, or relative recovery, of a probe-styled microdialysis setup is defined as:

$$\text{Recovery} = E_d = \frac{C_{out} - C_{in}}{C_{\infty} - C_{in}} \qquad \text{Equation 2.1}$$

where C_{in}, C_{out}, and C_{∞} are the concentrations for the analyte of interest in the inflow perfusate, outflow dialysate, and the tissue/fluid surrounding the probe, respectively. The perfusate flowing into the probe is normally devoid of the analyte of interest (C_{in} equals zero) and thus the equation can be simplified to:

$$\text{Recovery} = E_d = \frac{C_{out}}{C_{\infty}} \qquad \text{Equation 2.2}$$

In other words, the recovery term is a measure of how efficient the microdialysis probe (perfusate) is able to represent the analyte concentration in the tissue or solution.

Bungay et al. developed a steady-state mathematical model [72, 73] to calculate the expected microdialysis extraction fraction, E_d, from a constant concentration stationary ECF, given by:

$$E_d = \frac{C_{out} - C_{in}}{C_{\infty} - C_{in}} = 1 - \exp\left[-\frac{1}{Q_d (R_d + R_m + R_e)} \right] \qquad \text{Equation 2.3}$$

where Q_d is the perfusion flow rate and R_d, R_m, and R_e are the dialysate, membrane, and external medium resistances, respectively. Analytes sequentially diffuse across a region of the external medium, then the membrane, and finally through to the dialysate in order to exit the microdialysis probe. Since these resistances are in series and mass transfer flow is conserved (i.e. equivalent) across the three regions, the resistances are additive. Eq. 2.3 assumes that the transmembrane pressure is sufficiently small and that there is no

convective fluid flow through the membrane; that is, mass transport is primarily due to diffusion across a concentration gradient [13].

Jacobson et al. developed an empirical model [74] that related microdialysis extraction with the perfusion flowrate, active area of the membrane, and the mass transfer coefficient. The resulting equation is:

$$\frac{C_{out}}{C_{\infty}} = 1 - \exp(-K_0 A / Q_d) \qquad \text{Equation 2.4}$$

where K_0 is the analyte-specific mass transfer coefficient for the membrane, A is the active area of the microdialysis membrane, and the remaining terms are described previously. Extrapolating this equation to the case of zero flowrate reveals that C_{out} is expected to equal C_{∞}, i.e., resulting in full recovery of the analyte. The product ($-K_0A$) is equivalent to resistance terms, $1/(R_d + R_m + R_e)$, from Eq. 2.3, and the entire expression is equivalent to Bungay's expression for E_d in Eq. 2.3. Jacobson's group realized that different amino acids, even with similar molecular weights, exhibited different *in vivo* mass transport coefficients. Therefore, for most cases, K_0 values must be determined experimentally for each analyte-membrane combination.

2.3.4 Calibration Techniques

Obtaining the true interstitial concentration of an analyte (i.e. 100% extraction efficiency) via microdialysis is difficult with today's microdialysis probes, as it requires the perfusion flowrate to be extremely low. Typical sampling flowrates range between 0.5 and 2.0 µl/min [63] and even then, the dialysate will typically have an E_d of less than 30% at 0.5 µl/min and less than 20% at 1.0 µl/min for *in vitro* recovery of cytokines [75].

Operating at even lower flowrates increases the sample collection time significantly, since there is always some minimum volume of sample required for analysis. Calibration techniques allow for a more practical means of estimating what the true ECF concentration is. Several approaches exist to approximate the true concentration, each with their own limitations.

2.3.4.1 Flowrate Method

Jacobson et al. developed a calibration technique [74] known as the flowrate method, or the mass transfer method, where the perfusion flowrate is decreased gradually while changes in the dialysate concentrations are measured. At low flowrates, the change in dialysate concentration plateaus. By applying appropriate nonlinear regression analysis on this data, the concentration can be extrapolated for the zero flowrate condition, which can be approximated to be the true tissue concentration value. However, this method is not very accurate. Accuracy improves as lower and lower flowrates are used but this incurs the problem of long collection periods as described earlier.

2.3.4.2 No-net flux Method

Unlike the previous method which uses analyte-free perfusate, another method for calibrating the microdialysis probe involves perfusing known concentrations of the analyte of interest into the probe at a specific flowrate and then measuring the dialysate concentration that comes out (i.e. measuring before and after dialysis). This is known as the no-net flux method, or equilibrium dialysis, and was first conceived by Lonnroth et al

in 1987 [76]. The left hand side of Eq. 2.3 is assumed to be an unknown value P since neither the perfusion flowrate nor the resistances change. Thus it can be rearranged as

$$C_{out} - C_{in} = -P\left(C_{in} - C_{\infty}\right) \qquad \text{Equation 2.5}$$

where P is the proportion of analyte transport to and from the probe. The net difference between the dialysate concentration and perfusate concentration (C_{out} - C_{in}) is plotted as a function of varying perfusate concentrations (Fig. 2.8). Then, a simple linear regression analysis is performed. Whether the analyte ultimately diffuses into or out of the probe is assumed to be solely due to the concentration gradient between what is added to the perfusate and the tissue concentration itself. Theoretically, when the net difference (C_{out} - C_{in}) is zero, it implies that the perfusate concentration is equal to the tissue concentration, which is represented by x-intercept of the plot. This data from this technique is relatively simple to analyze and does not necessarily require the use of slow perfusion flowrates [73, 77].

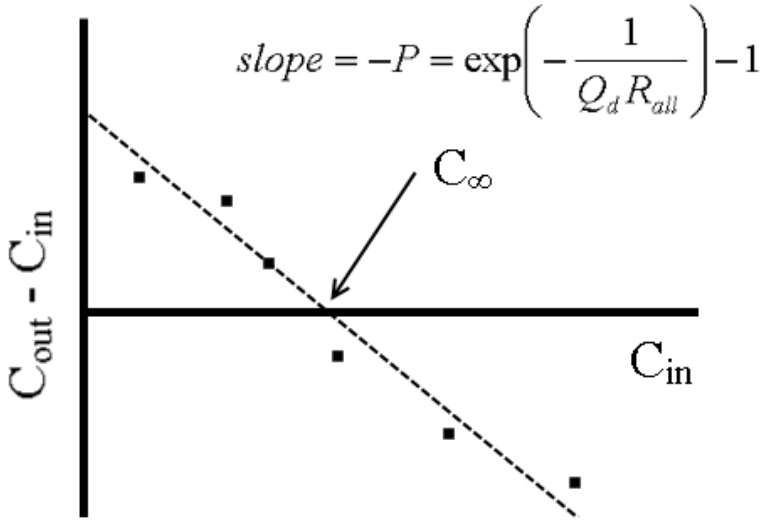

Figure 2.E: No-net flux method. Net difference between the dialysate and perfusate concentrations plotted against varying perfusate inlet concentration. The x-intercept represents where the perfusate concentration is equal to the tissue concentration. [67]

2.3.4.3 Retrodialysis

The retrodialysis technique determines E_d by measuring the loss of an analyte from the perfusate [78, 79]. The perfusate is doped with an analyte of known concentration of at least ten times that of the tissue concentration surrounding the probe [67]. For this method, it is necessary to dope the perfusate with an analyte that has very similar diffusion characteristics as the analyte of interest. Usually, a radiolabled version of the analyte of interest is used. High concentrations in the perfusate are required to ensure that the radio-labeled analyte crossing the membrane (from perfusate-side to tissue-side) is not limited by the concentration of unlabeled analyte (on the tissue-side), regardless of the concentration on the tissue side of the membrane [77]. By this assumption, C_∞ is negligible compared to the known C_{in} and the extraction fraction can be determined by

$$E_d = \frac{C_{in} - C_{out}}{C_{in}} \qquad \text{Equation 2.6}$$

However, extremely high concentrations of radiolabled analyte in the perfusate tend to make the membrane the diffusion-limiting site, and thus, should be avoided [80, 81].

2.3.5 Microdialysis on a Chip

Micrometer-scale total analysis systems (μTAS) are becoming more than just a novel research concept and beginning to be considered an important tool to improve global health. Also known as ‘lab-on-a-chip’ devices because of their likeness in size and similar fabrication processes with computer microprocessors, they are used in diverse applications such as biochemical assays, polymerase chain reactions, and blood sample

separation. Some advantages that microdevices offer include smaller volumes of reagents and potentially hazardous wastes, reduced cost, portability, and speed of analysis. The broad field of microfluidics has seen incredible advances in the last 20 years [82] although the very first μTAS, a micro gas chromatograph, was developed at Stanford University in the 1970s [83]. In particular, microfluidic devices using membranes for mass transport control have been garnering increasing amounts of interest over the past 10 years, as illustrated in Fig. 2.9. Some μTAS applications involving membranes include separation, purification, sample pre-treatment, and dialysis [84].

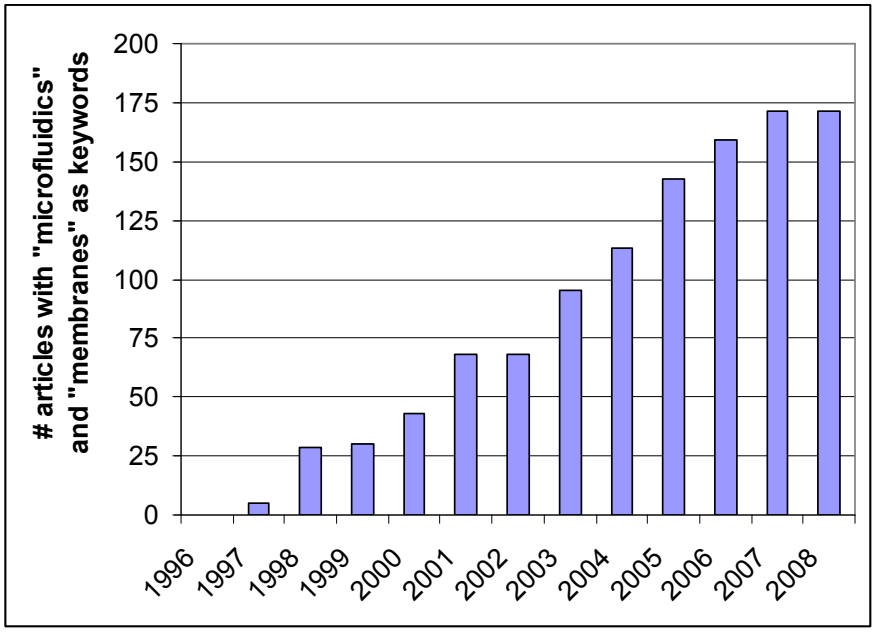

Figure 2.F: Graph showing an increasing interest in the microfluidics and membranes field over the last 12 years. [Source: Rutgers University Libraries Searchlight, with keywords: "microfluidics" and "membranes"]

2.3.5.1 Methods for integrating membranes into devices

There are several basic fabrication techniques to incorporate membranes into μTAS devices: membrane preparation during chip fabrication process, *in situ* preparation of membranes, and directly incorporating (commercial) membranes. Each method offers a series of advantages and disadvantages; ultimately, the decision depends on one's priorities for cost, ease of fabrication, MWCO control, and chemical compatibility.

One approach is to fabricate the membrane during the fabrication process of the chip. That is, the pores are created directly on the microfluidic chip itself. Many semiconductor microfabrication techniques are available to create pores in silicon wafers such as electrochemical etching [85], back etching [86], and ion beam track etching [87]. Some major advantages with using clean room technology include: using well established and understood semiconductor processes, excellent control of feature size (to the order of tens of nanometers), ability to make tailor-made structures, and avoiding sealing issues altogether. In fact, in most cases, there is no sealing process because the membrane is created as part of the chip substrate itself [84]. However, just like most other uses of semiconductor technologies, the production process is complex and expensive.

Another approach for integrating membranes is to fabricate them *in situ* on a pre-made microfluidic chip. Several variations for this method exist but usually involve selective polymerization. Polymerization of acrylate monomers occurs via UV light exposure, where the position and thickness of the membrane can be controlled simply by controlling where UV light hits [88]. Non-polymerized monomers are washed out afterwards. MWCO properties can vary depending on the ratio of monomer and cross-linking agent used, but ultimately requires trial and error experiments and educated

guesses for tailored specifications. The range of applicable materials is also very limited. Membranes can also form via interfacial polymerization at the interface between two solutions, as demonstrated by Kitamori et al. [89]. In this case, a thin polyamide membrane was created at the interface of an organic and an aqueous solution, both containing a certain monomer that reacts via a poly-condensation reaction to form. Again, there is only a limited range of membrane materials.

Lastly, in-house or commercial membranes can be directly incorporated into microfluidic devices by clamping or gluing the membrane between two microfluidic chips; it is also the most straight-forward of the options. Commercial membranes are sold as flat sheets and come in varying materials, sizes, and MWCOs and may undergo surface modification to functionalize the membrane with trypsin [90] or bovine serum albumin [91], for example. The clamping method offers flexible configurations because it is possible to swap in/out different types of membranes depending on the application. However, creating a good seal can be difficult. When clamping hard substrates such as silicon and glass, the two surfaces that contact the membrane must have a high degree of flatness and even pressure must be applied to prevent leaking. Also, capillary forces can cause glue to get sucked into and block microfluidic channels and membrane pores.

In this thesis, a microdialysis chip intended for continuous dialysis of blood proteins during cardiopulmonary bypass procedures is presented. The device sandwiches a commercial membrane between two microfluidic chips and bonded with epoxy for cost savings and ease of manufacturability. The microdialysis chip is designed with high throughput, extraction efficiency, and robustness in mind.

Chapter 3 - On-chip Microdialysis System

In this chapter, a microdialysis chip is developed for continuous blood protein extraction for, but not limited to, CPB operations. The fabrication steps are based on semiconductor technology and soft lithography, both of which will be discussed in detail.

3.1 Theory

Fluid dynamics and mass transport theories are used to predict and explain the performance of the microdialysis device. Optimization of overall device performance remains a difficult task since the 'device performance' is actually made up of a multitude of factors. Changing an operating parameter one way may be favorable for one factor but adversely affect another factor.

3.1.1 Mass Transfer Prediction

In the proposed microdialysis chip, there are two flows separated by a semipermeable membrane (Fig. 3.1) and is intended for *in vitro* use. Blood flows through the reservoir channel while a saline solution flows through the perfusate channel. Analytes in the reservoir fluid are dialyzed across the membrane, into the perfusion fluid.

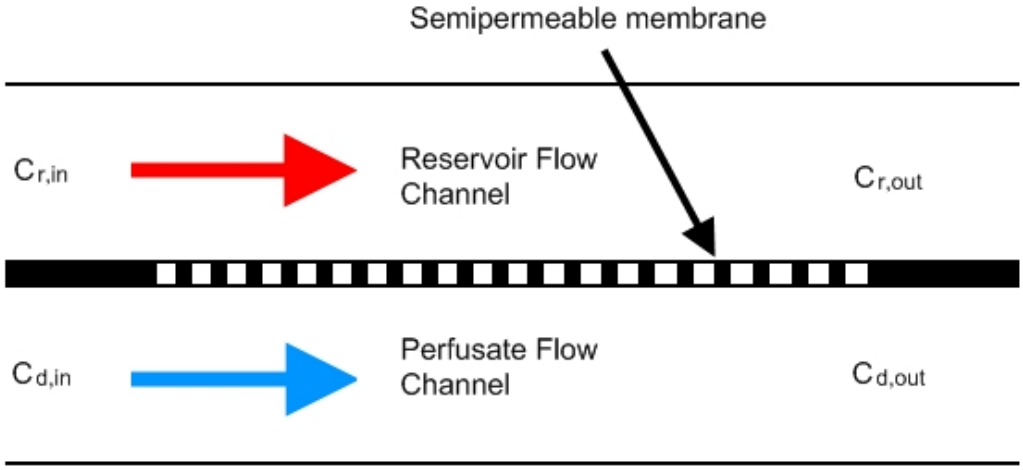

Figure 3. 1: A side-view diagram showing the layer reservoir channels and the layer of perfusion channels on opposite sides of a porous membrane [13]

The mass transfer coefficient, K_0, is assumed to be constant over the diffusion path and over time. The convective mass flux across the reservoir channel is given by

$$d\dot{m} = -Q_r dC_r \qquad \text{Equation 3.1}$$

where Q_r is the flowrate through the reservoir channel and C_r is the analyte concentration in the reservoir solution. Rearranging Eq. 3.1 yields

$$dC_r = -\frac{d\dot{m}}{Q_r} \qquad \text{Equation 3.2}$$

The convective mass flux of the perfusate is given by

$$d\dot{m} = -Q_d dC_d \qquad \text{Equation 3.3}$$

and another rearrangement yields

$$dC_d = -\frac{d\dot{m}}{Q_d} \qquad \text{Equation 3.4}$$

where Q_d is the flowrate through the perfusion channel and C_d is the analyte concentration in the perfusate solution.

The mass flux across the membrane can also be given as

$$d\dot{m} = K_0\left(C_r - C_d\right)dA \qquad \text{Equation 3.5}$$

where K_0 is the membrane's overall mass transfer coefficient (also referred to as the membrane's molecular permeability) and A is the diffusional area. By subtracting Eq. 3.4 from Eq. 3.2,

$$dC_r - dC_d = -\frac{d\dot{m}}{Q_r} - \frac{d\dot{m}}{Q_d} = -d\dot{m}\left(\frac{1}{Q_r} + \frac{1}{Q_d}\right) \qquad \text{Equation 3.6}$$

By substituting Eq. 3.5 into Eq. 3.6,

$$d\left(C_r - C_d\right) = -K_0\left(C_r - C_d\right)\left(\frac{1}{Q_r} + \frac{1}{Q_d}\right)dA \qquad \text{Equation 3.7}$$

Eq. 3.7 can then be rearranged into

$$\frac{d\left(C_r - C_d\right)}{\left(C_r - C_d\right)} = -K_0\left(\frac{1}{Q_r} + \frac{1}{Q_d}\right)dA \qquad \text{Equation 3.8}$$

By integrating Eq. 3.8 along the membrane diffusional area, A_m

$$\ln\frac{C_{r,out} - C_{d,out}}{C_{r,in} - C_{d,in}} = -K_0 A_m\left(\frac{1}{Q_r} + \frac{1}{Q_d}\right) \qquad \text{Equation 3.9}$$

where $C_{r,out}$ and $C_{r,in}$ are the outlet and inlet concentrations of the reservoir channel. $C_{d,out}$ and $C_{d,in}$ are the outlet and inlet concentrations of the perfusion channel. A_m is the diffusional surface area. Q_r and Q_d are the flowrates through the reservoir and dialysate channels. $C_{d,in}$ is always zero for this work; that is, a saline solution, free of the analyte of interest, enters the perfusion channel of the device. $C_{r,in}$ and $C_{r,out}$ are assumed to be equals since the reservoir flowrate, Q_r, is much greater than the perfusion flowrate, Q_d. In

other words, the amount of analytes diffusing out of the reservoir solution is negligible because it is constantly being replenished with more reservoir solution. Also, because Q_r is much greater than Q_d, the fraction $1/Q_r$ in Eq. 3.9 can be ignored. Therefore, Eq. 3.9 is simplified to

$$\ln\left(1-\frac{C_{out}}{C_{\infty}}\right)=-K_0 A_m\left(\frac{1}{Q}\right) \qquad \text{Equation 3.10}$$

where C_{out} is the dialysate concentration, C_{∞} is the reservoir concentration, and Q is the perfusion flowrate. Eq. 3.10 can be rearranged to represent the extraction efficiency (also known as "relative recovery") as a function of perfusion flowrate

$$E_d=\frac{C_{out}}{C_{\infty}}=1-e^{-\frac{K_0 A_m}{Q}} \qquad \text{Equation 3.11}$$

where a high extraction efficiency is achieved when $(K_0 A_m) >> Q$.

3.1.2 Fluid Pressure and Resistance

Balancing the hydraulic pressures in the dual-compartment microdialysis system is important to ensure that diffusion is the primary mode of mass/analyte transport, instead of convection. If the hydraulic pressure in the reservoir channel is much greater than that of the perfusion channel, the dialysate concentration will increase by having blood plasma cross the membrane and enter the perfusion channel. However, this may also cause large particles in the reservoir solution, mainly blood cells, to become lodged or lyse as it tries to squeeze into the pores. On the other hand, if the hydraulic pressure in the perfusion channel is much greater than that of the reservoir channel, perfusate may

flow across the membrane, thereby diluting the reservoir solution and reducing the dialysate sample volume.

The pressure drop for a viscous incompressible fluid flowing through a constant cross-section is a function of the channel geometry and flowrate, which is given by,

$$\Delta P = QR \qquad \text{Equation 3.12}$$

where ΔP is the pressure drop, Q is the fluid flowrate, and R is the geometric resistance term.

For a rectangular channel, the resistance term is given by

$$R_{rect} = \frac{12\mu L}{WH^3}\left[1 - \frac{H}{W}\left(\frac{192}{\pi^5}\sum_{n=1,3,5,\ldots}^{\infty}\frac{1}{n^5}\tanh\left(\frac{n\pi W}{2H}\right)\right)\right]^{-1} \qquad \text{Equation 3.13}$$

where μ is the fluid dynamic viscosity, L is the length of the channel, W is the length of the long edge of the channel cross-section, and H is the length of the short edge of the channel cross-section. For square, channels, W and H are equivalent.

For a circular channel, such as the cylindrical pores of the membranes or tubing, the resistance term is given by

$$R_{circ} = \frac{8\mu L}{\pi r^4} \qquad \text{Equation 3.14}$$

where r is the radius of the channel and L is the thickness of the membrane or length of tubing.

3.2 Device Design and Fabrication

The microdialysis chip made up of three main components: a polydimethylsiloxane (PDMS) layer for the reservoir channel, another PDMS layer for the perfusion channel, and a polymer track-etch membrane (with either 100 or 400 nm diameter pores) bonded in between (Fig. 3.2). The design and fabrication protocol created for this thesis are a result of a series of many developmental iterations.

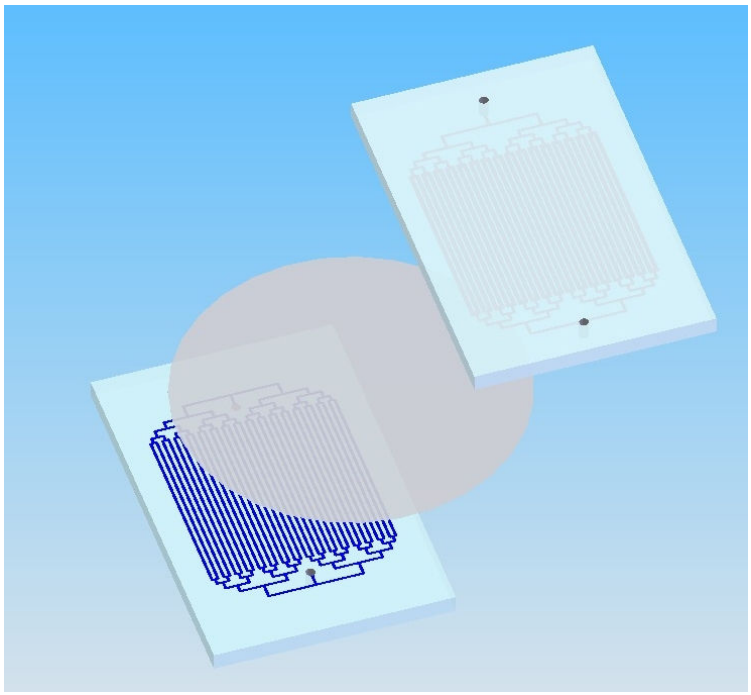

Figure 3.2: Exploded view of the three main components (right to left): PDMS layer for the reservoir channel, a thin polymer membrane, and a PDMS layer for the perfusion channel.

3.2.1 General Design Considerations

According to Eq. 3.11, maximizing the diffusion area increases the extraction efficiency. It is also important to consider the size of the overall device for ease of manufacturing and to maintain the μTAS form factor. Using these constraints, commercial track-etched membranes, 47 mm in diameter, were selected. The size of the

perfusion and reservoir channels were designed to maximize the diffusion area while fitting within the membrane's perimeter.

Instead of using a single-channel design, where the one channel would be several millimeters wide, a multiple parallel-channel design has two main advantages: 1) increased rigidity of the device, which is important because PDMS is very soft and flexible, and 2) provides structural support for the fragile, thin membrane (~10 μm thick). However, one must also consider the adverse affects of reducing channel width for the sake of having multiple parallel channels, such as increasing hydraulic resistance and shear stress. Since the perfusion flow is driven by a syringe pump, i.e. flowrate-controlled, a large hydraulic resistance increases the pressure drop in the channel and increases the chance for PDMS-membrane delamination. Also, high shear stresses are known to cause cell lysis as well as platelet activation.

To ensure consistent and repeatable results from the microdialysis chip, the perfusion channel and reservoir channel PDMS layers must be properly aligned with respect to one another, so that the diffusion area does not vary from one produced device to another (Fig. 3.3). The diffusion area is defined as areas where the perfusion channels and reservoir channels overlap. Since each channel is only several hundred microns wide, extra care must be taken in the alignment and bonding process. Small lateral misalignments and/or rotational misalignments can reduce the diffusion area quite drastically.

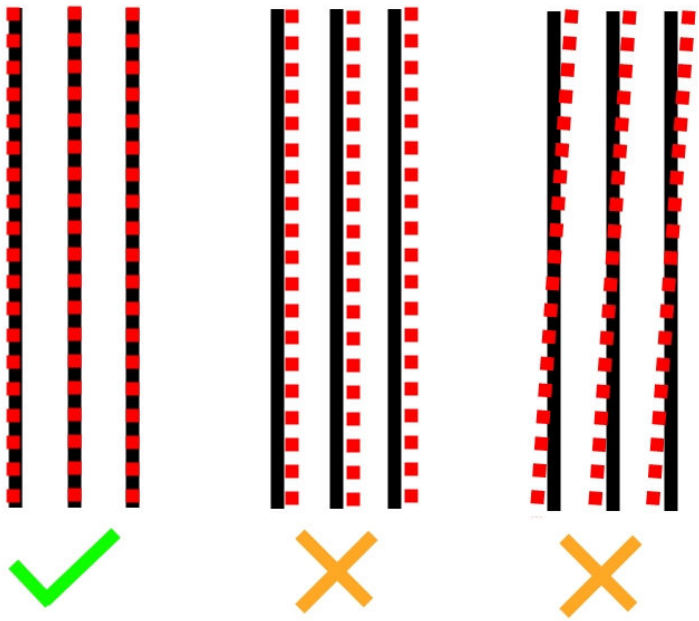

Figure 3.3: Demonstrating how improperly aligned channels can affect the diffusion area. Solid lines represent one layer of parallel channels and the dotted lines represent the other layer. Left: proper alignment results in full overlap. Center: even a small lateral shift can result in no overlap. Right: a small rotational shift can also reduce overlap areas.

To overcome this problem, the reservoir channels are designed to be slightly wider than the perfusion channels, making the alignment and bonding process more forgiving. There are several advantages for making the reservoir channel width wider than the perfusion channel: 1) the reservoir solution, blood, is sensitive to high shear stresses, which is reduced by widening the channel, 2) the reservoir flowrate can increase to further satisfy the $Q_r >> Q_d$ assumption in Eq. 3.10, and 3) if the perfusion channel is wider than the reservoir channel, diffusion becomes limited by the reservoir channel's width.

3.2.1.1 First design: no bifurcation

The first channel design consisted of a short inlet channel that led directly to a series of parallel channels. A computational fluid dynamics (CFD) analysis (COMSOL Inc., Burlington, MA) showed that the flow velocity is highest in the center channels and quickly decreases for channels farther away, as shown the velocity field contour plot in Fig. 3.4, where red denotes high velocity and blue denotes low velocity. Predicting device performance is made difficult by not having uniform flowrates among the parallel channels. It is also not an efficient way of using the diffusion areas, since there is essentially no flow going through a majority of the channels farthest from the center. Hydraulic resistance is a function of the path length, as shown in Eq. 3.13. Since the outer channels in Figure 3.4 require a much longer detour to reach the outlet than the center channels, where it is essentially a straight path, the flowrates cannot be expected to be evenly distributed.

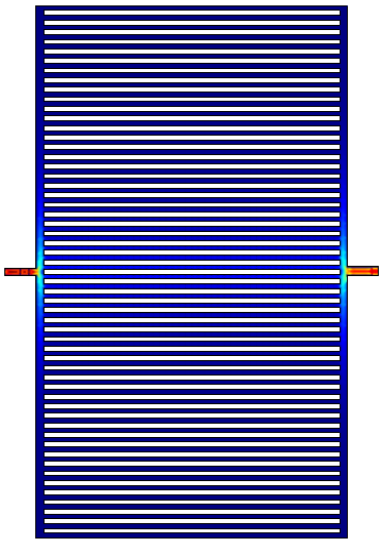

Figure 3.4G: CFD analysis of the non-bifurcating channel design. Fluid enters from the short channel on the left and exits on the right. Most of the flow goes through the center channels, while the outer channel have negligible flowrates.

3.2.1.2 Final Design: Bifurcating Tree

A bifurcating tree design is used to ensure that the flowrates in each of the parallel channels are equal, as seen in the CFD analysis in Fig. 3.5. At each bifurcation stage, the flowrate is divided equally into the next bifurcation stage. Inherent to the bifurcation design, there are 2^n channels, where n is the number of bifurcating stages. For this device, there are 32 channels (n = 5).

Although both the perfusion and reservoir layers use the bifurcating tree design, they are given a slightly different design from one another. Fig. 3.6 shows the two layers properly aligned, in such a way that the long channels in the center have maximum overlap areas. However, one can notice areas in the bifurcating tree sections where there are no overlap. This staggered design minimizes the amount of interaction, whether it's diffusion or convection, in areas that make theoretical calculations more difficult.

Although minimized, it is impossible to avoid all overlap in the staggered areas without having to make drastic design and manufacturing changes.

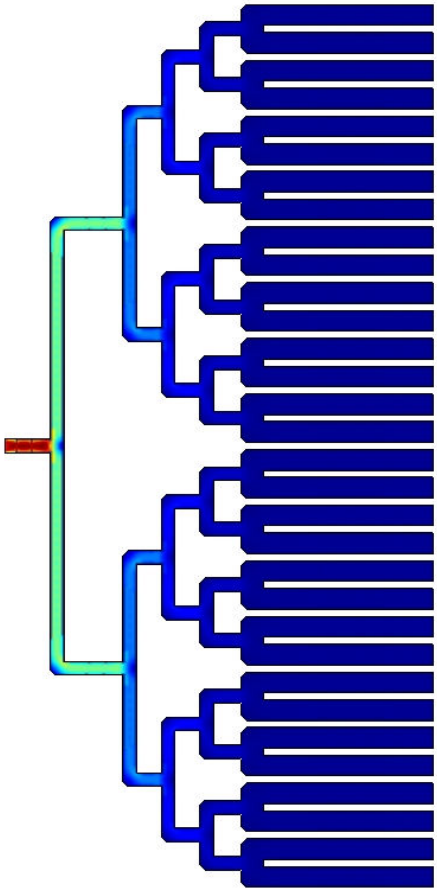

Figure 3.5: Bifurcating channel design: a CFD analysis showing a surface plot of the velocity field. Red denotes high velocity and blue denotes low velocity. At each bifurcation stage, the flowrate splits up equally. This is only a partial model due to computational constraints.

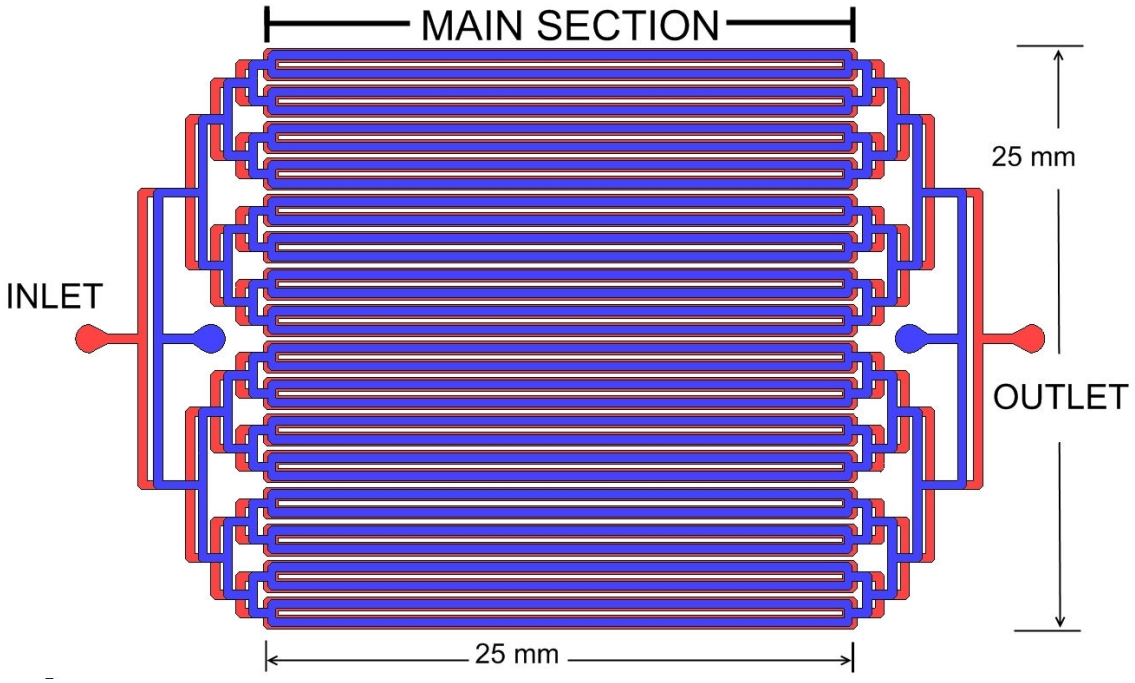

Figure 3.6: Stacked view of the perfusion layer (blue) aligned on top of the reservoir layer (red). The staggered design in the bifurcating tree section is intended to minimize interaction between the two layers, except for the main section in the center.

3.2.2 Photolithography and Soft Lithography

The microfluidic channels are created using photolithography and soft lithography techniques. SU-8 negative photoresist (MicroChem, Boston, MA) is a UV light-sensitive material used for its ability to create thick and high aspect ratio structures. When exposed to UV light, negative photoresist become insoluble to photoresist developer, whereas unexposed portions are dissolved by the developer. Using the dark field masks shown in Fig. 3.7 and a mask aligner (EVG620, EV Group, Austria), perfusion and reservoir structures were created on silicon wafers. The schematic of the procedure is shown in Fig. 3.8 and the full recipe is given in Tables 1 and 2.

The channels in the bifurcating trees for the perfusion and reservoir masks are 400μm wide. The widths of the main channel are 400 and 600 μm for the perfusion and

reservoir channels, respectively. The length of the main section is 25 mm long for both layers. The recipe in Table 1, using SU-8 2025, creates a layer of photoresist 30 µm thick while the recipe in Table 2, using SU-8 2150, creates a layer of photoresist 130 µm thick.

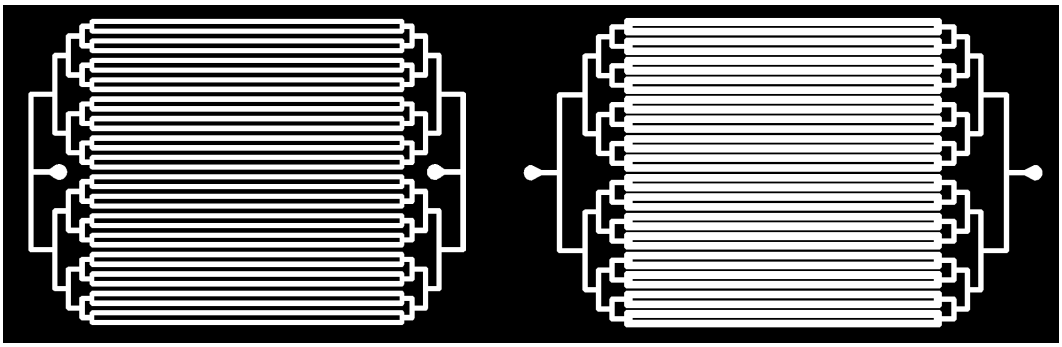

Figure 3.7H: Dark-field masks for photolithography. Left: Perfusion mask. Right: Reservoir mask.

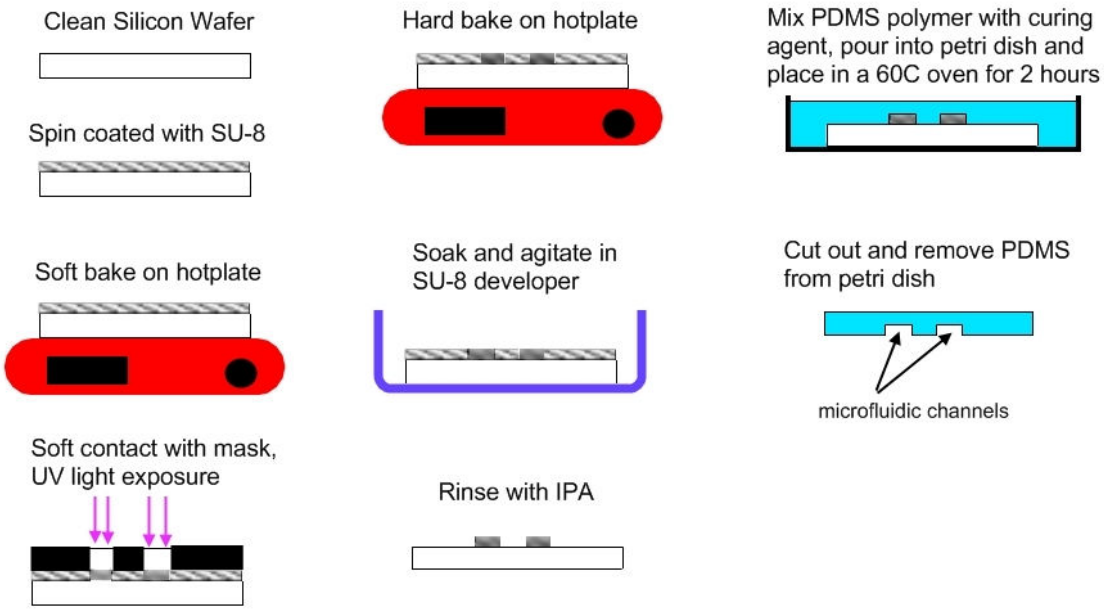

Figure 3.8: Soft-lithography steps used to create microfluidic channels in PDMS.

Table 1: Photolithography recipe for 30 micron thick Perfusion Channel

Perfusion Channel - 30 micron thickness			
#	**Step**	**Description**	**Time**
1	Cleaning Procedures	Soak silicon wafer in acetone solution	10 min
		Soak silicon wafer in isopropyl alcohol (IPA) solution	10 min
		Soak silicon wafer in deionized (DI) water	10 min
		Rinse under running DI water	1 min
		Blow dry with filtered nitrogen or filtered air	1 min
		Bake in vented oven at 200C	30 min
2	Spin Coating	SU-8 2025, 500 RPM for 5 sec @ accl. 100 RPM/sec, then 2875 RPM for 30 sec @ accl. 300 RPM/sec	---
3	Softbake	Place on hot plate at 65C	2 min
		Place on hot plate at 95C	5 min
4	Exposure	Set exposure dose to	300 mJ/cm^2
5	Post-exposure Bake	Place on hot plate at 65C	1 min
		Place on hot plate at 95C	3 min
6	Develop	Soak in SU-8 developer solution, agitate	5 min
7	Rinse	Rinse in IPA	---

Table 2: Photolithography recipe for 130 micron thick Reservoir Channel

Reservoir Channel - 130 micron thickness			
#	**Step**	**Description**	**Time**
1	Cleaning Procedures	Soak silicon wafer in acetone solution	10 min
		Soak silicon wafer in isopropyl alcohol (IPA) solution	10 min
		Soak silicon wafer in deionized (DI) water	10 min
		Rinse under running DI water	1 min
		Blow dry with filtered nitrogen or filtered air	1 min
		Bake in vented oven at 200C	30 min
2	Spin Coating	SU-8 2150, 500 RPM for 10 sec @ accl. 100 RPM/sec, then 3000 RPM for 30 sec @ accl. 300 RPM/sec	---
3	Softbake	Place on hot plate at 65C	6 min
		Place on hot plate at 95C	37 min
4	Exposure	Set exposure dose to	250 mJ/cm^2
5	Post-exposure Bake	Place on hot plate at 65C	5 min
		Place on hot plate at 95C	13 min
6	Develop	Soak in SU-8 developer solution, agitate	16 min
7	Rinse	Rinse in IPA	---

The photolithography step creates the "master," a negative mold comprised of photoresist on a silicon wafer from which many PDMS molds can be made from [92]. The master is placed inside a petri dish, with the photoresist-side facing up. PDMS (Dow Corning Sylgard 184, Dow Corning, Midland, MI) molds are created by mixing the base and curing agent at a ratio of 10:1 by mass, then pouring the mixture into the petri dish. This can then be allowed to cure at room temperature overnight or in a 60^0C oven for 2 hours to solidify. Cured PDMS is cut and peeled from the master mold and inlet/outlet access holes are punched out with an 18G flat-tipped needle so that Intramedic PE-10 polyethylene tubing (Becton Dickinson, Franklin Lakes, NJ) can be inserted with a snug fit. Once the tubing is inserted, a fast-curing sealant is applied around the base of the tubing to prevent leakage and accidental removal.

3.2.3 Bonding to membrane

The bonding portion of the production process is the most critical, yet most difficult, step. Several experiments were performed to find the most effective bonding method between the polycarbonate (PC) track-etched membrane (Fig. 3.9) and PDMS pieces. No method can be declared a decisive winner because each offers benefits as well as drawbacks.

3.2.3.1 Thermal

Putting the two materials together and placing it in a 160^0C to 180^0C oven for 5 or more hours resulted in a very strong, non-reversible bond. Unfortunately, extreme wrinkling of the membrane was observed after the bonded device is removed from the

oven. Membrane wrinkling is one of the main manufacturing problems because it typically leads to partial or complete blockage of the channels, rendering the entire device unusable. As the temperatures of the PDMS layers and PC membrane rises in the oven, PDMS expands more than the membrane because of its larger thermal expansion coefficient. Eventually, this is followed by the two materials being permanently bonding to one another, at their disproportionately expanded state, once sufficient time and temperature has been reached. As a result, the membrane takes on a "wrinkled" appearance, creating peaks and valleys in the membrane, which are easily tall enough to partially or completely obstruct the 30 μm tall perfusion channels. Although making perfusion channels thicker than 30 μm can help with channel-blockage issues, that change would also lower the extraction efficiency of the device by increasing the diffusion length, thereby increasing the residence time the perfusate would require to reach equilibrium with the reservoir channel concentration.

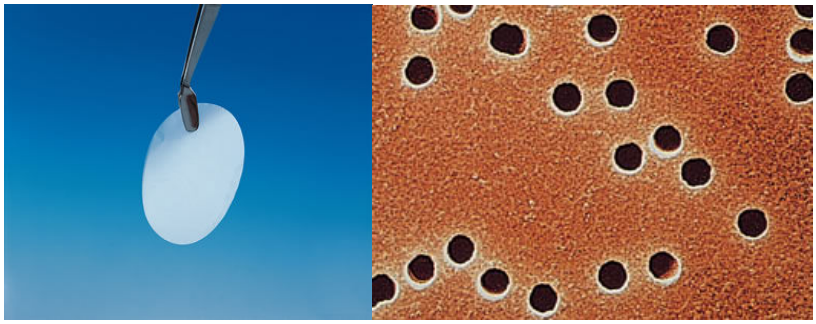

Figure 3.9: Commercial track-etched membranes. Left: a circular membrane, 47 mm in diameter, held by a tweezer. Right: an SEM image of the cylindrical pores on the membrane. [93]

3.2.3.2 Thin film deposition

Although Whitesides et al. were able to irreversibly bond PDMS to materials such as itself, glass, silicon, polyethylene, and polystyrene by simply exposing the surfaces to oxygen plasma and bringing the surfaces into contact, it failed to work for materials such as polyimide, PMMA, and polycarbonate [92]. Cremer et al. were able to produce an irreversible bond between a thin film of titanium dioxide and PDMS by using Whitesides' oxygen plasma method.

Utilizing the works of Whitesides and Cremer, experiments were performed to see if the PC membranes could first be coated with a thin film of titanium dioxide and then bond it to PDMS, as Cremer had done in a similar manner. A thin film of pure titanium was sputtered onto a PC membrane via magnetron DC sputtering (PVD75, Lesker, Clairton, PA). Titanium oxidizes into titanium dioxide on its own when exposed to air, but surface treating it with oxygen plasma also helps. Freshly cured PDMS and titanium dioxide-coated PC membranes were treated with oxygen plasma using a variety of power and time settings to find an optimal recipe. Once the membrane contacted PDMS, it was left at room temperature over night with weights laying on top. These experiments produced moderate to excellent bonding strength, similar to that of the thermal bonding method but without the wrinkling issues. However, the bond disappears once the membrane is exposed to water. Currently, it is not clear if the bond fails between PDMS and titanium dioxide or between titanium dioxide and polycarbonate, but further research into this method may find a way to overcome the water issue.

3.2.3.3 Epoxy Stamping

Of the methods mentioned thus far, the most effective method for bonding membranes (where, in this case, "bonding" is referred to in the mechanical sense) to PDMS is by using a biocompatible epoxy (Epo-Tek 301, EpoTek, Billerica, MA) as an intermediate layer between PDMS and the membrane [94]. A major advantage for using a "mortar" (e.g. glue, PDMS, or even brick mortar) to join surfaces together is that it is forgiving for rough and imperfect surfaces, such as that found on a porous membrane. Assuming the epoxy is capable of filling the micro-sized pores of the membrane, part of its adhesive capability may be due to the bonding of epoxy on one end of a pore, to the epoxy on the other end; thereby, interlocking the membrane. Because the microfluidic channels embedded into the PDMS layer are only 30 μm and 130 μm thick for the perfusion and reservoir channels, respectively, steps must be taken to prevent epoxy from getting into the channels and causing partial or complete blockage. More importantly, excess epoxy can spread onto the diffusion areas of the membrane, clogging the pores. In addition to these problems, the strength of the bond is usually not very strong when only a thin layer of epoxy is used.

Stamping consists of placing the bonding side of both PDMS layers onto a thin layer of epoxy and joining the three layers together as shown in Fig. 3.10. Once joined, the device is given 24 hours to cure to achieve full bonding strength. The simplest and quickest method to create a thin layer of epoxy is to pour some epoxy onto a flat surface and use a flat edge to spread the epoxy until a uniform thin layer is achieved. Using a spin coating machine has the advantage of being able to create repeatable uniform thicknesses, unlike the manual method of spreading a thin layer by hand. However, spin

coating is best used for slow curing adhesives because the spinning process can completely drive off the solvent in epoxies before the bonding surfaces can come together. For this reason, uncured PDMS is preferred for its longer curing time but seems to suffer from a weaker bonding strength than epoxy.

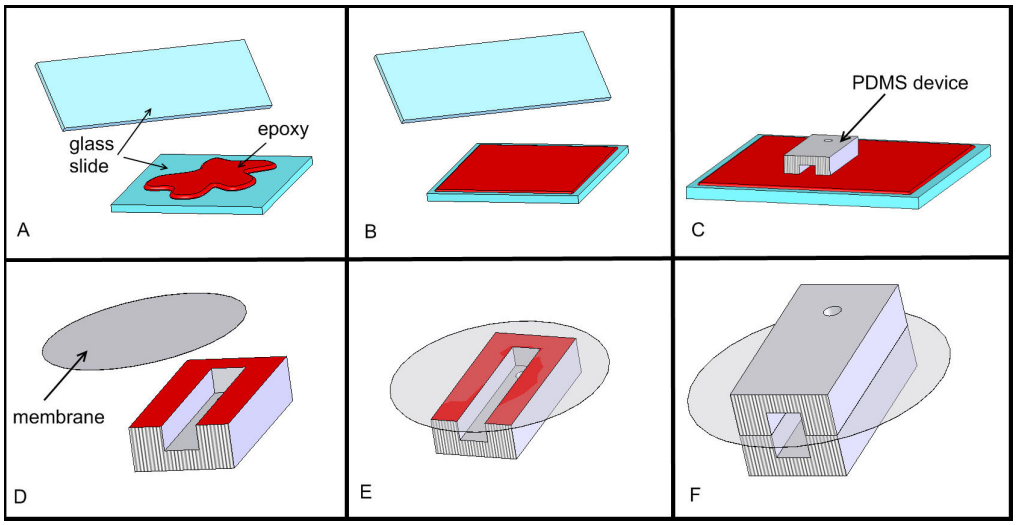

Figure 3.10: Schematic for the epoxy stamping procedure. A) a small amount of epoxy is placed on top of a clean glass slide; B) an object with a flat edge, such as another glass slide, is used as a squeegee on the epoxy until a thin, uniform layer of epoxy remains; C) the first PDMS layer is placed onto the thin layer of epoxy, with the channel side facing down; D) and E) a membrane is placed on top of the epoxy-side of the first PDMS layer; F) steps A-C are repeated for the second PDMS layer and aligned with the first layer under a dissection microscope.

3.3 Numerical Studies - Electric Circuit Model

In order to establish a starting baseline for channel geometry, membrane pore size, tubing length, and flowrate parameters, a Matlab program was written to solve a circuit diagram representing the experimental setup, as shown in Fig. 3.11. The objective was to determine a set of conditions for which diffusion of analytes across the membrane pores, from the reservoir channel to the perfusion channel, was the primary mode of

transport. In other words, convective flux was to be minimized and only in the direction of reservoir-to-perfusate, if it exists at all.

In the circuit diagram, there are two flowrate sources: 1) the reservoir fluid (blood) is driven by a pressure head generated by the CPB pump, represented by a voltage source and 2) the perfusate (lactated Ringer's solution) is driven by a syringe pump at a specific flowrate, represented by a current source. The reservoir source undergoes its first pressure drop due to the resistance in the reservoir channel's inlet tubing. Comparatively, the perfusion source is not followed by a resistor for the perfusion channel's inlet tubing since it is driven by a current source and its pressure drop does not affect the rest of the circuit. The two nodal points on either side of the pore resistor represent the pressure difference that determines the flowrate through the membrane pores. An assumption is made that the pressure at the reservoir node is always greater than or equal to the pressure at the perfusate node. Under this assumption, the perfusate should not be able to enter the reservoir channel, which would dilute the reservoir solution. This assumption is also necessary to provide enough known variables to solve the set of linear equations described below; otherwise, since the pore's resistance can either be a function of the blood plasma's viscosity or the Ringer's solution's viscosity, depending on which direction fluid travels. This assumption can be verified by solving for the entire circuit and checking to see if the reservoir node pressure is greater than or equal to the perfusate node pressure, if not, that particular solution is invalid.

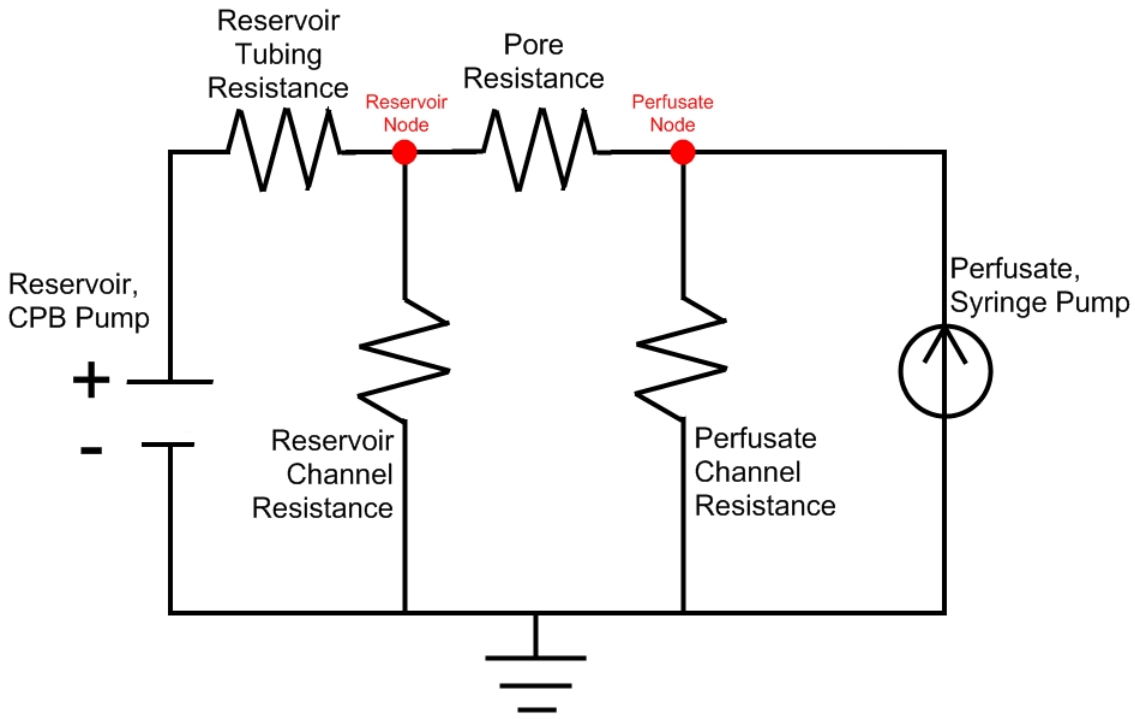

Figure 3.11: A circuit diagram representing the microdialysis chip. The reservoir side is given a voltage source to represent the pressure source given by the CPB pump. The perfusate side is given a current source to represent the predetermined flowrate put out by a syringe pump. Resistors represent hydrodynamic resistance, which is a function of channel geometry and fluid viscosity.

Since convective flow through the pores can occur throughout the entire length of the channel, the problem is simplified by dividing the pressure at the nodes in half when calculating flowrate through the pores, thereby representing the average pressure over the length of the channel. Finally, the perfusate and reservoir solutions experience pressure drops due to their respective PDMS channels, where they eventually reach the end of the device and into collection tubes, which are at atmospheric pressure. Although there is tubing connected to the outlet ports of the device, this tubing is much shorter than the inlet tubing and assumed to have negligible resistance.

Using Kirchhoff's current law (KCL), which states that the sum of currents flowing into a nodal point is equal to the sum of currents flowing out of the nodal point, and Ohm's law,

$$\Delta V = IR_{elec} \qquad \text{Equation 3.15}$$

where ΔV is the voltage drop which is analogous to a pressure drop, I is the current which is analogous to flowrate, and R_{elec} is the electrical resistance which is analogous to the pressure drop equation in Eq. 3.12 if the solutions are assume to behave as Newtonian fluids..

At the 'Reservoir Node' (see circuit diagram in Fig. 3.11), applying KCL gives

$$0 = \frac{P_{CPB,source} - P_{Rsrv}}{R_{Tubing}} - \frac{P_{Rsrv}}{R_{Rsrv}} - Q_{pore} \qquad \text{Equation 3.16}$$

where $P_{CPB,source}$ is the pressure provided by the CPB circuit, P_{Rsrv} is the pressure at the reservoir node, R_{Tubing} is the resistance in the tubing leading from where the reservoir tubing connects with the CPB circuit to the reservoir-side of the device, R_{Rsrv} is the resistance through the reservoir channels, and Q_{pore} is the flowrate crossing the membrane.

At the 'Perfusate Node,' applying KCL gives

$$0 = Q_{Perf,source} + Q_{Pore} - \frac{P_{Perf}}{R_{Perf}} \qquad \text{Equation 3.17}$$

where $Q_{perf,source}$ is the syringe pump flowrate that is set by the user, P_{Perf} is the pressure at the perfusate node, and R_{Perf} is the resistance through the perfusate channels.

The flowrate through the membrane is given by applying the hydraulic equivalence of Ohm's law,

$$Q_{Pore} = \frac{1/2\left(P_{Rsrv} - P_{Perf}\right)}{R_{Pore}} \qquad \text{Equation 3.18}$$

where the "½" refers to taking the average pressure difference between the channels, as noted earlier.

For simplification, blood is assumed to be a non-Newtonian fluid in this analysis. The blood flowrate entering the reservoir channel is given by applying the hydraulic equivalence of Ohm's law,

$$Q_{Rsrv,source} = \frac{P_{CPB,source} - P_{Rsrv}}{R_{Tube}} \qquad \text{Equation 3.19}$$

The overall hydraulic resistance in the reservoir channel is given by applying Eq. 3.13,

$$R_{Rsrv} = \frac{12\mu L}{W_{Rsrv} {H_{Rsrv}}^3 N_{Chan}} \left[1 - \frac{H_{Rsrv}}{W_{Rsrv}} \left(\frac{192}{\pi^5} \sum_{n=1,3,5,\ldots}^{\infty} \frac{1}{n^5} \tanh\left(\frac{n\pi W_{Rsrv}}{2H_{Rsrv}}\right)\right)\right]^{-1} \qquad \text{Equation 3.20}$$

where μ_{Blood} is the dynamic viscosity of blood at 35°C, L is the length for both the perfusion and reservoir channels, W_{Rsrv} is the width of a single reservoir channel, H_{Rsrv} is the height of the reservoir channels, and N_{Chan} is the number of channels. Without the N_{Chan} term, the equation would only solve the resistance through a single channel.

The overall resistance in the perfusion channels is given by applying Eq. 3.13,

$$R_{Perf} = \frac{12\mu L}{W_{Perf} {H_{Perf}}^3 N_{Chan}} \left[1 - \frac{H_{Perf}}{W_{Perf}} \left(\frac{192}{\pi^5} \sum_{n=1,3,5,\ldots}^{\infty} \frac{1}{n^5} \tanh\left(\frac{n\pi W_{Perf}}{2H_{Perf}}\right)\right)\right]^{-1} \qquad \text{Equation 3.21}$$

where μ_{LRS} is the dynamic viscosity of lactated Ringer's solution at room temperature, W_{Perf} is the width of a single perfusion channel, and H_{Perf} is the height of the perfusion channel.

The overall resistance in the membrane pores is given by applying Eq. 3.14,

$$R_{Pore} = \frac{8\mu_{Plasma} T_{Membrane}}{\left[\pi\left(D_{Pore}/2\right)^4\right] N_{Pore}} \qquad \text{Equation 3.22}$$

where μ_{Plasma} is the dynamic viscosity of human blood plasma at 35°C, $T_{Membrane}$ is the thickness of the membrane, D_{Pore} is the pore diameter give in Table 3, and N_{Pore} is the number of pores available in the active diffusion area, A_m. The SEM image in Fig. 3.9 (right) shows that the pores can be approximated as straight, uniform tubes.

The number of pores is a function of the pore density and the available diffusion area given by the equation

$$N_{Pore} = \rho_{Pore} A_m = \rho_{Pore}\left(N_{Chan} W_{Perf} L\right) \qquad \text{Equation 3.23}$$

where ρ_{Pore} is the pore density which varies depending on the manufacturer's specifications (see Table 3). A_m is a function of the perfusion channel's width since the perfusion channels are purposely designed to be narrower than the reservoir channels, making perfusion widths the limiting factor.

The hydraulic resistance of the polyethylene tubing (Intramedeic PE-10, Becton Dickinson, Franklin Lakes, NJ) connected to the reservoir inlet is given by,

$$R_{Tubing} = \frac{8\mu_{Blood} L_{Rsrv,Tubing}}{\pi\left(D_{Tubing}/2\right)^4} \qquad \text{Equation 3.24}$$

where $L_{Rsrv,Tubing}$ is the length of the reservoir inlet tubing and D_{Tubing} is the inner diameter of the tubing.

Table 3: Whatman Nucleopore Polycarbonate Track-etched Membranes

Pore Size (micron)	Pore Density (pores/cm^2)	Membrane Thickness (micron)
0.05	6x10^8	6
0.08	6x10^8	6
0.1	3x10^8	6
0.2	3x10^8	10
0.4	1x10^8	10
0.6	3x10^7	10
0.8	3x10^7	9

3.3.1 Observing Trends from Matlab Code

Although the above equations are not used to calculate analyte extraction efficiency, in this case, microdialysis performance is judged in terms of the perfusion flowrate recovery (PFR). PFR is the ratio of the flowrate exiting the perfusion outlet to the perfusion flowrate going in, given as

$$PFR = \frac{PerfusionOutletFlowrate}{PerfusionInletFlowrate} = \frac{Q_{Perf,source} + Q_{Pore}}{Q_{Perf,source}} \times 100 \qquad \text{Equation 3.25}$$

where $Q_{Perf,source}$ is the perfusion flowrate that is set by the syringe pump, and Q_{Pore} is the additional flowrate from blood plasma crossing over the membrane to the perfusion channels due to some pressure differential. Under ideal conditions where there is no fluid flux across the membrane, PFR equals 100% since there is no Q_{Pore} contribution. If the hydraulic pressure of the reservoir channel is much greater than the pressure of the perfusion channel, extracellular fluid may cross the membrane and into the perfusion channel, i.e. PFR > 100%, affecting E_d. In the reverse situation, where the perfusion channel's hydraulic pressure is much greater than the reservoir channel's pressure, i.e. PFR < 100%, meaning lactated Ringer's solution crosses over to the reservoir channel,

which dilutes the analyte concentration in blood and affecting E_d as well.

In order to see how PFR is affected by operating parameters such as: CPB pressure, perfusate flowrate, reservoir inlet tube length, and membrane pore size/density; two parameters varied at a given time. Meanwhile, the remaining parameters are held at a nominal value. Since commercial membranes are used in the devices, the membrane pore size, pore density, and thickness are essentially non-customizable except for what is already available in the product line. Because of this limitation, membrane selection is important and will be used as the recurring variable in Fig. 3.12-3.14.

Fig. 3.12-3.14 show how small pore sized membranes have a very stable PFR close to 100% across the span of the x-axis, while large pore sized membranes are very sensitive to the x-axis parameter. Because the relationship between pore diameter and pore resistance is $R_{Pore} \propto \frac{1}{D_{Pore}^{\ 4}}$, the small pore sized membranes have such large resistances that, relative to larger pore sized membranes, the flow on one side of the membrane is less likely to be able to influence the flow on the opposite side. Pore density has less of an impact, compared to the pore diameter, on overall resistance due to its $R_{Pore} \propto \frac{1}{\rho_{Pore}}$ relationship (where ρ_{Pore} is the pore density), and is not referred to explicitly when describing the membrane. A stable PFR around 100% across a wide range of design and operating parameters is a quality that a robust device should have. It means the device can operate predictably under varying conditions. Unfortunately, it can also be an indication that the membrane's pore resistance is too high (i.e. a completely impermeable membrane would inherently always have a PFR of 100%). Therefore, a compromise must be made between device robustness and analyte permeability.

There is negligible difference in PFR, between the 0.08 µm and 0.1µm pore size membrane but a significant difference in PFR, between the 0.1 µm and 0.2 µm pore size membrane (Fig. 3.12-3.14). Since there are no intermediate pore sizes available from the manufacturer, the 0.1 µm membrane is a reasonable compromise between MWCO and robustness. Fig. 3.12 shows a linear relationship between PFR and CPB pressure, where the intersection point represents the chosen nominal value and large deviations from this value dramatically affects PFR outcome. Meanwhile Fig. 3.13 and 3.14 show an exponentially decaying relationships between PFR with respect to perfusion flowrate and reservoir tubing length, where low perfusion flowrates and short reservoir tubing lengths produce the largest deviations from 100% PFR. On the other hand, using high perfusion flowrates is not necessarily the solution since it will lower E_d as seen in Eq. 3.11 .

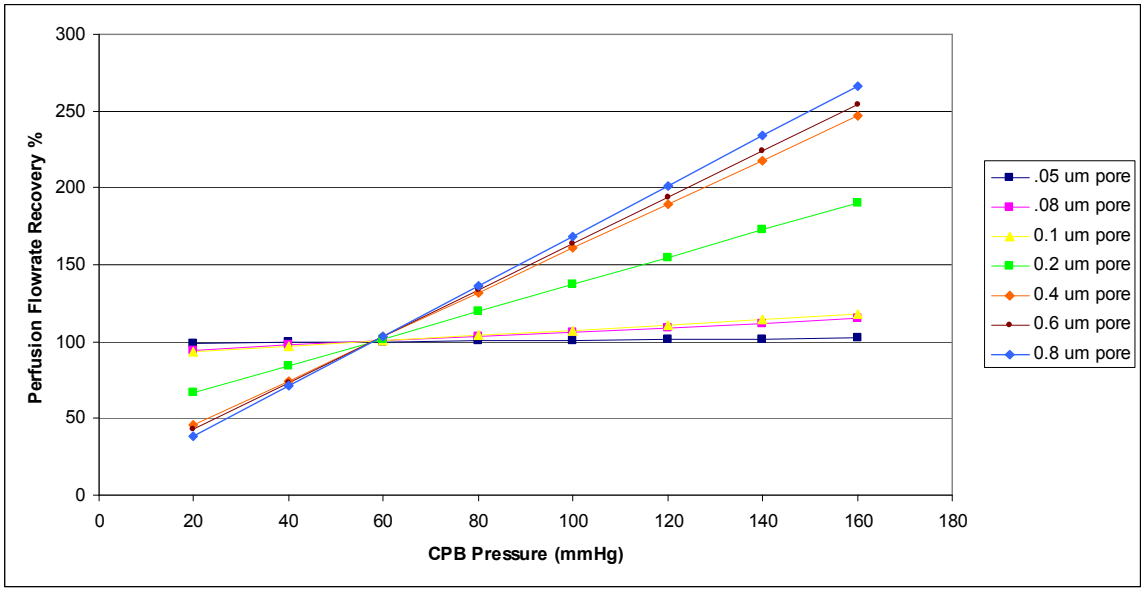

Figure 3.12: Results from Matlab model: Perfusion flowrate recovery vs CPB Pressure, for various pore sizes.

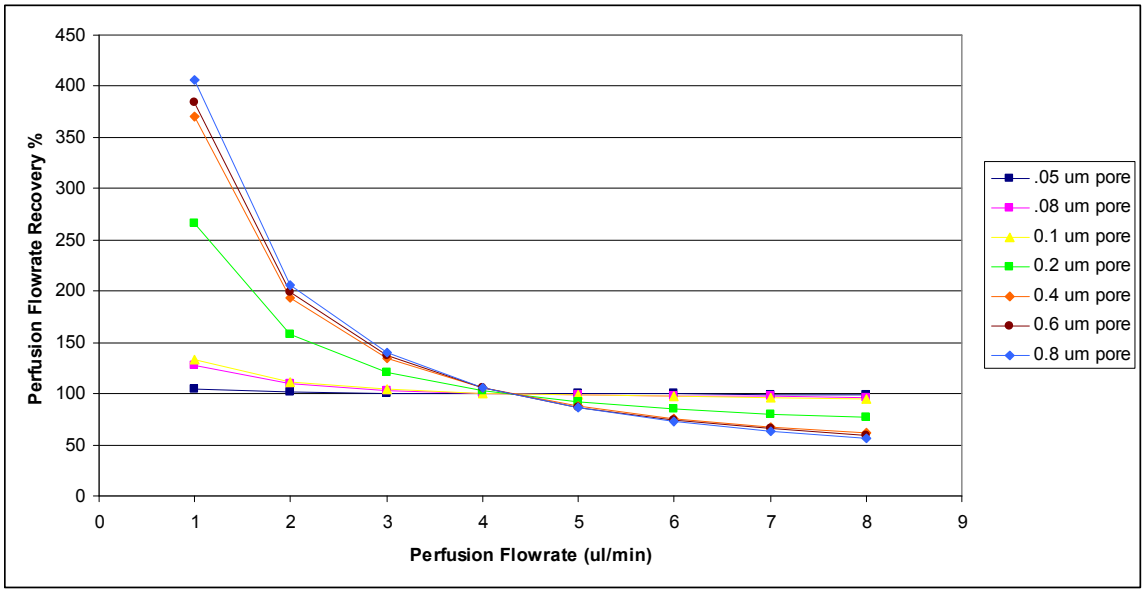

Figure 3.13: Results from Matlab model: Perfusion flowrate recovery vs Perfusion flowrate, for various pore sizes.

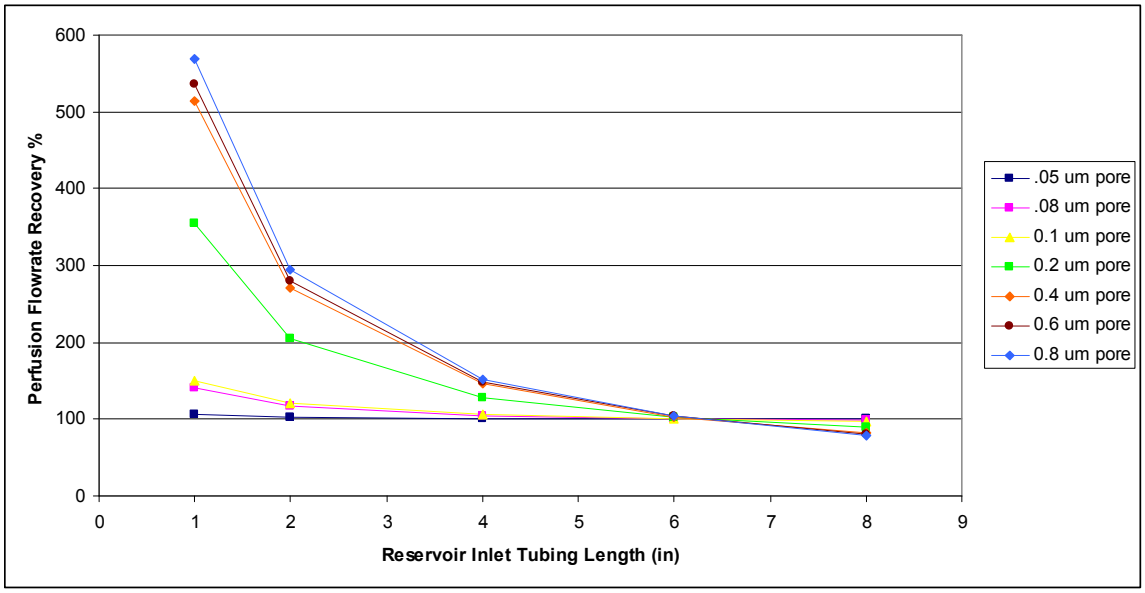

Figure 3.14: Results from Matlab model: Perfusion flowrate recovery vs Reservoir inlet tubing length, for various pore sizes.

Next, a similar analysis is performed using the Matlab program to observe the effects of the reservoir channel height, CPB pressure, perfusion flowrate, and reservoir

tubing length on PFR, as shown in Fig. 3.15-3.17. The important information to extract from these figures is the trend, rather than the PFR actual values, since the non-varying parameters are assigned non-optimized values. In these figures, PFR is most stable when the reservoir height is largest, for all three x-axis parameters. In this case, a reservoir channel height of 110 µm exhibits very little PFR change, from one end of the x-axis to the other, when compared to a reservoir channel height of 30 µm. A tall reservoir height has the additional benefit of reducing the chances of damaging blood and further activating the inflammatory response by reducing shear stress.

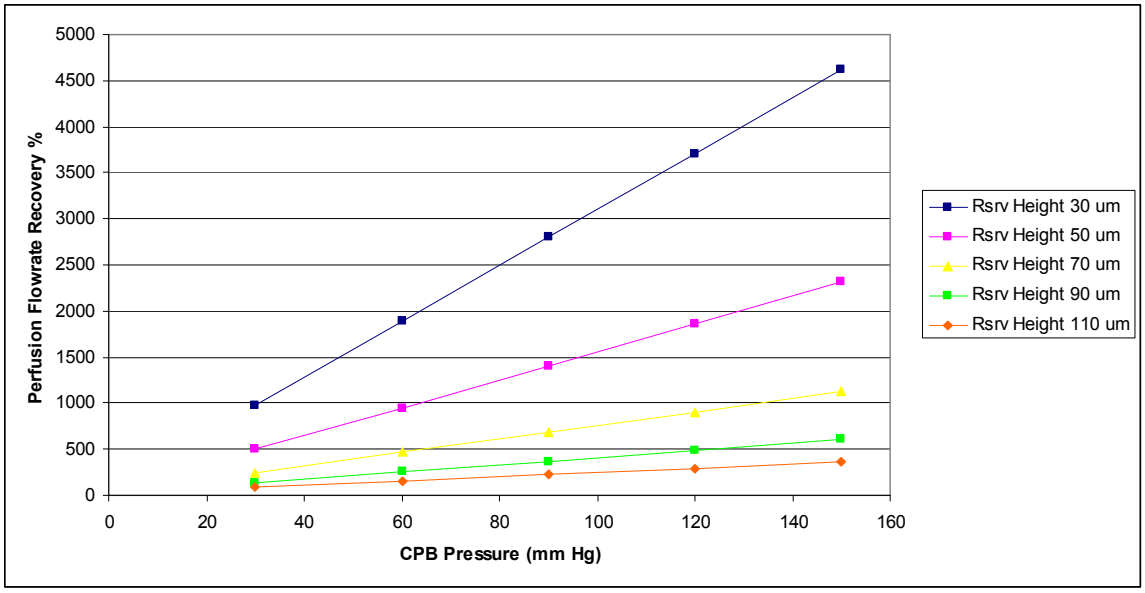

Figure 3.15: Results from Matlab model: Perfusion flowrate recovery vs CPB Pressure, for various reservoir channel heights.

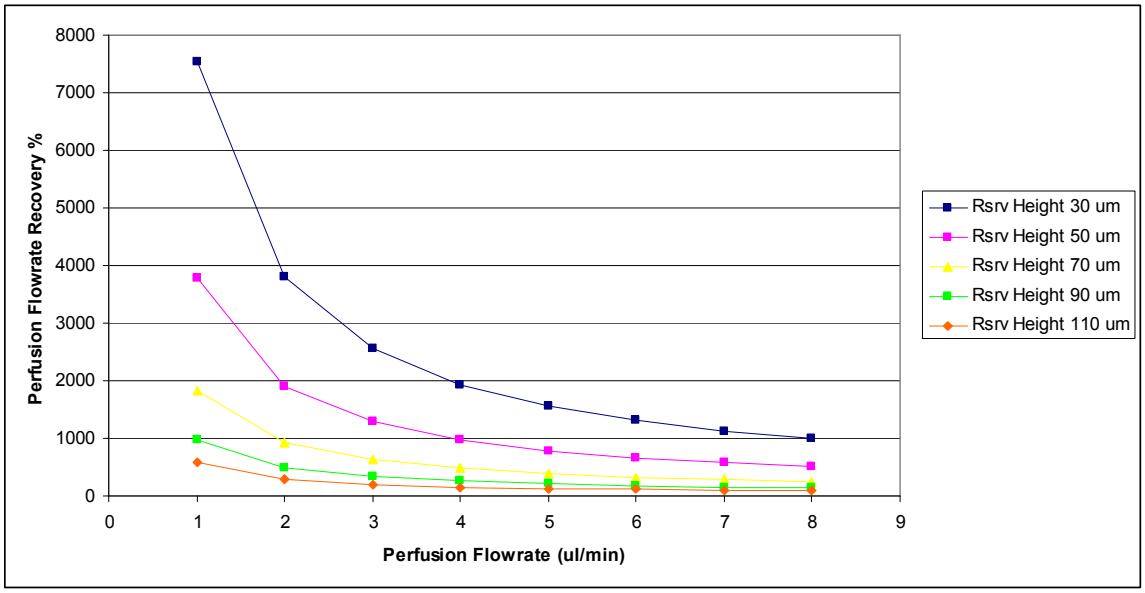

Figure 3.16: Results from Matlab model: Perfusion flowrate recovery vs Perfusion flowrate, for various reservoir channel heights.

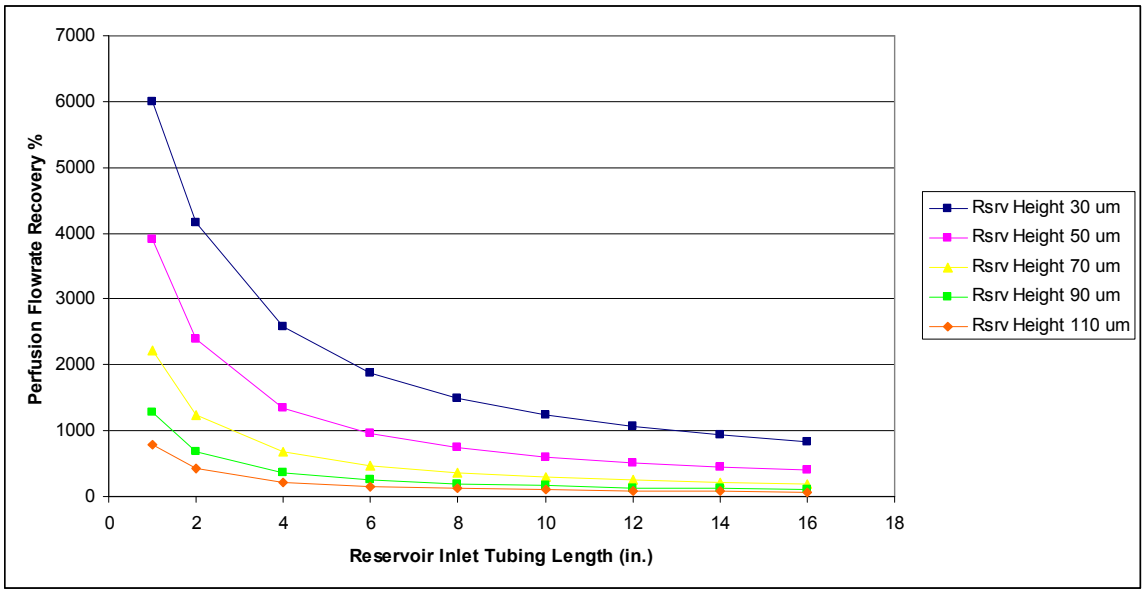

Figure 3.17: Results from Matlab model: Perfusion flowrate recovery vs Reservoir inlet tubing length, for various reservoir channel heights.

In contrast to the previous figures showing the effects of reservoir heights, Fig. 3.18-3.20 show that a shallow perfusion channel height is more stable than a taller height, and is preferred when designing for robustness. However, there is a limit to how shallow a channel height can be before significant problems arise during the fabrication process. Shallow channel heights suffer from a greater chance for epoxy to partially or completely block channels during the epoxy stamping procedure.

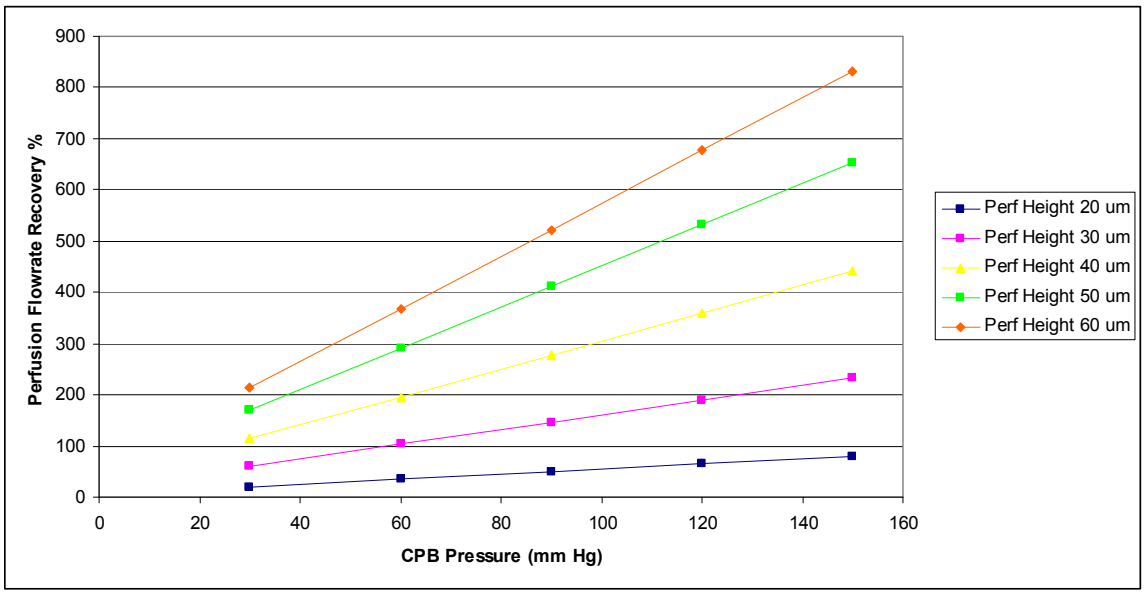

Figure 3.18: Results from Matlab model: Perfusion flowrate recovery vs CPB Pressure, for various perfusion channel heights.

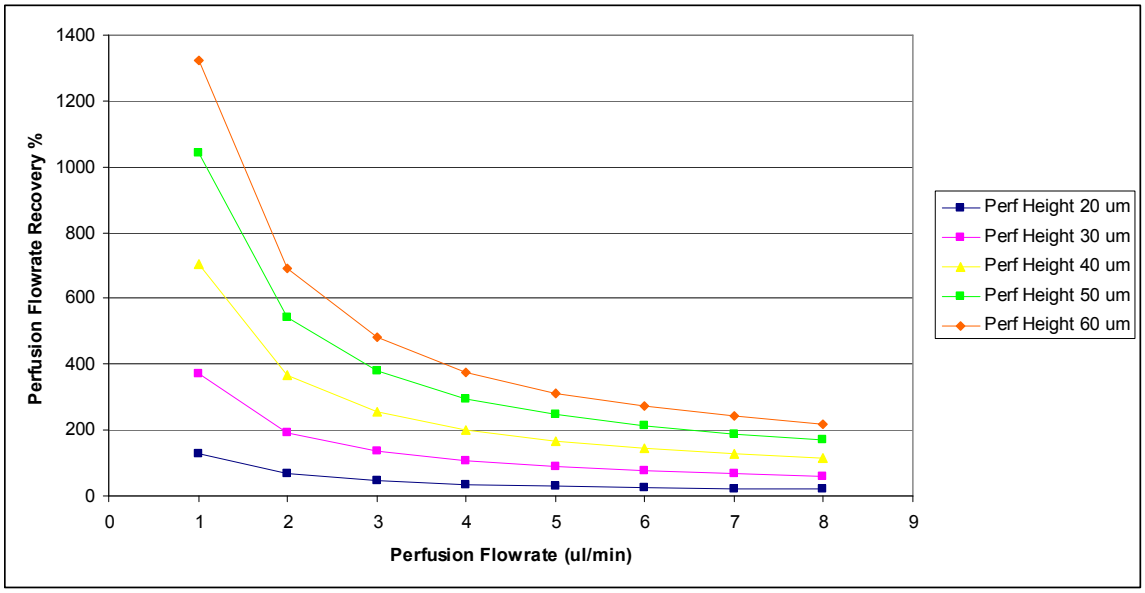

Figure 3.19: Results from Matlab model: Perfusion flowrate recovery vs Perfusion flowrate, for various perfusion channel heights.

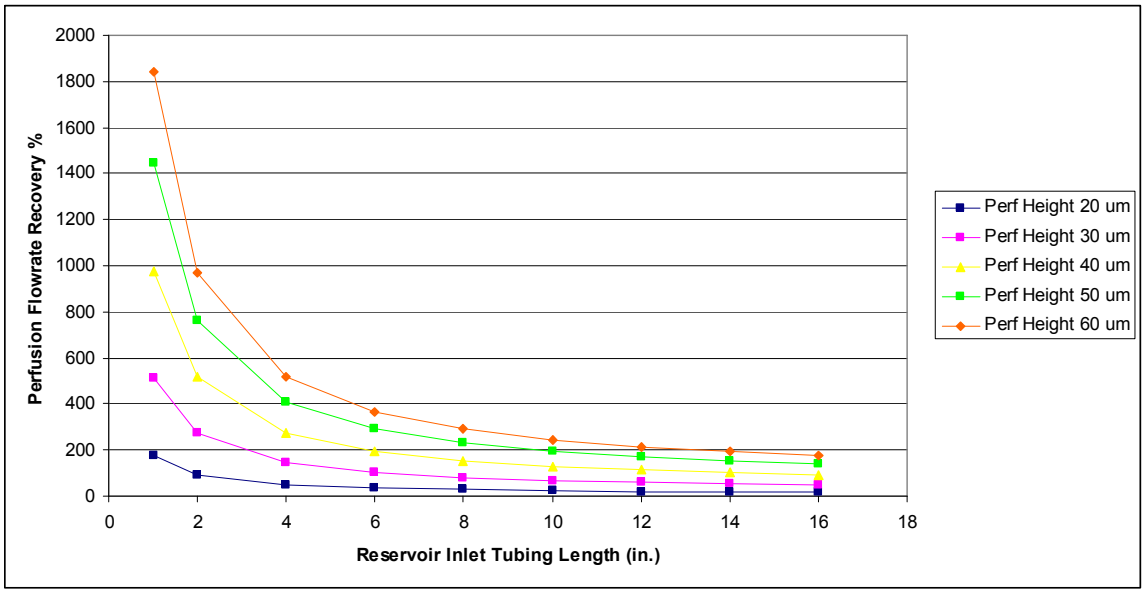

Figure 3.20: Results from Matlab model: Perfusion flowrate recovery vs Reservoir inlet tubing lengths, for various perfusion channel heights.

With the preceding Matlab simulation results and manufacturing constraints in mind, design parameters were finalized for use with blood in a mock CPB circuit, shown in Table 4. Although, theoretically, the objective is to maximize robustness and dialysis performance, in reality, compromises in these areas must be made for manufacturing reasons.

Table 4: Finalized Microdialysis Design for CPB integration

Perfusion Height	30 μm
Perfusion Width	400 μm
Reservoir Height	130 μm
Reservoir Width	600 μm
Channel Length	25 mm
Number of Channels	32
Membrane Pore Size	0.1 or 0.4 μm
Perfusion Flowrate (Syringe Pump)	4.1 μl/min
Membrane Bonding Method	Epoxy stamping

3.4 Microdialysis Experiments

In order to test the proof-of-concept of the proposed microdialysis device, bench-top experiments were conducted using a syringe pump, instead of a CPB pump, and a glucose/phosphate-buffered-saline (PBS) solution, instead of blood. Samples were then collected from the device and analyzed for glucose. These bench-tops experiments helped to establish protocols and techniques that were then used for the mock CPB circuit experiments.

Before a device was to be used, it was exposed to oxygen plasma (power: 100 W, time: 60 sec) for sterilization and to render the channel surfaces hydrophilic. Sterile DI water is then used to completely fill all of the microchannels, including the tubing. This

step is vital to reduce the risk of a bubble lodging itself into a channel, thereby blocking flow through that channel and disrupting the uniform flowrates across the 32 channels.

3.4.1 Experimental Setup: Glucose and PBS

Theoretically, changing perfusate and/or reservoir flowrates affect both the pressure balance across the membrane and the extraction efficiency of the device (see Eq. 3.11) simultaneously. Bench-top experiments were conducted to find flowrates that minimize convective flux across the membrane, while attempting to maximize analyte recovery.

For these experiments, a variation of the final design (Table 4) was used: the perfusion channel height was 20 μm, the reservoir channel height was 65 μm, the membrane had a 0.4 μm pore diameter, the reservoir fluid was a ~200 mg/dl glucose/PBS solution, and glucose-free PBS was used as the perfusate. The perfusate and reservoir solutions were infused into the device via individually controlled syringe pumps. In this case, the perfusion flowrate was held constant at 4 μl/min, while the reservoir flowrate varied between 41 μl/min and 75 μl/min. Before connecting the reservoir syringe to the device, a sample of the glucose/PBS solution was collected to be used as the reference concentration, C_∞. Once the device was connected and the syringe pumps were turned on at the appropriate flowrates, the first samples were not collected until a 30 minute waiting period had passed in order to allow the chemical and flow profiles to stabilize. This waiting period was also used after every change made to the flowrate. Samples were collected until there was at least 75 μl of solution in both collection tubes and the collection time was recorded. Glucose concentration and volume measurements were

made at the reservoir and perfusate outlet. Glucose concentration was measured with a biochemistry analyzer (YSI 2700 Select, YSI Life Sciences, Yellow Springs, OH) and volume was measured using a pipette.

To verify the accuracy of the numerical simulations with experimental values, the Matlab code used to simulate Fig. 3.11 was rewritten for the bench-top glucose/PBS experiment with the following modifications: the reservoir channel became flowrate driven via a syringe pump, instead of pressure driven by the CPB circuit; the reservoir inlet tubing resistance is ignored due to the reservoir being current-sourced; the channels' geometric resistances were modified to represent the changes made to the channel heights and widths, as described in the previous paragraph; and all dynamic viscosities were that of PBS since blood was not used. The revised circuit diagram is shown in Fig. 3.21.

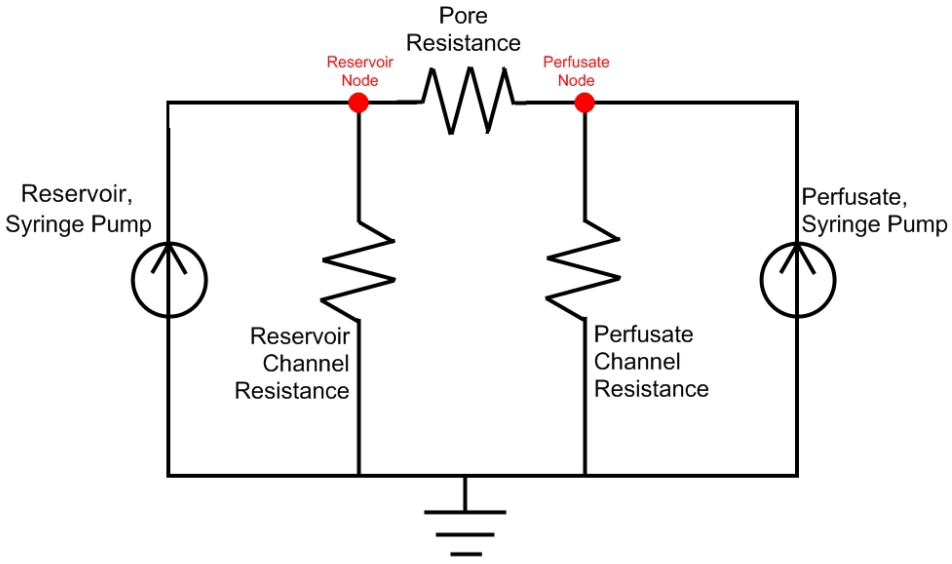

Figure 3.21: A revised circuit diagram for the bench-top glucose/PBS experiments, based off of Fig 3.11, where the reservoir channel is driven by a syringe pump, instead of a CPB pump. Thus, the reservoir inlet tubing resistance can be ignored and the reservoir inlet is now represented with a current source.

3.4.2 Results and Discussion: Glucose and PBS

Results for the experimental and theoretical volume recoveries, as a function of reservoir flowrate, are shown in Fig. 3.22, where volume recovery is defined as the volume measured at the outlet of either the perfusion channel (PERF), or reservoir channel (RSRV), divided by the volume of fluid infused by the respective syringe pump, which is determined by multiplying the flowrate by the collection time. A volume recovery greater than 100% implies that more volume exits that particular channel than was expected, and vice versa. As reservoir flowrate increases, the hydraulic pressure within the reservoir channels also increases, driving more and more reservoir solution to cross the membrane into the perfusion channel. As a result, the reservoir volume recovery decreases. Intuitively, the perfusion volume recovery increases as a result. Linear regression trendlines for perfusion and reservoir volume recovery data show an intersection point when the reservoir flowrate is 50 µl/min and the perfusate flowrate is 4 µl/min, at which point both channels have ~100% volume recovery. Theoretically, this point suggests that there is very little convective flux across the membrane, from either direction.

Despite the appearance that the theoretical values for the reservoir volume recovery matches closely to its corresponding experimental values (Fig. 3.22, solid and hollow square data points) and that the experimental perfusion volume recovery appears to be quite different than its predicted values, this outcome is partially due to the fact that the reservoir flowrate was significantly greater than the perfusion flowrate. For example, 4 µl/min "error" between the experimental and theoretical reservoir outlet flowrate is a relatively small difference compared to its original value ranging between 41 µl/min and

75 µl/min). How ever, when that additional 4 µl/min crosses into the perfusion channel, it doubles the original flowrate of 4 µl/min. Therefore, a better methodology for evaluating the accuracy of the numerical model would be to run both channels at similar flowrates.

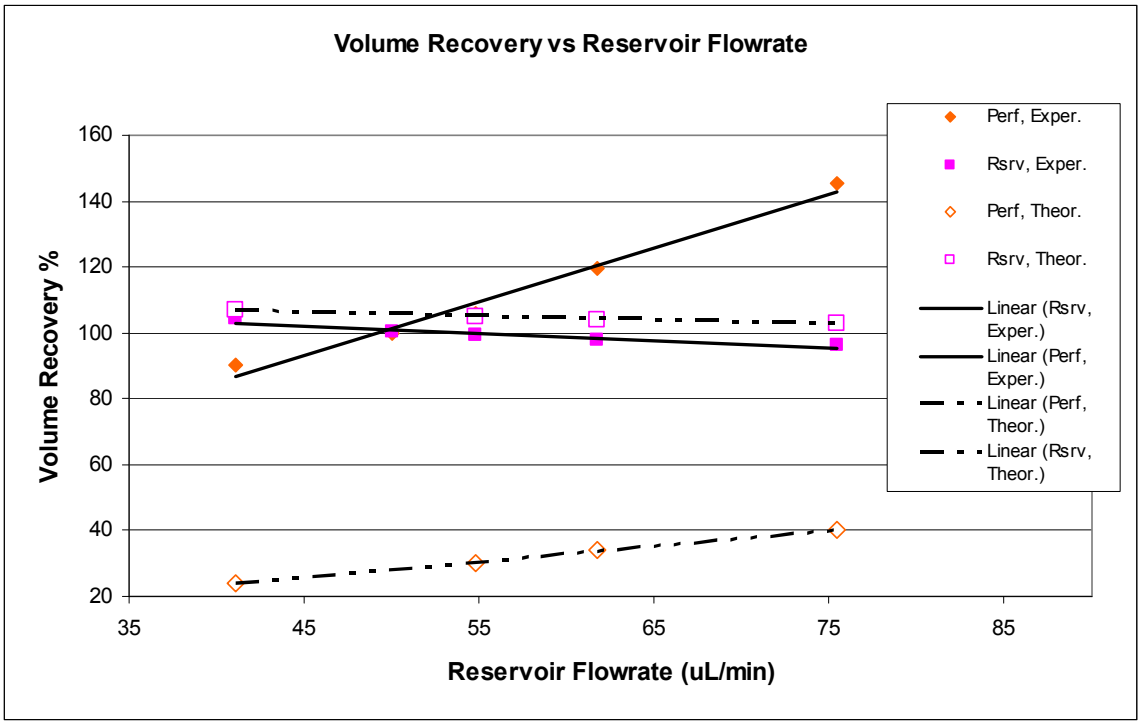

Figure 3.22: Theoretical (hollow) and experimental (solid) Volume Recovery values for perfusion (diamond) and reservoir (square) outlets, versus varying reservoir flowrates.

Glucose concentration recovery as a function of reservoir flowrate is shown in Fig. 3.23, where recovery is defined as the outlet concentration divided by the reference concentration, C_∞. The figure shows the outlet concentration recovery from both channels overlapping one another throughout the full range of flowrates tested. Both the perfusion and reservoir fluids reach very similar glucose concentrations throughout the entire range of reservoir flowrates, despite the direction of convective flux across the membrane. The

assumption that the two solutions are fully mixed by the time it exits the device by verifying that,

$$\dot{m}_{final,perf} C_{final,perf} + \dot{m}_{final,rsrv} C_{final,rsrv} = \dot{m}_{initial,total} C_{initial,total} \qquad \text{Equation 3.26}$$

where, $\dot{m}_{final,perf}$, $\dot{m}_{final,rsrv}$, and $\dot{m}_{final,total}$ are the glucose mass flow rates from the perfusion outlet, reservoir outlet, and the total from the perfusion and reservoir inlet, respectively. $C_{final,perf}$, $C_{final,rsrv}$, and $C_{initial,total}$ are the glucose concentration values from the perfusion outlet, reservoir outlet, and the total from the perfusion and reservoir inlet, respectively.

From solving Eq. 3.26, it was shown that the two solutions were indeed fully mixing while inside the device, most likely due to the larger 0.4 μm membrane pore size that was used. The slight dilution of the glucose/PBS reservoir solution is not expected to be a concern as long as the mass flow rate of the reservoir solution is significantly greater than that of the perfusate solution.

Based on the numerical studies, shown in Fig. 3.12-3.14, the effect that flowrate has on volume recovery can be decreased by using membranes with smaller pore sizes. While this may aid in reducing large changes in volume recovery, it may also reduce perfusate analyte recovery.

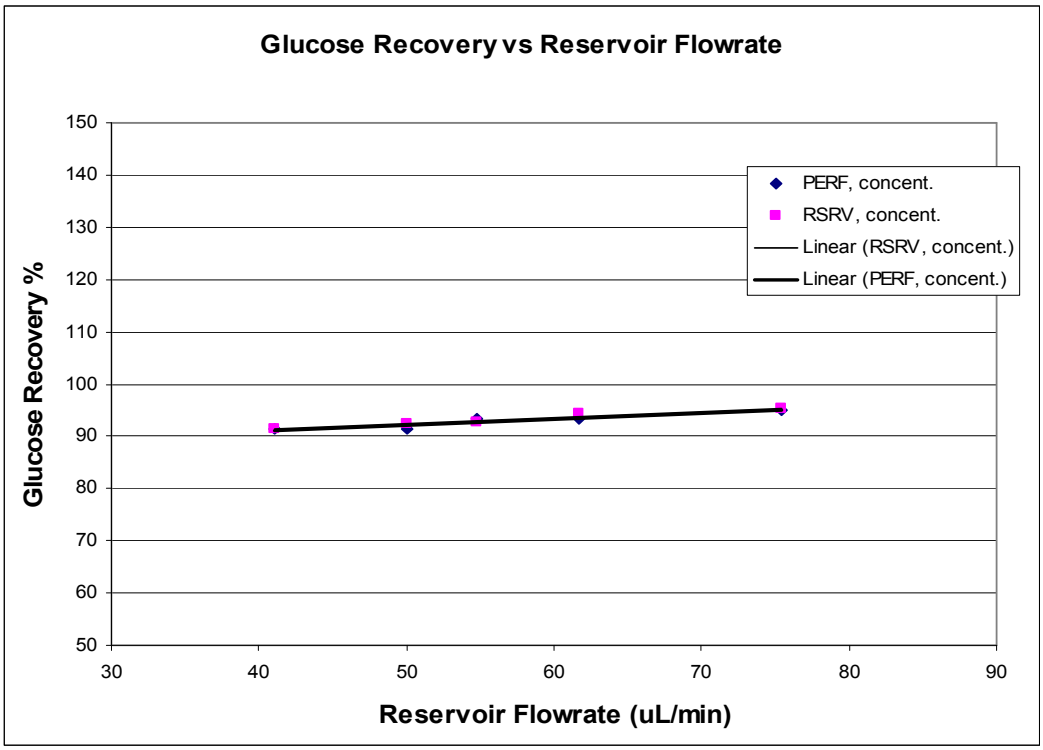

Figure 3.23: Glucose concentration recovery for perfusion and reservoir channels, for varying reservoir flowrates. Data shows that both channels end up with near-identical concentrations for a wide range of flowrates, causing the data points to overlap one another.

3.4.3 Introduction: Blood with Mock CPB Circuit

The microdialysis device, as described in Table 4, was used in a mock CPB circuit to test the recovery performance for the complements C3a, C4a, and C5a in human blood. Experiments were conducted under the supervision of Dr. Akif Undar, Director of the Pediatric Cardiac Research Laboratories at Hershey Medical Center (Hershey, PA). Two devices were tested on the same day, but separately: the first had a membrane pore diameter of 0.1 μm and the other had a 0.4 μm diameter. The devices were otherwise identical.

3.4.3.1 Experimental Setup: Blood with Mock CPB Circuit

A mock *in vitro* CPB circuit was primed by a perfusionist, where packed red blood cells (PRBCs) are hemodiluted with lactated Ringer's solution to obtain a hematocrit level of 26% and pumped through the circuit at 500 ml/min at an arterial circuit pressure of 100 mmHg. The Hershey Medical Center's blood bank provided PRBCs as a substitution for whole blood due to the limited availability of whole blood for non-medical, non-emergency usage. The "packed cells" are prepared by removing platelets, plasma, and sometimes white blood cells from whole blood. Although PRBCs contain little coagulation factors, 4 Units/ml of heparin was added to the circuit to simulate a real CPB circuit as accurately as possible. A heat exchanger maintained the blood at normothermic conditions. The perfusionist monitored and controlled blood pH-levels by supplying appropriate blood-gases

Prior to connecting the microdialysis devices to the CPB circuit, both the perfusion and reservoir channels were infused with a filtered 0.5% w/v solution of PBS and bovine serum albumin (BSA) at 60 µl/min and 4 µl/min, respectively, for 30 minutes. BSA is commonly used to minimize surface adsorption of the analyte to exposed areas such as the channel walls and membrane surface [95, 96].

The device's reservoir inlet tubing was then connected to the circuit at a sampling manifold located downstream of the arterial port of the membrane oxygenator, as shown in Fig. 3.24. The device's perfusion inlet tubing was connected to a syringe filled with lactated Ringer's solution, which was driven by a syringe pump. The perfusion flowrate was set to 4.1 µl/min while the reservoir flowrate was determined to be 40 µl/min, according to timed volume measurements. For the first 45 minutes, the fluid exiting the

device was not collected for analysis since this contained the PBS-BSA solution initially infused into the device. Once this waiting period had passed, reservoir outlet and perfusate outlet samples were collected in separate 1.5 ml microcentrifuge tubes for 15 minutes, every 15 minutes, for 1.5 hours (i.e. 6 samples).

At the half-way mark of each 15 minute sampling period, a 1 ml blood sample was collected from a different sampling port downstream of the membrane oxygenator. This blood sample provided a snapshot of analyte concentrations in the blood before it enters the reservoir channel, thereby providing a reference point to compare how much the reservoir solution was being diluted during dialysis, if at all. Collecting this blood sample at the 7 min. 30 sec. mark provided an estimate of the average analyte concentration during each 15 minute sampling period, in case C3a, C4a, and C5a levels fluctuated over time.

Collected samples were stored on ice, until the end of the experiment, when they were snap-frozen at -80^{O}C. Analysis was performed by Hershey Medical Center using a commercially available anaphylatoxin cytometric bead kit (BD Biosciences, San Jose, CA).

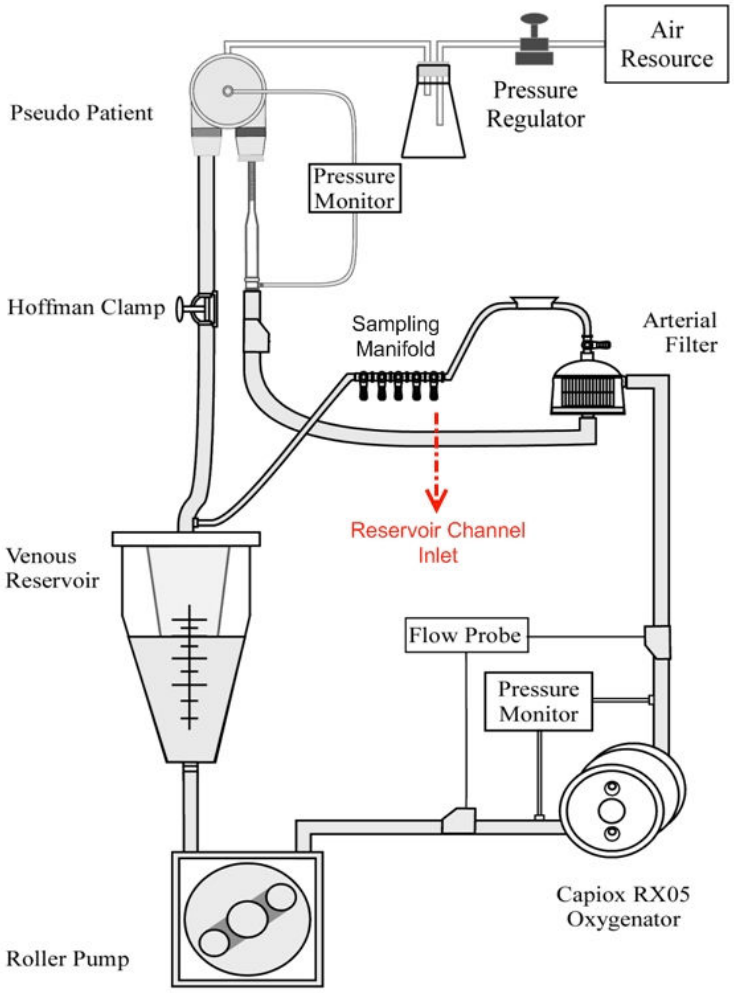

Figure 3.24: The setup for the mock CPB circuit experiments. A relatively small quantity of blood flow is routed to the reservoir channel of the microdialysis device, via a Luer connection at the sampling manifold on the arterial side of the oxygenator.

3.4.3.2 Results and Discussion: 0.1 μm membrane

A two-tailed paired t-Test was conducted on the data, where the null hypothesis, H_0, states that the two sample means are equal in concentration or relative recovery. The statistical significance value, α, used is 0.05.

For the 0.1 μm device, the average C3a, C4a, and C5a concentration recoveries are shown in Fig. 3.25 for the perfusion outlet, reservoir outlet, and CPB sample. The graph shown in Fig. 3.26 uses the same data as Fig. 3.25 but converts it to relative recovery (equivalent to extraction efficiency, E_d) for a quicker evaluation of device performance, simply by dividing the perfusion or reservoir outlet concentration with the CPB circuit concentration.

For C3a in the 0.1 μm device (Fig. 3.25, left), the perfusion channel appeared to reach an equilibrium point with the reservoir channel but at the expense of a diluted reservoir channel, as demonstrated by the higher C3a concentration from the CPB circuit. Using the CPB circuit concentration as reference, the relative recovery for the perfusion outlet and reservoir outlet are 79% and 74%, respectively (Fig. 3.26, left).

For C4a in the same device (Fig. 3.25, center), relative recovery for C4a in the perfusion and reservoir outlets were 75% and 56%, respectively (Fig. 3.26, center). However, the perfusion channel resulted in unexpectedly higher relative recovery than the reservoir channel.

The graph for C5a (Fig. 3.25, right) show yet another difference in device performance. Relative recovery for C5a in the perfusion and reservoir outlets were 70% and 93%, respectively (Fig. 3.26, right).

By looking at Fig. 3.26 as a whole, one notices that the relative recovery for the perfusion outlet varies only slightly, between 70-79%, while the reservoir outlet varies more widely between 74-93%. Unfortunately, it is not yet clear whether the consistency in the perfusion outlet's relative recovery is coincidental and, if not, why it would happen while the reservoir outlet recovery fluctuates significantly more. It is also not clear why C3a concentration from the perfusion and reservoir outlets were able to equilibrate during dialysis, but C4a and C5a concentrations were not. One theory is that the difference in molecular structures of the complements affects its permeability through the pores.

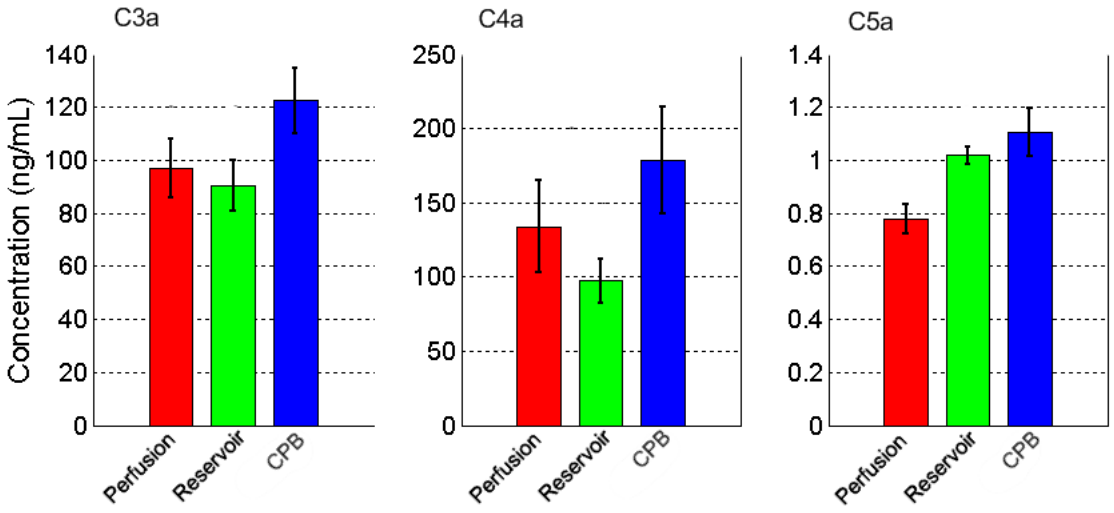

Figure 3.25: Analyte concentration for the 0.1 µm membrane device: (left) C3a, (center) C4a, and (right) C5a. Data represents an average of 6 data points over a 1.5 hour period. A two-sample paired t-Test was performed, where H_0 = two means are equal. The asterisk (*) represents a statistical significance level, $\alpha<0.05$.

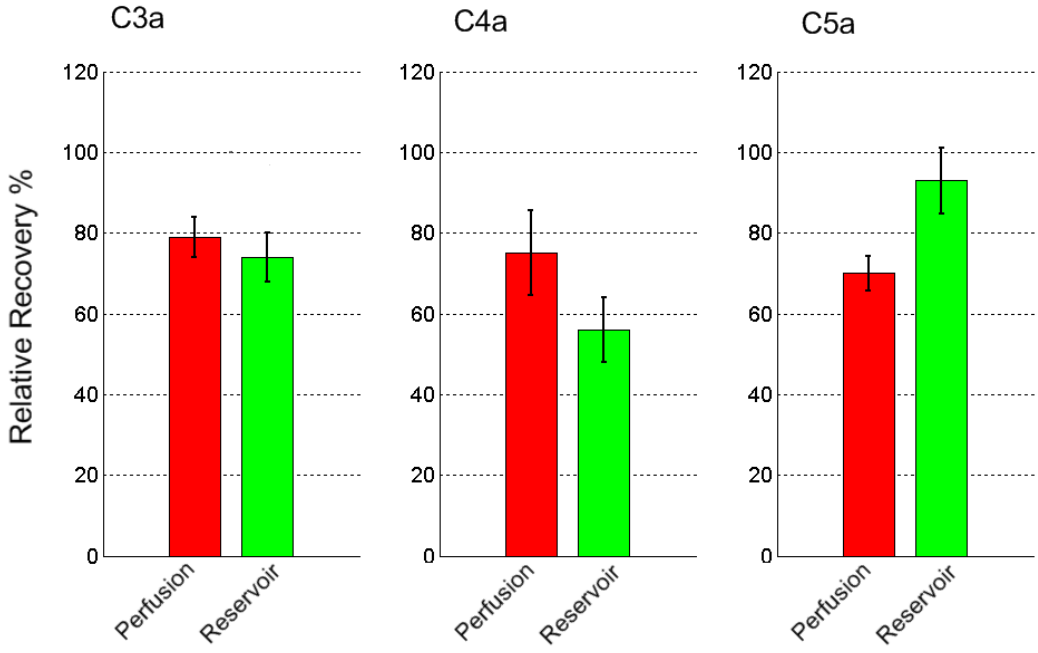

Figure 3.26: Relative recovery for the 0.1 µm membrane device: (left) C3a, (center) C4a, and (right) C5a. Data represents an average of 6 data points over a 1.5 hour period. The asterisk (*) represents a statistical significance level, $\alpha<0.05$.

The p-values for a two-tailed paired t-Test and correlation coefficient values for Fig. 3.25 and 3.26 are summarized in Table 5 and 6, respectively. According to these two tables, the noticeable differences in the paired recovery values of the 0.1 µm membrane device is unlikely to be coincidental and for the most part, the paired recovery values show medium to high positive correlation, and surprisingly, with low and negative correlations as well in C5a. Essentially, no statistical significance can be found for the 0.1 µm device.

Table 5: 100 nm membrane: p-values, pairwise t-test. Blue/bold values denote acceptance of the null hypothesis.

	Perf/Rsrv	Perf/CPB	Rsrv/CPB	Perf_RR% / Rsrv_RR%
C3a	0.020	0.000	0.000	0.012
C4a	0.004	0.004	0.001	0.001
C5a	0.000	0.000	**0.070**	0.001

Table 6: 100 nm membrane: correlation coefficient

	Perf/Rsrv	Perf/CPB	Rsrv/CPB	Perf_RR% / Rsrv_RR%
C3a	0.912	0.830	0.654	0.859
C4a	0.941	0.797	0.745	0.761
C5a	-0.142	0.727	0.128	0.465

3.4.3.3 Results and Discussion: 0.4 µm membrane

The 0.4 µm device appeared to have yielded more consistent and overall better performance than the 0.1 µm device. From Fig. 3.27, one can clearly see more mean concentrations being comparable to one another, evidence of good recovery performance for the perfusion and reservoir channels. The reservoir outlet mean relative recoveries for C3a and C5a, shown in Fig. 3.28, are close to 100% (105% and 106%, respectively), whereas the reservoir outlet mean relative recovery for C4a is slightly greater, at 118%.

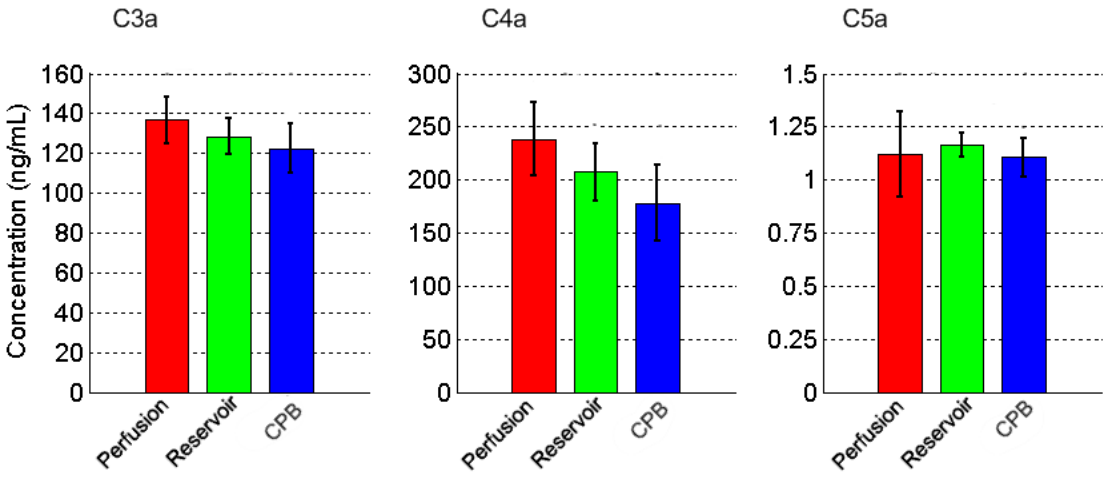

Figure 3.27: Analyte concentration for the 0.4 µm membrane device: (left) C3a, (center) C4a, and (right) C5a. Data represents an average of 6 data points over a 1.5 hour period. A two-sample paired t-Test was performed, where H_0 = two means are equal. The asterisk (*) represents a statistical significance level, $\alpha<0.05$.

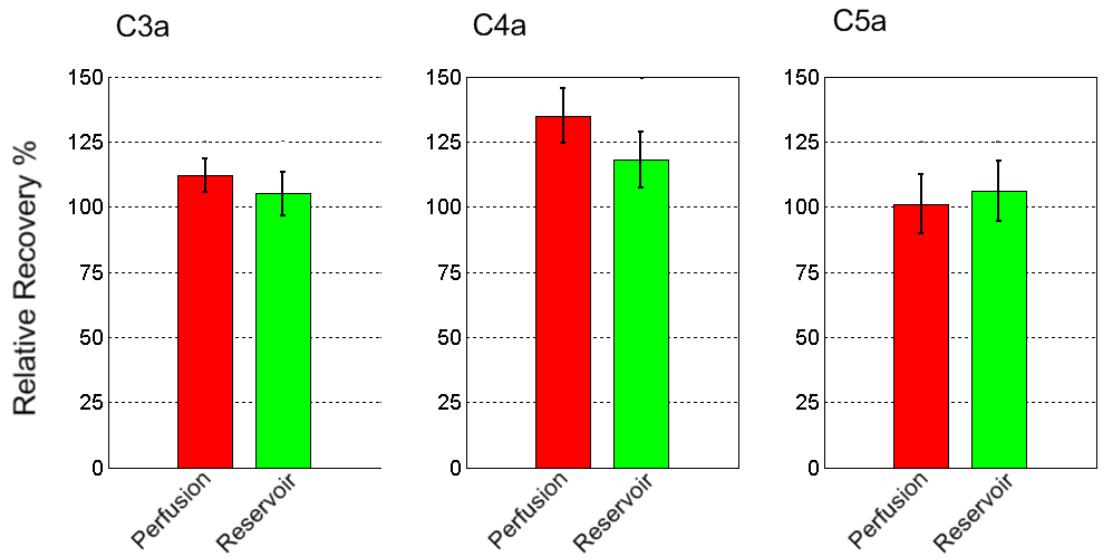

Figure 3.28: Relative recovery for the 0.4 µm membrane device: (left) C3a, (center) C4a, and (right) C5a. Data represents an average of 6 data points over a 1.5 hour period. The asterisk (*) represents a statistical significance level.

The p-values for a two-tailed paired t-Test and correlation coefficient values for Fig. 3.27 and 3.28 are summarized in Table 7 and 8, respectively. According to these two

tables, the noticeable differences in the paired recovery values of the 0.4 µm membrane device is unlikely to be coincidental and for the most part, the paired recovery values show medium to high positive correlation in most cases, and similar to C5a in the 0.1 µm device, the C5a results here had low negative correlations as well. In both cases, Fig. 3.31 in the next section demonstrates these results. The changes in concentration of C5a is so minimal and seemingly noisy that one cannot expect a strong correlation.

Table 7: 400 nm membrane: p-values, pairwise t-test. Blue/bold values denote acceptance of the null hypothesis.

	Perf/Rsrv	Perf/CPB	Rsrv/CPB	Perf RR% / Rsrv RR%
C3a	**0.089**	0.004	**0.210**	**0.092**
C4a	0.002	0.000	0.002	0.001
C5a	**0.610**	**0.821**	**0.278**	**0.515**

Table 8: 400 nm membrane: correlation coefficient

	Perf/Rsrv	Perf/CPB	Rsrv/CPB	Perf RR% / Rsrv RR%
C3a	0.587	0.836	0.592	0.486
C4a	0.944	0.987	0.956	0.871
C5a	-0.008	0.839	-0.253	-0.341

3.4.3.4 Time Course Data

The time course data is given in Fig. 3.29-3.31 in order to observe the standard deviations for a given sample measured using a cytometric bead assay. Although both the 0.1 µm and 0.4 µm devices follow the trend of the CPB concentration over time, albeit roughly at times, the 0.4 µm device clearly has a better extraction efficiency throughout

the time course. The standard deviations, as denoted by the error bars, remain fairly consistent for the C3a and C4a plots, Fig. 3.29 and Fig. 3.30, respectively. However, the C5a plot for the 0.1 μm device had a significant jump in standard deviation at t = 15 min. and t = 75 min., as seen in Fig. 3.31. In the same figure, the 0.4 μm device had a single inconsistently large standard deviation in the reservoir outlet at the 75 minute marks as well. The fact that, at the 75 minute mark, the reservoir outlets for both devices experienced similar results (large standard deviation) does not seem like a coincidence. Perhaps some form of human error, such as mishandling the samples during collection, could have caused this outcome.

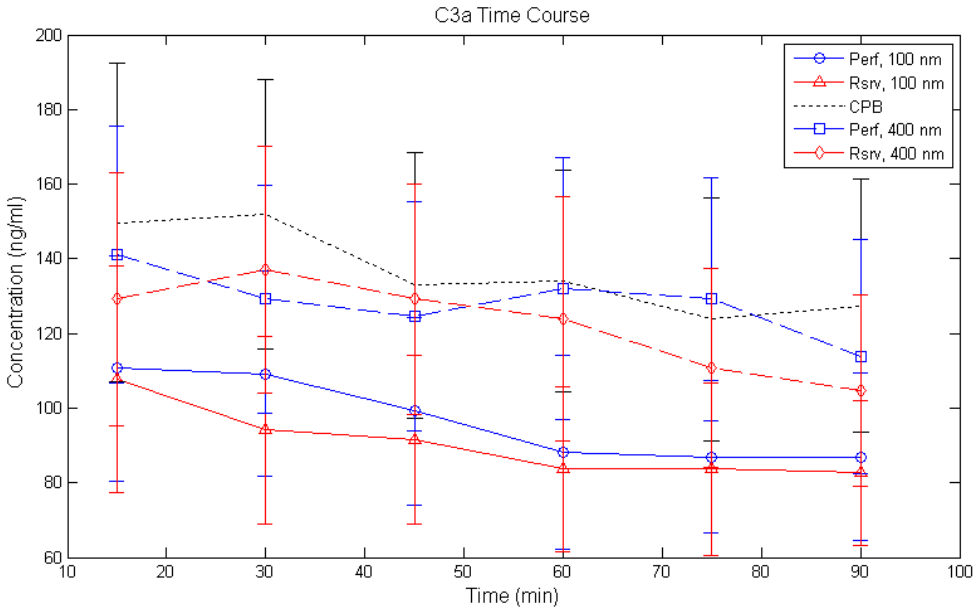

Figure 3. 29: Time course data with error bars representing 2 standard deviations for C3a.

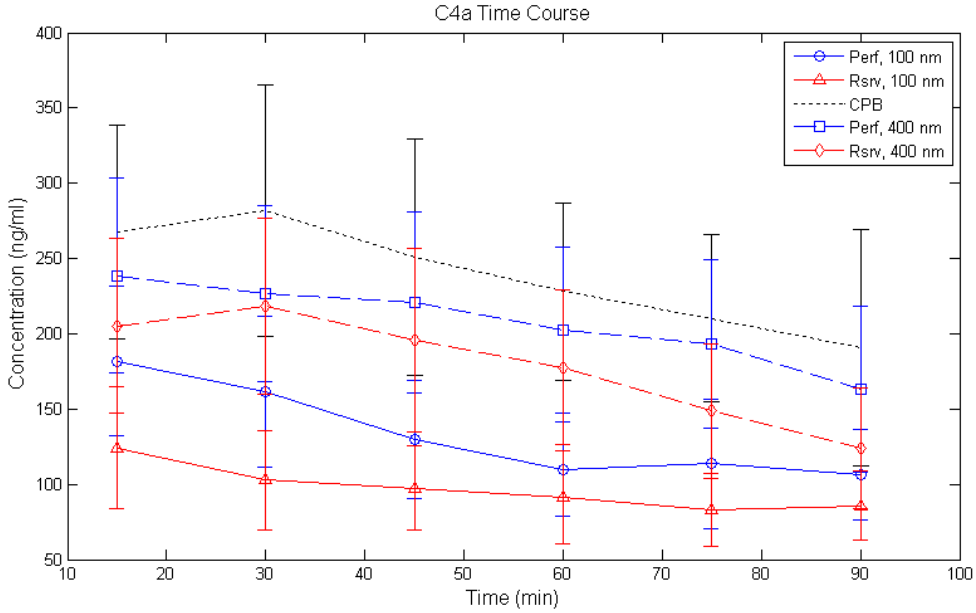

Figure 3. 30: Time course data with error bars representing 2 standard deviations for C4a.

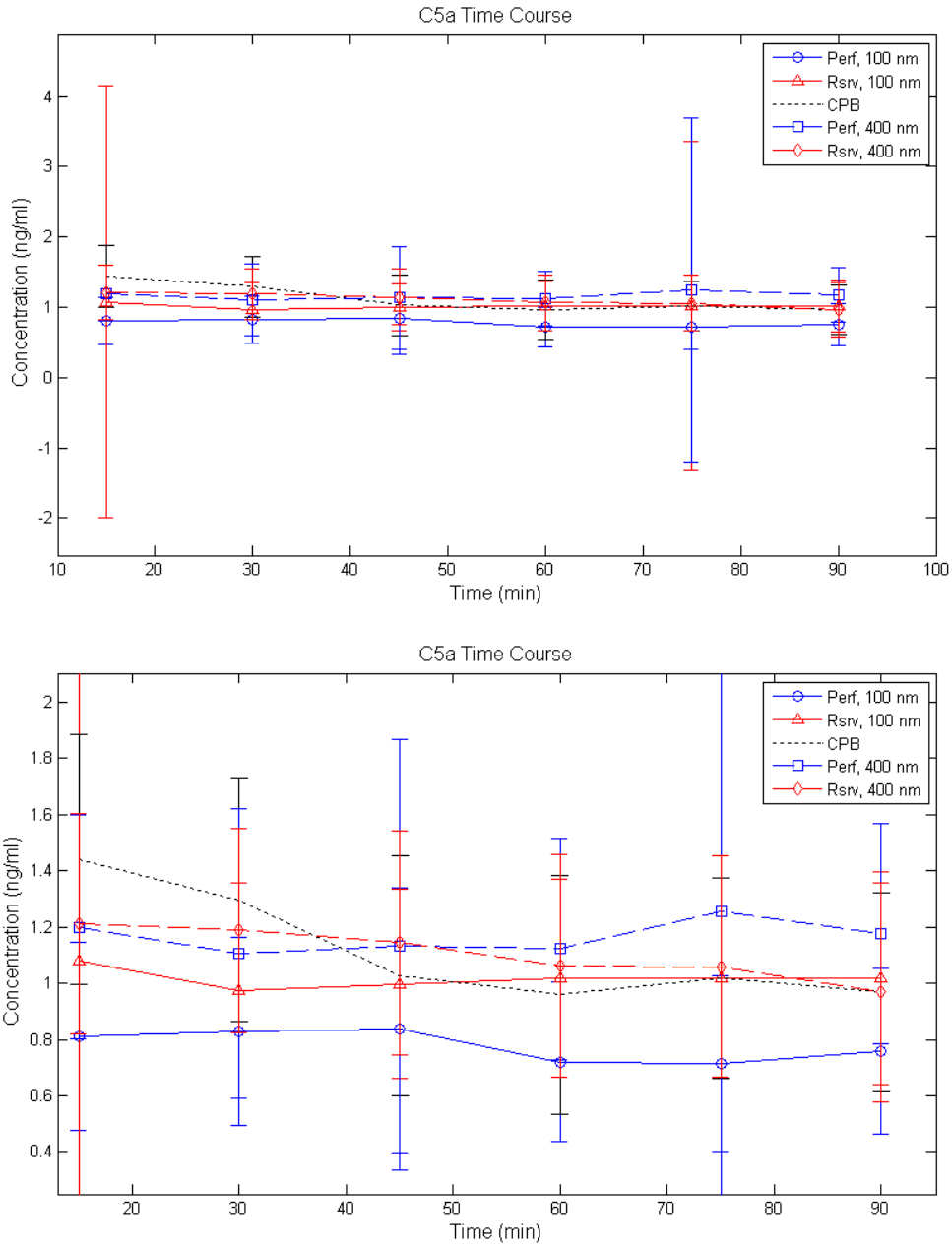

Figure 3.3 1: Time course data with error bars representing 2 standard deviations for C5a. (Top) Zoomed out to see full extent of error bars at 15 and 75 min. (Bottom) Zoomed in.

Chapter 4 - Conclusions and Future Work

It appears that the larger pore-sized device resulted in an overall better performing microdialysis device even though there was an initial concern about the increased risk of convective flux across the membrane. Although the pore resistance in the 0.1 μm device was calculated to be 51 times greater than the 0.4 μm device, there seems to be less reservoir solution dilution in the larger pore-sized device. Another significant benefit from using the larger membrane pore size is the increased perfusate extraction efficiency.

If whole blood or human patients are used in the experiment, other problems may develop and have to be accounted for, such as biofouling of the membrane from platelet activation and influences of blood temperature on device performance. When biofilm forms on the membrane surface, it can block pores and decrease membrane permeability. During an open-heart procedure, surgeons will typically cool the patient's body to intentionally induce hypothermia and eventually bring them back to normothermic conditions. This large temperature change will affect the blood viscosity and therefore, the hydraulic pressure within the microdialysis device, but can be remedied by adjusting the perfusion flowrate and adjusting calibration values for C_∞ as needed.

In the future, one major change in the microdialysis setup would be to use a peristaltic pump, in between the CPB circuit sampling manifold and the reservoir inlet tubing of the device. The use of a peristaltic pump will improve consistency by changing the reservoir channels mode of transport from pressure-based to flowrate-based. During an actual CPB procedure, the arterial circuit pressure may vary from patient to patient, vary over time, and vary depending on the blood viscosity, which itself can vary due to hematocrit and temperature. A peristaltic pump will give the microdialysis operator more control of the flow conditions within the device. During mock CPB circuit experiments, it was also noted that the pressure gauges were very sensitive to the placements of the circuit tubing and sampling manifold, since this inherently affects the head pressure in the circuit. Therefore, relying on the circuit pressure readings to determine expected reservoir flowrate may yield erroneous predictions.

The fabrication procedure should also be improved upon; more importantly, a more reliable bonding method is needed. Currently, the benefit from using a low viscosity epoxy is the ability to create a thin layer of epoxy for stamping, which minimizes additional diffusion distances required for the analyte to cross over from the reservoir channel to the perfusion channel. However, this low viscosity property also increases the chances of the epoxy spreading into the channels as well as spreading to membrane surfaces beyond the template dictated by the PDMS channels. Since each of the perfusion channels are only 400 μm wide, the available diffusion area may decrease significantly. Furthermore, the

Due to the epoxy's transparent nature, especially since its thickness is only tens of microns, it is difficult to visually see when epoxy spreads out beyond the intended

membrane areas or into the channels themselves. The only method to perform quality control checks is to perform microdialysis experiments (e.g. dialyzing glucose) on a large set of devices, of the same design, and compare the extraction efficiency results. If the variance is small, poorly made devices can be spotted easily and the rest would be deemed acceptable for actual CPB usage. If the variance is large, it may be difficult to distinguish which devices are not built to specifications.

To improve the bonding performance, further research into dry bonding techniques is necessary. Since titanium-dioxide-coated polycarbonate membranes have been shown to provide excellent bonding strength in air, but not when exposed to liquids, other combinations of thin film material and membrane material may overcome this limitation.

Compared to currently available, commercial microdialysis probes, this proposed device has better extraction efficiency performance, especially at high flowrates (~4 μl/min). Its *in vitro* design makes it less invasive for the patient and reduces the risk of infections, whereas microdialysis probes are designed to be placed directly on tissue or in ECF. Although it is beyond the scope of this project, this microdialysis device is intended to work in conjunction with a microimmunoassay module (also a μTAS device) that can continuously track the changing inflammatory protein markers, such as that created by Yang et al. [16, 97] and currently being investigated by Sasso et al. [98-100]. The microdialysis chip would therefore serve to continuously prepare a cell-free solution that contains similar levels of analyte concentration as that in the blood.

Bibliography

1. Daly, R.C., et al., *Fifty years of open heart surgery at the Mayo Clinic.* Mayo Clin Proc, 2005. **80**(5): p. 636-40.
2. Perrault, L.P., et al., *On-pump, beating-heart coronary artery operations in high-risk patients: an acceptable trade-off?* Ann Thorac Surg, 1997. **64**(5): p. 1368-73.
3. Lukassen, P. [cited; Available from: http://www.mrtwee.nl/Perfusionist.htm.
4. Martin, R., et al., *Hemolysis during cardiopulmonary bypass.* J Cardiothorac Anesth, 1989. **3**(6): p. 737-40.
5. Vercaemst, L., *Hemolysis in cardiac surgery patients undergoing cardiopulmonary bypass: a review in search of a treatment algorithm.* J Extra Corpor Technol, 2008. **40**(4): p. 257-67.
6. Hensel, M., et al., *Hyperprocalcitonemia in patients with noninfectious SIRS and pulmonary dysfunction associated with cardiopulmonary bypass.* Anesthesiology, 1998. **89**(1): p. 93-104.
7. Sistino, J.J. and J.R. Acsell, *Systemic inflammatory response syndrome (SIRS) following emergency cardiopulmonary bypass: a case report and literature review.* J Extra Corpor Technol, 1999. **31**(1): p. 37-43.
8. de Mendonca-Filho, H.T., et al., *Circulating inflammatory mediators and organ dysfunction after cardiovascular surgery with cardiopulmonary bypass: a prospective observational study.* Crit Care, 2006. **10**(2): p. R46.
9. Khabar, K.S., et al., *Circulating endotoxin and cytokines after cardiopulmonary bypass: differential correlation with duration of bypass and systemic inflammatory response/multiple organ dysfunction syndromes.* Clin Immunol Immunopathol, 1997. **85**(1): p. 97-103.
10. Moat, N.E., D.F. Shore, and T.W. Evans, *Organ dysfunction and cardiopulmonary bypass: the role of complement and complement regulatory proteins.* Eur J Cardiothorac Surg, 1993. **7**(11): p. 563-73.
11. Westaby, S., *Complement and the damaging effects of cardiopulmonary bypass.* Thorax, 1983. **38**(5): p. 321-5.
12. Westaby, S., *Organ dysfunction after cardiopulmonary bypass. A systemic inflammatory reaction initiated by the extracorporeal circuit.* Intensive Care Med, 1987. **13**(2): p. 89-95.
13. Hsieh, Y.C., *On-chip Microdialysis System with Flow-Through Glucose Sensing Capabilities*, in *Dept. of Bioengineering*. 2006, Pennsylvania State University.
14. Hsieh, Y.C. and J.D. Zahn, *On-chip microdialysis system with flow-through sensing components.* Biosens Bioelectron, 2007. **22**(11): p. 2422-8.

15. Yang, S., A. Undar, and J.D. Zahn, *A microfluidic device for continuous, real time blood plasma separation.* Lab Chip, 2006. **6**(7): p. 871-80.
16. Yang, S., A. Undar, and J.D. Zahn, *Continuous cytometric bead processing within a microfluidic device for bead based sensing platforms.* Lab Chip, 2007. **7**(5): p. 588-95.
17. Fung, Y.C., *Stochastic flow in capillary blood vessels.* Microvasc Res, 1973. **5**(1): p. 34-48.
18. Yen, R.T. and Y.C. Fung, *Effect of velocity of distribution on red cell distribution in capillary blood vessels.* Am J Physiol, 1978. **235**(2): p. H251-7.
19. Albelda, S.M., C.W. Smith, and P.A. Ward, *Adhesion molecules and inflammatory injury.* FASEB J, 1994. **8**(8): p. 504-12.
20. Andersen, L.W., et al., *Presence of circulating endotoxins during cardiac operations.* J Thorac Cardiovasc Surg, 1987. **93**(1): p. 115-9.
21. Benedetti, M., et al., *Blood--artificial surface interactions during cardiopulmonary bypass. A comparative study of four oxygenators.* Int J Artif Organs, 1990. **13**(8): p. 488-97.
22. Cohn, L.H. and L.H. Edmunds, *Cardiac surgery in the adult*. 3rd ed. 2008, New York: McGraw-Hill Medical. xx, 1704 p.
23. Cremer, J., et al., *Systemic inflammatory response syndrome after cardiac operations.* Ann Thorac Surg, 1996. **61**(6): p. 1714-20.
24. Gillinov, A.M., et al., *Complement and neutrophil activation during cardiopulmonary bypass: a study in the complement-deficient dog.* Ann Thorac Surg, 1994. **57**(2): p. 345-52.
25. Gillinov, A.M., et al., *Inhibition of neutrophil adhesion during cardiopulmonary bypass.* Ann Thorac Surg, 1994. **57**(1): p. 126-33.
26. Gravlee, G.P., *Cardiopulmonary bypass : principles and practice*. 2nd ed. 2000, Philadelphia: Lippincott Williams & Wilkins. xvi, 768 p.
27. Kirklin, J.K., et al., *Complement and the damaging effects of cardiopulmonary bypass.* J Thorac Cardiovasc Surg, 1983. **86**(6): p. 845-57.
28. Kirklin, J.W., et al., *Studies in extracorporeal circulation. I. Applicability of Gibbon-type pump-oxygenator to human intracardiac surgery: 40 cases.* Ann Surg, 1956. **144**(1): p. 2-8.
29. Nilsson, L., L. Bagge, and S.O. Nystrom, *Blood cell trauma and postoperative bleeding: comparison of bubble and membrane oxygenators and observations on coronary suction.* Scand J Thorac Cardiovasc Surg, 1990. **24**(1): p. 65-9.
30. Nilsson, L., et al., *Bubble and membrane oxygenators--comparison of postoperative organ dysfunction with special reference to inflammatory activity.* Scand J Thorac Cardiovasc Surg, 1990. **24**(1): p. 59-64.
31. Utley, J.R. and E.A. Ashleigh, *Pathophysiology and techniques of cardiopulmonary bypass*. 1982, Baltimore: Williams & Wilkins. xiv, 197 p.
32. van Velzen-Blad, H., et al., *Cardiopulmonary bypass and host defense functions in human beings: II. Lymphocyte function.* Ann Thorac Surg, 1985. **39**(3): p. 212-7.
33. Lillehei, C.W., *Controlled cross circulation for direct-vision intracardiac surgery; correction of ventricular septal defects, atrioventricularis communis, and tetralogy of Fallot.* Postgrad Med, 1955. **17**(5): p. 388-96.

34. Kirklin, J.W., et al., *Intracardiac surgery with the aid of a mechanical pump-oxygenator system (gibbon type): report of eight cases.* Proc Staff Meet Mayo Clin, 1955. **30**(10): p. 201-6.
35. Utley, J.R., *Cardiopulmonary bypass surgery.* Curr Opin Cardiol, 1992. **7**(2): p. 267-75.
36. Stoney, W.S., et al., *Air embolism and other accidents using pump oxygenators.* Ann Thorac Surg, 1980. **29**(4): p. 336-40.
37. Jakob, H., et al., *In-vitro assessment of centrifugal pumps for ventricular assist.* Artif Organs, 1990. **14**(4): p. 278-83.
38. Oku, T., et al., *Hemolysis. A comparative study of four nonpulsatile pumps.* ASAIO Trans, 1988. **34**(3): p. 500-4.
39. Lynch, M.F., D. Peterson, and V. Baker, *Centrifugal blood pumping for open heart surgery.* Minn Med, 1978. **61**(9): p. 536-8.
40. Wheeldon, D.R., D.W. Bethune, and R.D. Gill, *Vortex pumping for routine cardiac surgery: a comparative study.* Perfusion, 1990. **5**(2): p. 135-43.
41. Kress, D.C., et al., *Pump-induced hemolysis in a rabbit model of neonatal ECMO.* ASAIO Trans, 1987. **33**(3): p. 446-52.
42. Palder, S.B., et al., *Prolonged extracorporeal membrane oxygenation in sheep with a hollow-fiber oxygenator and a centrifugal pump.* ASAIO Trans, 1988. **34**(3): p. 820-2.
43. Moore, F.D., Jr., et al., *The effects of complement activation during cardiopulmonary bypass. Attenuation by hypothermia, heparin, and hemodilution.* Ann Surg, 1988. **208**(1): p. 95-103.
44. Utley, J.R., *Pathophysiology of cardiopulmonary bypass: current issues.* J Card Surg, 1990. **5**(3): p. 177-89.
45. Elliott, M.J., *Perfusion for pediatric open heart surgery.* Semin Thorac Cardiovasc Surg, 1990. **2**(4): p. 332-40.
46. Kirklin, J.K., *Prospects for understanding and eliminating the deleterious effects of cardiopulmonary bypass.* Ann Thorac Surg, 1991. **51**(4): p. 529-31.
47. Parker, D.J., et al., *Changes in serum complement and immunoglobulins following cardiopulmonary bypass.* Surgery, 1972. **71**(6): p. 824-7.
48. Hirayama, T., et al., *Evaluation of red cell damage during cardiopulmonary bypass.* Scand J Thorac Cardiovasc Surg, 1985. **19**(3): p. 263-5.
49. Hoffman, J.F., *Cation transport and structure of the red-cell plasma membrane.* Circulation, 1962. **26**: p. 1202-13.
50. Kreel, I., et al., *A syndrome following total body perfusion.* Surg Gynecol Obstet, 1960. **111**: p. 317-21.
51. Warren, J.B., A.J. Brady, and G.W. Taylor, *Vascular smooth muscle influences the release of endothelium-derived relaxing factor.* Proc Biol Sci, 1990. **241**(1301): p. 127-31.
52. Kilbridge, P.M., et al., *Induction of intercellular adhesion molecule-1 and E-selectin mRNA in heart and skeletal muscle of pediatric patients undergoing cardiopulmonary bypass.* J Thorac Cardiovasc Surg, 1994. **107**(5): p. 1183-92.
53. Wilson, I., et al., *Inhibition of neutrophil adherence improves postischemic ventricular performance of the neonatal heart.* Circulation, 1993. **88**(5 Pt 2): p. II372-9.

54. Haslett, C., et al., *The pulmonary vascular sequestration of neutrophils in endotoxemia is initiated by an effect of endotoxin on the neutrophil in the rabbit.* Am Rev Respir Dis, 1987. **136**(1): p. 9-18.
55. Ratliff, N.B., et al., *Pulmonary injury secondary to extracorporeal circulation. An ultrastructural study.* J Thorac Cardiovasc Surg, 1973. **65**(3): p. 425-32.
56. Till, G.O., et al., *Intravascular activation of complement and acute lung injury. Dependency on neutrophils and toxic oxygen metabolites.* J Clin Invest, 1982. **69**(5): p. 1126-35.
57. Smith, P.L., et al., *Cerebral consequences of cardiopulmonary bypass.* Lancet, 1986. **1**(8485): p. 823-5.
58. Sasaki, S., et al., *Partial cardiopulmonary bypass in rats for evaluating ischemia-reperfusion injury.* ASAIO J, 1996. **42**(6): p. 1027-30.
59. Dodds, A.W. and R.B. Sim, *Complement : a practical approach*. Practical approach series. 1997, Oxford: IRL Press at Oxford University Press. xxi, 274 p.
60. Mondino, B.J., Y. Sidikaro, and H. Sumner, *Anaphylatoxin levels in human vitreous humor.* Invest Ophthalmol Vis Sci, 1988. **29**(7): p. 1195-8.
61. Schleuning, M., et al., *Complement activation during storage of blood under normal blood bank conditions. Effects of proteinase inhibitors and leukocyte depletion.* Blood, 1992. **79**(11): p. 3071-5.
62. Hed, J., M. Johansson, and M. Lindroth, *Complement activation according to the alternate pathway by glass and plastic surfaces and its role in neutrophil adhesion.* Immunol Lett, 1984. **8**(6): p. 295-9.
63. Webster, J.G., *Encyclopedia of medical devices and instrumentation*, Wiley-Interscience: Hoboken, N.J.
64. Chaurasia, C.S., et al., *AAPS-FDA Workshop White Paper: microdialysis principles, application, and regulatory perspectives.* J Clin Pharmacol, 2007. **47**(5): p. 589-603.
65. Clough, G.F., *Microdialysis of large molecules.* AAPS J, 2005. **7**(3): p. E686-92.
66. Schutte, R.J., S.A. Oshodi, and W.M. Reichert, *In vitro characterization of microdialysis sampling of macromolecules.* Anal Chem, 2004. **76**(20): p. 6058-63.
67. Plock, N. and C. Kloft, *Microdialysis--theoretical background and recent implementation in applied life-sciences.* Eur J Pharm Sci, 2005. **25**(1): p. 1-24.
68. Groth, L. and A. Jørgensen, *In vitro microdialysis of hydrophilic and lipophilic compounds.* Analytica Chimica Acta, 1997. **355**(1): p. 75-83.
69. Mary, S., et al., *Assessment of the recovery of three lipophilic psoralens by microdialysis: an in vitro study.* International Journal of Pharmaceutics, 1998. **161**(1): p. 7-13.
70. Patterson, S.L., K.A. Sluka, and M.A. Arnold, *A novel transverse push-pull microprobe: in vitro characterization and in vivo demonstration of the enzymatic production of adenosine in the spinal cord dorsal horn.* J Neurochem, 2001. **76**(1): p. 234-46.
71. Huang, Q., B. Seibig, and D. Paul, *Polycarbonate hollow fiber membranes by melt extrusion.* Journal of Membrane Science, 1999. **161**(1-2): p. 287-291.
72. Bungay, P.M., P.F. Morrison, and R.L. Dedrick, *Steady-state theory for quantitative microdialysis of solutes and water in vivo and in vitro.* Life Sci, 1990. **46**(2): p. 105-19.

73. Bungay, P.M., et al., *Microdialysis of dopamine interpreted with quantitative model incorporating probe implantation trauma.* J Neurochem, 2003. **86**(4): p. 932-46.
74. Jacobson, I., M. Sandberg, and A. Hamberger, *Mass transfer in brain dialysis devices--a new method for the estimation of extracellular amino acids concentration.* J Neurosci Methods, 1985. **15**(3): p. 263-8.
75. Ao, X. and J.A. Stenken, *Microdialysis sampling of cytokines.* Methods, 2006. **38**(4): p. 331-41.
76. Lonnroth, P., P.A. Jansson, and U. Smith, *A microdialysis method allowing characterization of intercellular water space in humans.* Am J Physiol, 1987. **253**(2 Pt 1): p. E228-31.
77. Chefer, V.I., et al., *Overview of brain microdialysis.* Curr Protoc Neurosci, 2009. **Chapter 7**: p. Unit7 1.
78. Larsson, C.I., *The use of an "internal standard" for control of the recovery in microdialysis.* Life Sci, 1991. **49**(13): p. PL73-8.
79. Scheller, D. and J. Kolb, *The internal reference technique in microdialysis: a practical approach to monitoring dialysis efficiency and to calculating tissue concentration from dialysate samples.* J Neurosci Methods, 1991. **40**(1): p. 31-8.
80. Le Quellec, A., et al., *Microdialysis probes calibration: gradient and tissue dependent changes in no net flux and reverse dialysis methods.* J Pharmacol Toxicol Methods, 1995. **33**(1): p. 11-6.
81. Lonnroth, P. and L. Strindberg, *Validation of the 'internal reference technique' for calibrating microdialysis catheters in situ.* Acta Physiol Scand, 1995. **153**(4): p. 375-80.
82. Janasek, D., J. Franzke, and A. Manz, *Scaling and the design of miniaturized chemical-analysis systems.* Nature, 2006. **442**(7101): p. 374-80.
83. Shuichi, S., *Micro total analysis system (&mgr;TAS).* Electronics and Communications in Japan (Part II: Electronics), 1999. **82**(2): p. 21-29.
84. de Jong, J., R.G. Lammertink, and M. Wessling, *Membranes and microfluidics: a review.* Lab Chip, 2006. **6**(9): p. 1125-39.
85. Tjerkstra, R.W., et al., *Multi-walled microchannels: free-standing porous silicon membranes for use in μTAS.* Microelectromechanical Systems, Journal of, 2000. **9**(4): p. 495-501.
86. Gielens, F.C., et al., *Microsystem technology for high-flux hydrogen separation membranes.* Journal of Membrane Science, 2004. **243**(1-2): p. 203-213.
87. Metz, S., et al., *Polyimide microfluidic devices with integrated nanoporous filtration areas manufactured by micromachining and ion track technology.* JOURNAL OF MICROMECHANICS AND MICROENGINEERING, 2004. **14**(3): p. 324-331.
88. Song, S., A.K. Singh, and B.J. Kirby, *Electrophoretic concentration of proteins at laser-patterned nanoporous membranes in microchips.* Anal Chem, 2004. **76**(15): p. 4589-92.
89. Hisamoto, H., et al., *Chemicofunctional membrane for integrated chemical processes on a microchip.* Anal Chem, 2003. **75**(2): p. 350-4.
90. Gao, J., et al., *Integrated microfluidic system enabling protein digestion, peptide separation, and protein identification.* Anal Chem, 2001. **73**(11): p. 2648-55.

91. Wang, P.C., J. Gao, and C.S. Lee, *High-resolution chiral separation using microfluidics-based membrane chromatography.* J Chromatogr A, 2002. **942**(1-2): p. 115-22.
92. Duffy, D.C., et al., *Rapid Prototyping of Microfluidic Systems in Poly(dimethylsiloxane).* Analytical Chemistry, 1998. **70**(23): p. 4974-4984.
93. Whatman.
94. Chueh, B.H., et al., *Leakage-free bonding of porous membranes into layered microfluidic array systems.* Anal Chem, 2007. **79**(9): p. 3504-8.
95. Daniel, K.D., et al., *Multi-reservoir device for detecting a soluble cancer biomarker.* Lab Chip, 2007. **7**(10): p. 1288-93.
96. Trickler, W.J. and D.W. Miller, *Use of osmotic agents in microdialysis studies to improve the recovery of macromolecules.* J Pharm Sci, 2003. **92**(7): p. 1419-27.
97. Yang, S., *Microfluidic Devices for On-line Monitoring of Clinically Relevant Proteins During Cardiopulmonary Bypass Procedures*, in *Department of Bioengineering*. 2006, Pennsylvania State University.
98. Sasso, L., Zahn, J.D. *Continuous microfluidic biosensing with conjugated paramagnetic beads*. in *2008 ASME IMECE*. Boston, Mass.
99. Sasso, L., Zahn, J.D. *Continuous microfluidic immunosensing with antibody conjugated paramagnetic beads*. in *MicroTAS 2008, The Twelth International Conference on Miniaturized Systems for Chemistry and Life Sciences*. San Diego, CA.
100. Sasso, L., Zahn, J.D., Undar, A. *A microfluidic immunosensor to monitor systemic inflamation during CPB*. in *Fifth International Conference on Pediactric Mechanical Circulatory Support Systems and Pediactric Cardiopulmonary Perfusion*. 2009. Dallas, Texas.

Appendix A: Preliminary Experiments

Preliminary experiments were conducted using channels with simple single-channel devices. These were done as proof-of-concept tests of various bonding methods and as practice for sample collection and analysis techniques. The PDMS device consisted of a single channel, 2 mm wide, 12 mm long, and 100 μm deep, for both the reservoir and perfusion sides. A polycarbonate membrane with 100 nm pore sizes were used. A syringe pump was used to control each of the channel's flowrate.

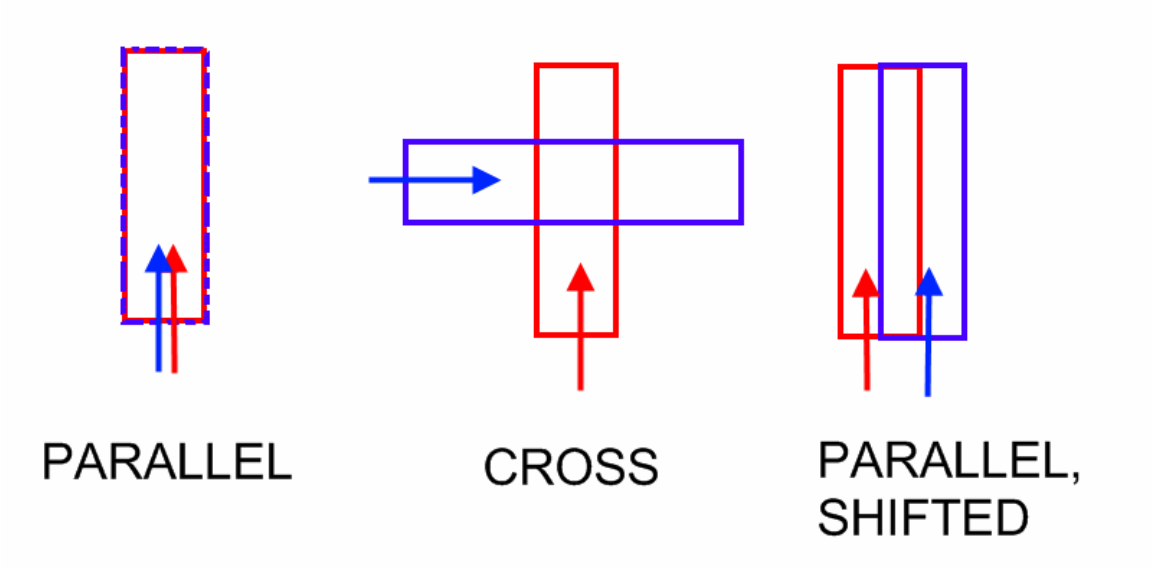

Figure A. 1: Various orientations of the channels: (left) reservoir channel is directly over perfusion channel; (middle) reservoir channel is perpendicular to perfusion channel; and (right) the two channels are offset laterally by one-half the channel width. Arrows denote direction of flow.

First, the "parallel" configuration was used, as shown in Fig. A.1, where both channels are aligned directly over one another. The reservoir solution consisted of a 1.27 g/l glucose/PBS mixture and pumped at a flowrate 40 µl/min while the perfusate solution was pumped at various flowrates, as shown in Fig. A.2.

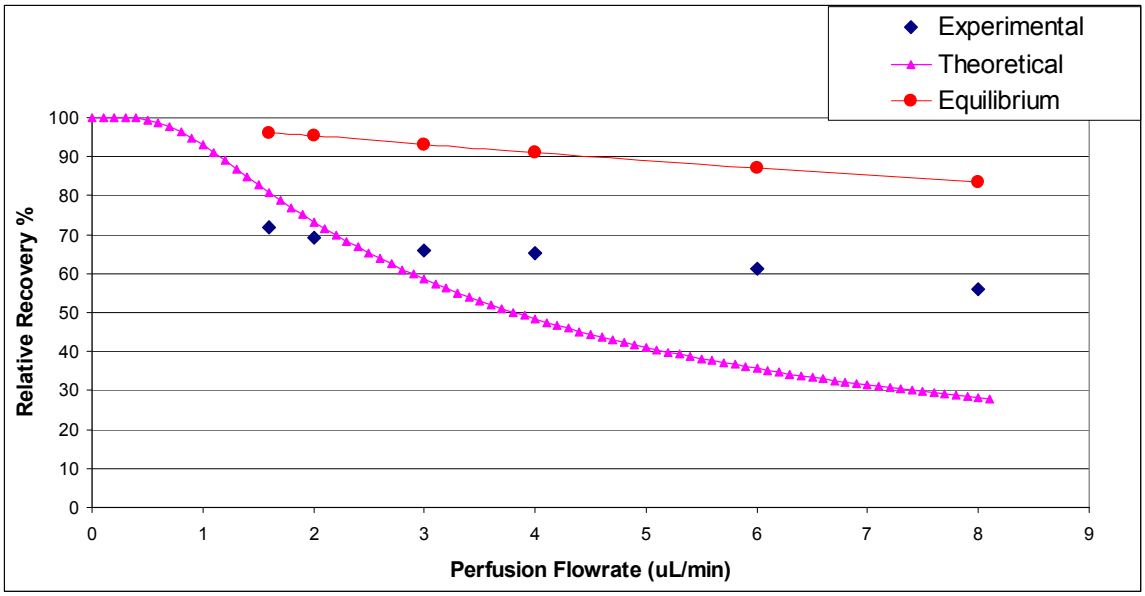

Figure A. 2: Glucose recovery at the perfusion outlet shown in Fig. A.1 (left), "parallel" configuration.

The theoretical relative recovery values in Fig. A.2 were computed using the membrane permeability value, K_0, determined by KaleidaGraph's (Synergy Software, Reading, PA) regression analysis of the experimental data itself. Thus, the resulting K_0 value is assumed to be only relevant to each own respective data set. The result clearly shows that the change in perfusion flowrate has little effect on the relative recovery, perhaps signifying that the two solutions are crossing through the membrane from their respective channels and mixing with one another. However, the two concentrations do not reach the theoretical equilibrium concentration value (shown in Fig. A.2), which

assumes that both solutions have infinite time for analytes to cross the membrane. One should also note that, under this configuration, the membrane does not remain flat and parallel to the plane where the two PDMS layers come in contact. In fact, it bows in the shape of a "U" due to the relatively wide and unsupported width of the channel. This results in an unexpected change in effective channel depth, thereby affecting the hydraulic pressure within the channel. This configuration also places the inlet and outlet holes of each channel, directly over the other channel. This does not allow the flow to stabilize first, before diffusion across the membrane is supposed to occur. In order to remedy these two problems, alternative alignment configurations were used, such as the "cross" and "shifted parallel" configurations shown in Fig. A.1 (middle and right).

In the cross configuration, the two channels are oriented perpendicular from one another, thereby decreasing the diffusion area, but also limiting the amount of bowing of the membrane. This setup also allows the flow to stabilize in its respective channel before the fluid reaches the diffusion area. The theoretical and experimental values were calculated using the same method as in the parallel configuration and shown in Fig. A.3. As one can see, the relative recovery values are significantly lower than that of the parallel configuration due to the decreased diffusion area. However, the experimental values do follow an exponential trend, as noted by the agreement with the expected values in Fig. A.3. The plot also demonstrates that bulk mixing is not occurring or is negligible.

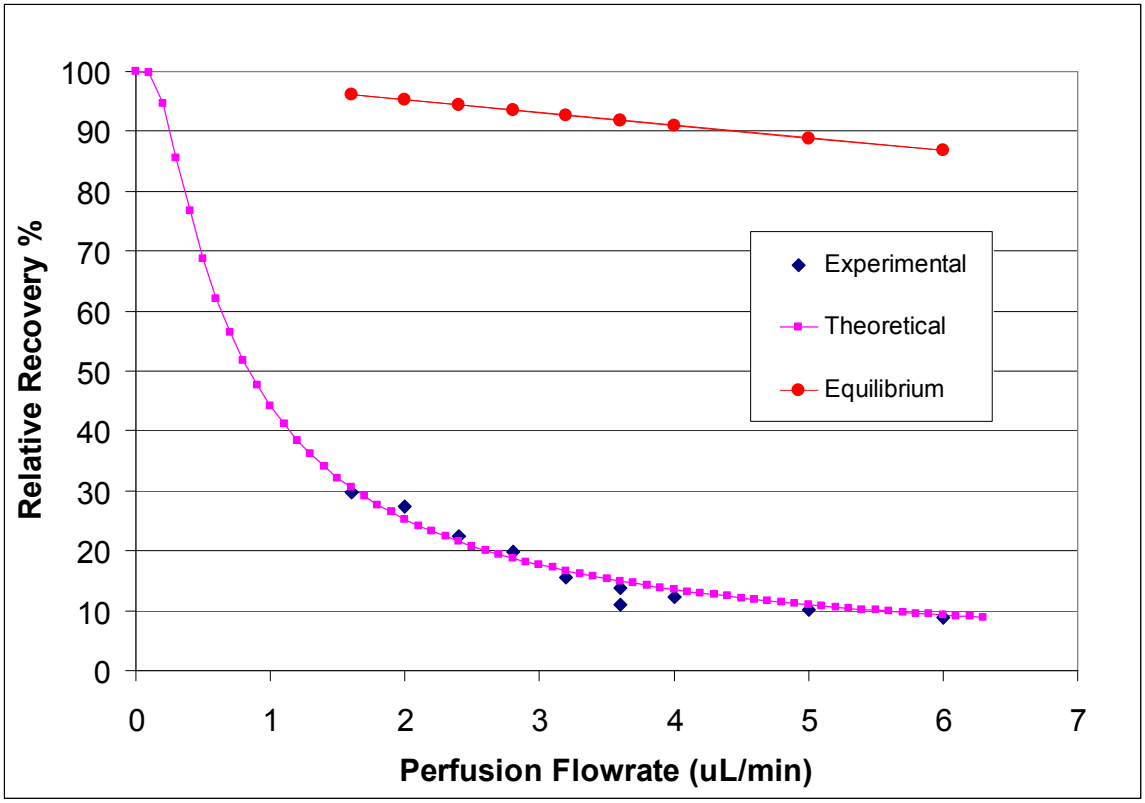

Figure A. 3: Glucose recovery at the perfusion outlet shown in Fig. A.1 (middle), "cross" configuration.

Finally, the shifted parallel configuration was used also to limit bowing across the width of the membrane, by shortening the width of the diffusion area, and to limit the deleterious effects of the inlet and outlet holes in the PDMS channel to be so close to the diffusion area. Once again, the experimental values are shown to follow an exponential trend and does not seem to experience mixing between the two channels, as shown in Fig. A.4.

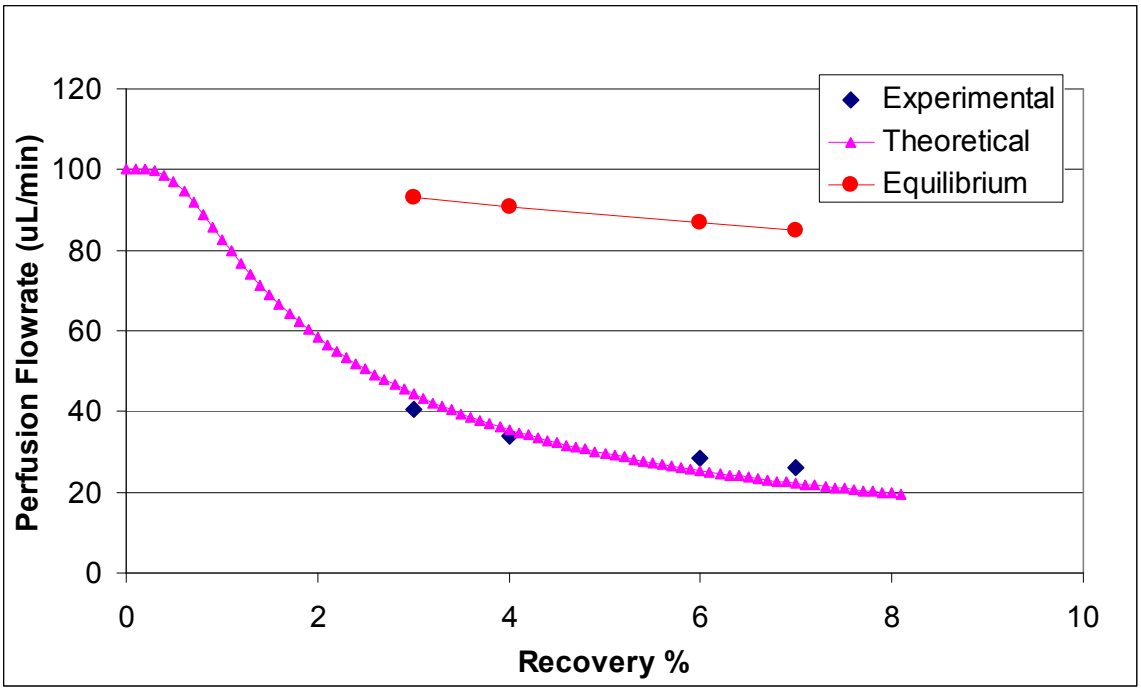

Figure A. 4: Glucose recovery at the perfusion outlet shown in Fig. A.1 (right), "shifted parallel" configuration.

Appendix B: Matlab Code

```
clear all;
display(' '); display(' '); display(' ');display(' '); display(' ');
display(' ');
display('************************************************************ ');
% display(datestr(now));
display('************************************************************ ');


display(' ');
Width_Blood_um = input('Width of blood channel (um): ');
Width_Blood_m = Width_Blood_um .* 10^-6;
length_Width_Blood = length(Width_Blood_m);

Height_Blood_um = input('Height of blood channel (um): ');
Height_Blood_m = Height_Blood_um .* 10^-6;
length_Height_Blood = length(Height_Blood_m);

Width_Perfus_um = input('Width of perfus channel (um): ');
Width_Perfus_m = Width_Perfus_um .* 10^-6;
length_Width_Perfus = length(Width_Perfus_m);

Height_Perfus_um = input('Height of perfus channel (um): ');
Height_Perfus_m = Height_Perfus_um .* 10^-6;
length_Height_Perfus = length(Height_Perfus_m);

Length_mm = input('Length of channel (mm): ');
Length_m = Length_mm .* 10^-3;


N = input('Number of channels: ');

Tube_rsrv_inlet_in = input('What is the length of PE-10 tubing for the
Reservoir Inlet (in): ');
Tube_rsrv_inlet_m = Tube_rsrv_inlet_in.*.0254; % convert in to meters
length_Tube = length(Tube_rsrv_inlet_m);

display(' ');

Q_perf_uLmin = input('What is perfusion flowrate (uL/min): ');
Q_perf_in = sym(Q_perf_uLmin.*1.667e-11);
length_Q_perf = length(Q_perf_in);
```

```
P_CPB_mmHg = input('What is the CPB pump pressure into reservoir
(mmHg): ');
P_CPB_Pa = sym(P_CPB_mmHg.*133.3);
length_P_CPB = length(P_CPB_Pa);

Pore_diam_um = input('Pore size (um): (0.05, 0.08, 0.1, 0.2, 0.4, 0.6,
or 0.8) = ');
length_Pore = length(Pore_diam_um);

% FOR LOOP in order of importance for analysis
% Pore Size >> Blood Height >> Blood Width >> Perfus Height >> Perfus
Width >>
% Tube L >> CPB Press >> Q_perfus
% END


string_varying_variables = input('Note: ','s');


for index_Pore = 1:length_Pore
    for index_Height_Blood = 1:length_Height_Blood
        for index_Width_Blood = 1:length_Width_Blood
            for index_Height_Perfus = 1:length_Height_Perfus
                for index_Width_Perfus = 1:length_Width_Perfus
                    for index_Tube = 1:length_Tube
                        for index_CPB = 1:length_P_CPB
                            for index_Q_perfus = 1:length_Q_perf


            ResistCalc_AUTO(Width_Blood_m(index_Width_Blood),...
            Height_Blood_m(index_Height_Blood),...
            Width_Perfus_m(index_Width_Perfus),...
            Height_Perfus_m(index_Height_Perfus),...
            Tube_rsrv_inlet_m(index_Tube),...
            Q_perf_in(index_Q_perfus),...
            P_CPB_Pa(index_CPB),...
            Pore_diam_um(index_Pore),...
            Length_m, N, string_varying_variables);

                            end
                        end
                    end
                end
            end
        end
    end
end


display(' ');
display('Data has been written to Excel file');
display('^^^^^^^^^^^^ E N D ^^^^^^^^^^^^');
display('==============================');
display(' ');display(' ');display(' ');
clear all
```

```
function [] = ResistCalc_AUTO(Width_Blood_m_fun, Height_Blood_m_fun,
Width_Perfus_m_fun, Height_Perfus_m_fun, Tube_rsrv_inlet_m_fun,
Q_perf_in_fun, P_CPB_Pa_fun, Pore_diam_um_fun, Length_m_fun, N_fun,
string_varying_variables_fun)

    % Declare Symbolic Variables
    syms P_rsrv Resist_rsrv Q_rsrv_in Q_pore P_perf Resist_perf
Resist_pores
    syms Resist_tube


    dyn_visc_blood = 3.5e-3;  %N-s/m^2 at 35C
    dyn_visc_perf = 1e-3;   %N-s/m^2
    dyn_visc_plasma = 1.6e-3;

    % Calculate Pore Resistance
    pore_boolean = 0;

    while (pore_boolean == 0)

        if Pore_diam_um_fun == .05
            Pore_density = 6e8*(100)^2;
            Pore_thk = 6e-6;
            pore_boolean = 1;
        elseif Pore_diam_um_fun == .08
            Pore_density = 6e8*(100)^2;
            Pore_thk = 6e-6;
            pore_boolean = 1;
        elseif Pore_diam_um_fun == .1
            Pore_density = 3e8*(100)^2; % converts from per cm^2, to
                                        per m^2
            Pore_thk = 6e-6; % [m]
            pore_boolean = 1;
        elseif Pore_diam_um_fun == .2
            Pore_density = 3e8*(100)^2;
            Pore_thk = 10e-6;
            pore_boolean = 1;
        elseif Pore_diam_um_fun == .4
            Pore_density = 1e8*(100)^2; % converts from per cm^2, to
                                        per m^2
            Pore_thk = 10e-6; % [m]
            pore_boolean = 1;
        elseif Pore_diam_um_fun == .6
            Pore_density = 3e7*(100)^2;
            Pore_thk = 10e-6;
            pore_boolean = 1;
        elseif Pore_diam_um_fun == .8
            Pore_density = 3e7*(100)^2; % converts from per cm^2, to
```

```
                                          per m^2
            Pore_thk = 9e-6; % [m]
            pore_boolean = 1;
        else
            display(' ');
            display('Please enter correct pore size')
            display(' '); display(' ');
        end  %if statement

    end  % while statement

    Pore_diam_m = Pore_diam_um_fun*10^-6; % converts pore size diameter
                                             from [um] to [m]

    Diff_Area_m2 = N_fun*Length_m_fun*min(Width_Perfus_m_fun,
                        Width_Blood_m_fun); % area is based on
                                          whichever width dimension is
                                          smallest
    Num_Pores = Pore_density*Diff_Area_m2;
    Num_Pores;

    Fudge_rsrv_sumseries = 0;
    Fudge_perf_sumseries = 0;

    %%% additional fudge factor for Rectangular Duct Resistances
    %%% (simplified equation does not apply due to low aspect ratio

    for ii=1:2:13
        Fudge_rsrv_sumseries = Fudge_rsrv_sumseries +
        (1/ii^5)*tanh(ii*pi*Width_Blood_m_fun/(2*Height_Blood_m_fun));

        Fudge_perf_sumseries = Fudge_perf_sumseries +
      (1/ii^5)*tanh(ii*pi*Width_Perfus_m_fun/(2*Height_Perfus_m_fun));
    end

    Fudge_rsrv = (1 - Height_Blood_m_fun/Width_Blood_m_fun *
                  (192/pi^5*Fudge_rsrv_sumseries))^-1;
    Fudge_perf = (1 - Height_Perfus_m_fun/Width_Perfus_m_fun *
                  (192/pi^5*Fudge_perf_sumseries))^-1;

%     Fudge_rsrv = 1;
%     Fudge_perf = 1;

    %>>>>>>>>>>>>>> SYMBOLIC EQUATIONS <<<<<<<<<<<<<<<<<

    eq1 = (P_CPB_Pa_fun-P_rsrv)/Resist_tube - P_rsrv/Resist_rsrv -
            Q_pore;

    eq2 = Q_perf_in_fun + Q_pore - P_perf/Resist_perf;

    eq3 = Q_pore - (P_rsrv/2-P_perf/2)/Resist_pores;

    eq4 = Resist_rsrv - (12*dyn_visc_blood*Length_m_fun/
            (Width_Blood_m_fun*Height_Blood_m_fun^3)/N_fun)*Fudge_rsrv;
```

```
    eq5 = Resist_perf - 12 * dyn_visc_perf*Length_m_fun/
            (Width_Perfus_m_fun*Height_Perfus_m_fun^3)/N_fun*
            Fudge_perf;

    eq6 = Resist_pores - 8*dyn_visc_plasma*Pore_thk/(pi*
            (Pore_diam_m/2)^4) / Num_Pores;

    eq7 = Resist_tube - 8*dyn_visc_blood*Tube_rsrv_inlet_m_fun/
            (pi*(0.28e-3/2)^4);

    eq8 = Q_rsrv_in - (P_CPB_Pa_fun-P_rsrv)/Resist_tube;

    S = solve(eq1, eq2, eq3, eq4, eq5, eq6, eq7, eq8);

    %>>>>>>>>>>>>> SYMBOLIC EQUATIONS <<<<<<<<<<<<<<<<<

    format short eng

    P_rsrv = single(S.P_rsrv); % Pa
    P_perf = single(S.P_perf); % Pa

    Resist_rsrv = single(S.Resist_rsrv);
    Resist_perf = single(S.Resist_perf);
    Resist_pores = single(S.Resist_pores);
    Resist_tube = single(S.Resist_tube);
    Q_rsrv_in = single(S.Q_rsrv_in)/1.667e-11; % uL/min
    Q_perf_in_fun = single(Q_perf_in_fun)/1.667e-11; % uL/min
    Q_pore = single(S.Q_pore)/1.667e-11; % uL/min

    Q_rsrv_out = single(S.P_rsrv/S.Resist_rsrv)/1.667e-11; % uL/min
    Q_perf_out = single(S.P_perf/S.Resist_perf)/1.667e-11; % uL/min

    P_CPB_mmHg_fun = single(P_CPB_Pa_fun)/133.3;



    note = string_varying_variables_fun;


      % % % % % % % % % % % % % % % % % % % % % % % % % % % % % % % % %
      % %
      % %        S T O R I N G   D A T A   I N   E X C E L
      % %
      % % % % % % % % % % % % % % % % % % % % % % % % % % % % % % % % %

    Header_title = {'0','Note','Reservoir Channel Width
(um)','Reservoir Channel Height (um)',...
        'Perfusion Channel Width (um)','Perfusion Channel Height
(um)','Channel Length (mm)',...
        'Number of Channels','Reservoir Tubing Length (in)','Pore Size
(um)',...
        'Perfusion Flow Rate (uL/min)','CPB Inline Pressure (mmHg)',...
```

```
        'Reservoir Pressure (Pa)','Perfusion Pressure (Pa)','Reservoir
Channel Resistance',...
        'Perfusion Channel Resistance','Pore Resistance','Reservoir
Tubing Resistance',...
        'Reservoir Flowrate-In (uL/min)',...
        'Pore Flowrate (uL/min)','Reservoir Flowrate-Out (uL/min)',...
        'Perfusion Flowrate-Out (uL/min)', 'Perf Flowrate Rec%'};

    xlswrite('VolumeCalc_AUTO',Header_title,'Sheet1');
%
%     targetSheet = worksheets.Item('Sheet1');
%     targetSheet.Activate;


    % % Check Excel sheet to make sure where data was last written,
prevents
    % % writing over previous data
    [numrow, numcol] = size(xlsread('VolumeCalc_AUTO','Sheet1'));

    row = num2str(numrow + 1);
    col = 'A';
    location = [col row];

    write_excel = {0,note, Width_Blood_m_fun*1e6,
            Height_Blood_m_fun*1e6, Width_Perfus_m_fun*1e6,...
            Height_Perfus_m_fun*1e6, Length_m_fun*1e3, N_fun,
            Tube_rsrv_inlet_m_fun/.0254, Pore_diam_um_fun,...
            Q_perf_in_fun, P_CPB_mmHg_fun, P_rsrv, P_perf, Resist_rsrv,
            Resist_perf, Resist_pores, Resist_tube, Q_rsrv_in, Q_pore,
            Q_rsrv_out, Q_perf_out, Q_perf_out/Q_perf_in_fun*100};

    xlswrite('VolumeCalc_AUTO',write_excel,'Sheet1',location);


    % display(' ');
    % display('Data has been written to Excel file');
    % display('^^^^^^^^^^^^ E N D ^^^^^^^^^^^^');
    % display('================================');
    % display(' ');display(' ');display(' ');
    % clear all;

end % function
```